Imperial College London

Quantum Behaviour in Nano-Mechanical Systems

by

Muhammad Tahir

Thesis submitted

for the degree of

Doctor of Philosophy of Imperial College London

and for the

Diploma of Imperial College

Condensed Matter Theory Group

Department of Physics

The Blackett Laboratory

Imperial College of Science, Technology and Medicine

London

March, 2010

Abstract

The emerging field of nano-electro-mechanical systems (NEMS), in which the single mode of a nanomechanical oscillator plays the role of an active device, is receiving much attention due to its technological importance. The characteristic component that gives the name to these devices is an oscillator of nanometer size coupled to the electrons on the dot that transfer electrons one-by-one between a source and a drain lead. From a fundamental point of view, it is important to understand the interplay between the electronic transport and the nanomechanical motion of the oscillator quantum mechanically.

This thesis contains the description and analysis of the dynamics of a nanomechanical oscillator coupled to a resonant tunnel junction (RTJ) and its realization as a shuttle device. The models we consider describe both the mechanical and electrical degrees of freedom quantum mechanically; Firstly, a RTJ coupled to a nanomechanical oscillator. Secondly, we report a first complete quantum mechanical analysis of a charge shuttle. We introduce a new non-perturbative quantum mechanical description for the strong interaction of both the electrical and the mechanical object, which is beyond the existing experiments. We describe a nonequilibrium Green's function formalism: a well suited technique to treat this kind of far from equilibrium systems, which can deal with very small to very large applied bias. The numerical implementation of these models are discussed in detail, and the transient and the steady state behavior of the system is also considered here for the quantum dynamics of the oscillator as a function of time. This will provide useful insight for the design of experiments aimed at studying the quantum behavior of an oscillator.

Contents

1 Introduction **9**
1.1 Nanoelectromechanical systems 9
1.2 Quantum dynamics 11
1.3 Experimental realization 14
1.4 Theoretical implementation for quantum behaviour in nano-mechanical systems 21
1.5 This thesis 23

2 Green's function theory **25**
2.1 Introduction 25
2.2 Single particle Green's function 26
2.3 Green's function and Perturbation Theory 28
2.4 General model formulation: Time-independent 29
2.4.1 Retarded and advanced Green's function 31
2.4.2 The Self-energy 33
2.4.3 Langreth's theorem 34
2.4.4 Dyson's equation and the Lesser Green's function 35
2.4.5 The Current from lead α 38
2.5 Time-dependent non-equilibrium Green's function 39
2.6 Formulation for a general time-dependent model 40
2.6.1 Time-dependent density matrix $\rho(t,t)$ 45
2.6.2 Time-dependent Current from lead α 48

3 A Simple Model for NEMS **50**
3.1 Introduction 50
3.2 Formulation 52
3.3 Green's function and quantum transport 55
3.4 Average Energy 60
3.5 Current noise and Fano factor 62
3.6 Discussion of results 65
3.7 Conclusions 73

4 Time-dependent dynamics of simple NEMS model **74**
4.1 Introduction . . . 74
4.2 Model calculations . . . 75
4.3 Time-dependent dot population $\rho(t)$ . . . 78
4.4 Time-dependent Current from lead α . . . 81
4.5 Average energy and the Fano factor . . . 82
4.6 Discussion of Results . . . 82
4.7 Conclusions . . . 92

5 Time-dependent transport via a quantum shuttle **94**
5.1 Introduction . . . 94
5.2 Formulation . . . 95
5.3 The self-energy and the Green's function . . . 97
5.4 The Density matrix $\rho_{n,n'}(t,t)$ and the correlation function . . . 99
5.5 Time-dependent Current from lead α . . . 103
5.6 Average energy . . . 106
5.7 Discussion of Results . . . 106
5.8 Conclusions . . . 116

6 Summary and outlook **118**
6.1 Summary . . . 118
6.2 Technique modified . . . 122
6.3 Future outlook . . . 123

A Time dependent current **125**

B Self-energy **130**

Bibliography **135**

Acknowledgement

This research would not have been possible without the invaluable guidance given to me by my supervisor Prof. Angus MacKinnon over last three years. I am grateful to my supervisor for the enthusiastic commitment to this project, lot of freedom and very insightful advice and for continuous encouragement and unlimited patience due to which I completed this work. Thanks for being such a great advisor to work under!

I would like to pay my deep gratitude to Dr. Kashif Sabeeh for continuous discussions, encouragement and moral support. Truly, he is the person who has provided me with the motivation to achieve new educational heights.

It has been inspiring to be a part of the Condensed matter theory group at Imperial College London and I have benefitted from many interactions here. In particular I would like to thank Tanja Duric for her help in the solution of some of the numerical problems I encounter during these years. Thanks to rest of my officemates- Sam Genway, Wei Hsiung Wee, Kilian Frensch, Tristan West, Angela Demetriadou, Aimee G. Bailey, Chris P. Race - who have provided an increasingly fun atmosphere in which to carry out research work.

I would like to acknowledge the financial support from Pakistan Higher Education Commission (HEC) to carry out this work at Imperial College London. Thanks to them for providing me this great opportunity to improve my studies in such a world ranked institution.

This thesis was as much my effort as it was due to sacrifices and support of my parents and my wife. I would like to thank my parents for that they put our education

above every thing else. This future is the result of their blessings and love. My wife has been source of encouragement during my Ph.D. and has taken everything in her stride with a smile on her face. She has been a calming influence during the last year. I can not thank her enough for everything she has done and endured during writting-up to make things easier for me.

Finally, I want to pay my gratitude to my brothers, sisters, family and friends for their unconditional love, and encouragement they have shown me not only in the course of my studies, in my life as well. Even though I know that words are not enough to fully thank their love and moral support, I want to offer them my immeasurable love and thanks.

Muhammad Tahir,

Imperial College London

March 2010.

List of figures:

1.1 Schematic diagram of a NEMS device... 15

1.2 Schematic realization of a NEMS device... 16

1.3 Most recent realization of a NEMS device... 18

1.4 Schematic diagram of a quantum shuttle device... 20

2.1 Schematic diagram of the simple model... 30

3.1 Schematic diagram of constructing the simple NEMS model... 50

3.2 Differential conductance against applied bias and coupling strength... 65

3.3 Diagram showing differential conductance against gate voltage... 68

3.4 Average energy of the nanomechanical oscillator against applied voltage... 67

3.5 Average energy of the nanomechanical oscillator against gate voltage... 68

3.6 Diagram showing current-voltage characteristics... 69

3.7 Diagram showing shot noise... 70

3.8 Differential shot noise is shown in this diagram... 71

3.9 Fano factor as a function of Fermi energy... 72

4.1 Diagram showing empty, half full and occupied state of the dot... 84

4.2 Total average current with the rate of change of dot population... 84

4.3 The net average current against time ($2\pi/\omega$) and left Fermi energy... 85

4.4 Fourier/laplace transform of figure 4.3... 86

4.5 The net average current as a function of time with different coupling... 88

4.6 The net average current as a function of time with large tunneling rate... 88

4.7 Average energy of the nanomechanical oscillator for weak coupling...89

4.8 Average energy of the nanomechanical oscillator for strong coupling...89

4.9 Diagram showing comparison of quantum oscillator with the classical... 91

4.10 Fano factor as a function of time... 91

5.1 Shuttling dynamics in the net average current (electron per cycle)... 107

5.2 The net average current (electron per cycle)... 107

5.3 Diagram showing the tunneling dynamics of the average current... 109

5.4 Correlation function showing the shuttling and tunneling behavior... 110

5.5 Correlation function as a function of time and the left Fermi energy... 110

5.6 Total average current with the rate of change of dot population... 112

5.7 Average energy of the oscillator in the regime of shuttling... 113

5.8 Shuttling behavior of the average energy of the oscillator... 113

5.9 Tunneling behavior of the average energy of the oscillator... 115

Chapter 1

Introduction

In this chapter we give a short introduction to the world of a new generation of quantum devices, so-called nanoelectromechanical systems. We then focus our attention on a particular kind of device called a quantum shuttle. We briefly describe the basic operating regime and give an overview of the different theoretical models that have been proposed to describe the dynamics of nanoelectomechanical systems and particularly the quantum shuttle. We report on the two main realizations of nanoelectromechanical systems including its particular application as a shuttle device and close the chapter with an outline of the contents of this thesis.

1.1 Nanoelectromechanical systems

In recent years, much attention has been focussed on the concept and realization of nanoelectromechanical systems (NEMS)[1, 2, 3, 4, 5, 6, 7, 8] as a new generation of quantum electronic devices. NEMS are microelectromechanical systems (MEMS) not only scaled to

sub-micron but also with extreme surface to volume ratio, an unconventional characteristic range of operations and embedding circuitry. Microelectromechanical systems, for example, microscopic machines, sensors, computers, electronics, etc., with mechanical elements such as: beams, cantilevers, gears etc., are already being used in daily life, i.e., opening and closing valves, turning mirrors, regulating electric current or light flow. Whether we are dealing with MEMS or NEMS, the main system is a combination of electronic circuit and mechanical component called an electromechanical device. In MEMS, the electronic part was treated quantum mechanically and the mechanical part semi-classically/classically. Essentially the quantum behavior of the mechanical part of the system promises a revolution in the measurement of mass with ultra high sensitivity[9], extremely small displacements[10] and extremely weak forces[11], particularly at molecular level[12], such as machines, sensors, computers and electronics on the nano-scale. In MEMS electronic coherence, interference, and discrete levels are already observed, but shot noise is a problem, while in NEMS quantum effects become more interesting, especially with single phonon mode and single electron states as shown by the experiments[10, 13, 14, 15, 16].

A large number of new experimental techniques have been developed to fabricate and perform experiments with NEMS in the quantum regime; Examples of high-frequency mechanical nano-structures that have been produced are nano-scale resonators[10, 17], semiconductor quantum dots or single molecules[12, 16, 18, 19, 20, 21, 22], cantilevers[23, 24], vibrating crystal beams[10], and more recently graphene sheets[25] and carbon nanotubes[26, 27]. These devices are expected to open up a number of future applications including nanomechanical transport effects, signal processing which could be used in fundamental

research and perhaps even form the basis for new forms of mechanical computers. Many theoretical methods and models have been applied in order to account for the behavior of different types of NEMS and to make predictions and proposals for future experiments.

From a fundamental point of view, it is important to understand the interplay between the electronic transport and the nanomechanical motion of the oscillator quantum mechanically. The quantum transport through both single electronic levels in quantum dots and single molecules would allow us to study an ideal realization of a continuous variable quantum system. On this scale classical physics loses it validity, and we enter the exciting world of quantum mechanics.

1.2 Quantum dynamics

Quantum nano-structures are likely to become primary components of future electronic devices. Presently the majority of these structures, such as nanomechanical resonators, semiconductor quantum dots, single molecules, single electron transistors, and similar low dimensional structures, exist as prototypes in research laboratories or are just being contemplated[10, 13, 14, 16, 17]. These devices can be interesting in their own right as nontrivial dynamical systems with small inertial mass. Given the small mass of the nanomechanical oscillator and the strong electrostatic coupling, individual electrons travelling through the device can give a significant 'kick' to the nanomechanical oscillator at the nano scale. In turn, the motion of the oscillator will influence the electron current and so on. At cryogenic temperatures, certain electronic devices can behave in a quantum coherent fashion, existing in a quantum superposition of different charge states as electrons

are transmitted through the device. Interacting with such a device, the nanomechanical oscillator's centre-of-mass may be driven into a quantum state, such as a superposition of separated position states. The quantum mechanical nature of the coupled nanoelectromechanical system will manifest itself in certain signatures of the measured current and shot noise. Nanoelectromechanical oscillators comprise up to about 100 million atoms, so that by most standards, such quantum effects would be deemed macroscopic. It is important to appreciate that we are here referring to quantum effects in NEMS devices that possess both many electronic and mechanical degrees of freedom. These devices interact strongly with the surrounding environment consisting of photons, phonons, fluctuating defects in both the mechanical oscillator and the electronic device as well. The experimental and theoretical investigation of such systems will lead to a deeper understanding of how classical dynamics emerges as an approximation to quantum dynamics.

The nanoelectromechanical oscillator component has been found to behave classically, as might be expected in the first generation of experimental work to probe the dynamics of NEMS. These experiments are not yet quite refined enough to observe quantum interference effects that are washed-out by the resonator's environment. Despite this, the classical dynamics of NEMS has been found to be nontrivial and worthy of investigation. One line of investigation is to identify common features in the classical dynamics of the various NEMS devices, so as to bring some degree of coherence to the field. In this hallmark of NEMS theory and experiments, the electronic device behaves effectively as a thermal bath[28, 29] under conditions of weak coupling and wide separation of nanomechanical and electronic dynamical time-scales. In these limits, the nanomechanical oscillator undergoes

a thermal Brownian motion, characterized by a damping constant and an effective temperature which are determined by the electronic parameters of the device. The fact that the electronic device can be effectively replaced by a thermal bath is at first sight rather surprising, given that the voltage-driven electron current flowing through the device is a far-from-equilibrium, many electron state. The use of well-understood equilibrium concepts in the construction of theoretical models of less-well-understood non-equilibrium systems goes back to the early days of statistical mechanics and continues to find broad applications.

A particular application of a NEMS device is a quantum shuttle[16, 30, 31, 32], which may increase the understanding of quantum transport properties of NEMS and related quantum phenomena in nanoscopic systems. The characteristic component that gives the name to these devices is an oscillating quantum dot of nanometer size that transfer electrons one-by-one between a source and a drain lead. This device is a close analog of an electomechanical bell in which a metallic ball is placed between two parallel plate capacitor. When a high bias is applied across the plates, the ball starts oscillating between the source and drain. The oscillations in the bell are sustained by the external bias that pumps energy into the quantum mechanical oscillator and the transfer of charge is governed by tunneling events, the tunneling amplitude being modulated by the position of the oscillating mechanical system.

Different models for shuttle devices have been proposed in the literature since the first exciting work[30] of Gorelik, et al., in which, the investigation of the quantization of charge in the strong Coulomb blockade regime has been discussed. This system consists of a movable, micro-size metallic grain spatially confined in a harmonic potential between

source and drain leads. In the strong Coulomb blockade regime only a single excess electron at a time is allowed to occupy the grain. When a sufficiently high bias is applied between the leads, a single electron may tunnel onto the grain, and due to the electrostatic field between the leads, the charged grain is driven towards the drain, where the electron tunnels off. Due to the harmonic potential the uncharged grain is forced back towards the source and the process is repeated.

The mechanical part of the shuttle device has been treated classically in the Gorelik model including a damped oscillator and assuming incoherent electron tunneling process. The essential feature of the nanometer scale realization is that the quantity which is transferred in unit cycle needs the quantum mechanical description. In the quantum transport properties of a quantum shuttle; the quantized current can be determined by the frequency of the quantum mechanical oscillator, the interplay between the time scales of the electronic and mechanical degrees of freedom, and the suppression of stochastic tunneling events due to matching of the Fermionic and oscillator properties.

1.3 Experimental realization

An experimental realization will lead us to a deeper understanding of NEMS: how NEMS are designed and operated at such a very small scale of both the components, electrical and mechanical. Fig 1.1 shows the first experimental realization[14] of NEMS aimed at confirming the validity of the uncertainty principle[33] at the zero-point of the system.

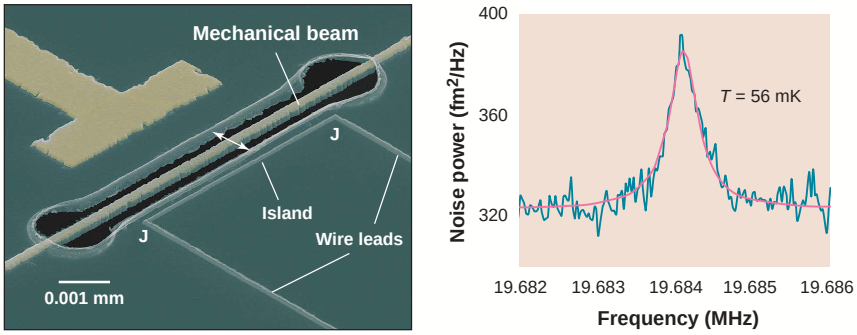


Figure 1.1: (Left) Electron micrograph of the device showing the mechanical beam and single-electron transistor wire leads and island. Electrons tunnel one at a time across electrically insulating junctions located at the corners (J). (Right) frequency spectrum of the thermal Brownian motion of the mechanical beam as measured by the single-electron transistor. The temperature of the beam inferred from the spectrum is 56 mK. This is the lowest measured beam temperature achieved in the experiment. The beam displacement units are in femtometers (1 fm = 10^{-15} m). M.D.LaHaye et al.,Science 304,74 (2004).

This is a Scanning Electron Mircoscope (SEM) micrograph showing the mechanical beam, SET, source-drain wire leads and the island. Due to the small diameter of the island, it has small capacitance and thus its charging energy exceeds the thermal energy. Due to coulomb blockade electrons tunnel one by one across the electrically insulating junctions located at the corners (J). The beam and the surrounding substrate are fashioned from a silicon nitride (SiN) membrane, a material that is commonly used for NEMS now-a-days because of its high strength to mass density ratio. The beam is coated with a layer of gold, forming the gate electrode. The SET island and the leads are made from aluminium. The mechanical resonator is located 600 nanometer away from the island. The fixed gate electrode at the upper left is used for displacement actuation. Fig 1.1 (b) shows that the single electron transistor (SET) detected noise spectrum converted to displacement

squared. Due to the thermal Brownian motion of the mechanical beam, a Lorentzian peak is clearly seen above the Amplifier noise background. For the experiment under discussion, the measured fundamental frequency that has been achieved is around 20 MHz at 56 mK. The observed level of position sensitivity is approaching low quantum numbers, which opens the possibility for a wealth of nanoelectromechanical experiments at millikelvin temperature: observation of nanoscopic fluctuations in nanomechanics, quantum limited feedback cooling and quantum squeezing. By improving the thermal characteristics of the experiment or by increasing the frequency of the mechanical mode, one can expect to approach the quantum ground state motion of the system.

Similar to the LaHaye et al. experiment, is an experiment[10] performed by Knobel et al. to explore and discuss the zero point properties of NEMS. This experiment involves the operation of the SET displacement detector as shown below in Fig 1.2.

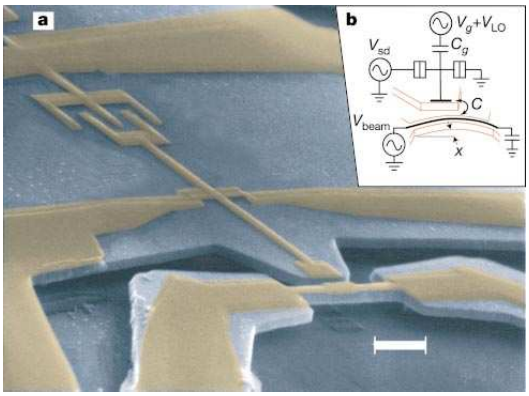


Figure 1.2: The device used in the experiment by R. G. Knobel and A. N. Cleland, Nature 424, 291 (2003). a) Scanning electron micrograph of the device, showing the doubly clamped GaAs beam, and the aluminum electrodes (coloured) forming the single electron transistor and beam electrode. Scalebar,1mm. The Al/AlOx/Al tunnel junctions have approximately $50 \times 50\, nm^2$ overlap. b) A schematic of the mechanical and electrical operation of the device.

In this experimental set up, they use a vibrating beam of crystal that is only 3 micrometers long, extremely sensitive to the detector, which is capable of detecting displacements as small as one thousandth of a nanometer or one hundredth of the size of a single atom. The beam may seem tiny by the standards of daily life but its mass is equivalent to that of about 100 million atoms. Demonstration of the uncertainty principle[33] for such a system would be a very striking manifestation of quantum mechanics well outside its traditional microscopic domain. The measured displacement sensitivity in this experiment is $2\text{x}10^{-15}$ $\text{mHz}^{-1/2}$, a sensitivity of 100, away from the quantum limit for this nanomechanical oscillator [13, 14, 15]. Fig. 1.2(b) is a false-coloured SEM micrograph showing the suspended, doubly clamped beam and SET. The substrate and the beam are fashioned from GaAs, and the SET and beam gate electrodes are thin layers of aluminium, with aluminium oxide forming the tunnel barriers. The beam is located 0.25 micrometer away from the island electrodes. The measured fundamental frequency for in plane motion is about 116 MHz at a temperature of 30 mK.

Beyond the above mentioned experiments, more recently a detector has been designed to approach the nano-scale regime of the mechanical oscillator as shown in Fig. 1.3.

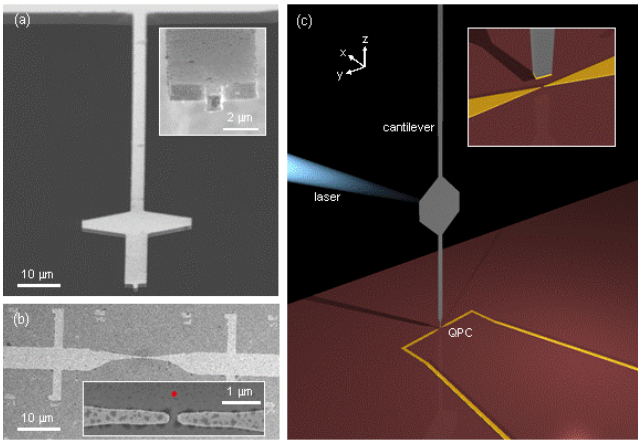


Figure 1.3: Components and geometry of the experimet by Poggio et al., Nature physics 4 635 (2008). a) Scaled schematic diagram of the experimental set-up. A close-up view of the QPC—with the cantilever in close proximity—is shown in the inset. The laser beam is part of the low-power interferometer used to calibrate displacement measurements made by the QPC. b) Scanning electron micrograph of the cantilever and its Au-coated tip (inset). c) Scanning electron micrograph of the QPC with a high-resolution view of the active region (inset). The red dot indicates the position of the cantilever tip during the experiment.

In this experiment[24], a quantum point contact is used as a sensitive displacement detector. This device is capable of sensing the low-temperature thermal motion of a nearby mechanical cantilever. An advantage of this approach has been claimed to include the versatility due to its off-board design, and with further development, capability to achieve quantum limited displacement detection. This experiment shows, how simply bringing a mechanical oscillator in close proximity to an off-board quantum point contact enables sensitive displacement measurements. In manipulating the device, the detector achieved a resolution of $10^{-12}\mathrm{Hz}^{-1/2}$, which is comparable to that achieved by optical interferometry on resonators of similar size. The fundamental advantage of this detector is that it can be applied to the measurements of oscillations with dimensions smaller than the optical

diffraction limit. In addition, by virtue of its off-board design, this device can be used in conjunction with sensitive cantilevers in a variety of force sensing applications including magnetic force microscopy. Although the resolution of this point contact device is limited by its imperfections, transducers of this type should have the properties required to reach the quantum limit of continuous position detection.

In addition to a simple NEMS device, an experimental realization of NEMS devices as a charge shuttle has been reported. A mesoscopic shuttle system similar in some respects to that proposed by Gorelik et al. has been experimentally realized by Blick et al[34]. This situation has been investigated both in the incoherent and in the quantum case. The shuttling phenomenon has been observed in Parks et al., experiment[16], where a C_{60} molecule is oscillating between two leads. In this experiment, Parks et al., have observed the quantization of current for various applied voltages, which exhibits step like features within the current-voltage (I-V) curve. The molecular shuttle between the electrodes in this experimental setup has been done at low amplitude and high frequency but provided a key evidence of the involvement of phonon levels in changing the current properties. This quantized behavior in the conductance characteristics of NEMS devices has been observed in a similar experiment[35]. Another method to drive the oscillations is to use an external AC electric field acting on a cantilever (Erbe et al[23].,), where the amplitude can be tuned independently of the source-drain voltage bias.

More recently, in an experiment[31], a 20 nm gold nanoparticle is embedded in the gap between two electrodes and attached to them through a monolayer of flexible organic molecules as shown in Fig. 1.4.

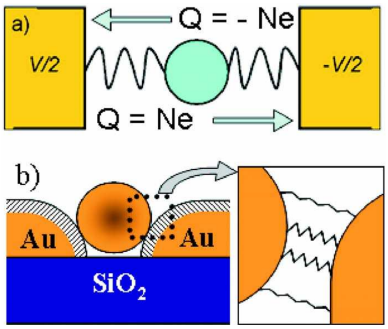


Figure 1.4: a) Theoretical model of an idealized shuttle junction and illustration of the shuttling process (Gorelik et al., PRL 80, 4526 (1998)) and b) experimental realization of the shuttle junction. The device consists of a 20 nm gold nanoparticle attached to two gold electrodes through monolayers of octanedithiol molecules serving as springs. The inset in b shows how the nanoparticle is attached to the electrode through a monolayer of elastic molecules; due to the curvature of the particle and electrode, some molecules are over stretched within the gap. [31]

The nanoparticle is set in motion by applying a voltage bias, which in turn transfers electrons from one electrode to the other. The device was built on the top of a silicon wafer coated with a $\sim$1 μm SiO_2 layer. This device is fabricated using electron beam-lithography in which 30 nm thick gold nanoelectrodes were separated by a gap of 10-20 nm. The nanoelectrodes are initially covered with a monolayer of 1, 8 octanedithiol having 1.2 nm thickness. The 20-nm diameter gold nanoparticle is absorbed by immersion of the electrode assembly into aqueous gold solution. The measured I-V characteristics of this device has been done at room temperature in a shielded dry box to protect the samples from moisture and to decrease electromagnetic noise. This experiment is very close to the original proposal by Gorelik, et al.

There are different models for the discussion and understanding the dynamical

properties of the electromechanical coupling using semiconductor fabrication technology. In these devices the transfer of charge is performed by a flexible semiconductor element such as a silicon beam resonator, cantilever, or silicon nanopillars[36]. The fundamental elements of these devices is large, around 100 nm, usually required an additional ac voltage to drive the oscillations of the mechanical element at its resonant frequency. The transport phenomena in these experiments has been described and discussed classically but needs a quantum mechanical description. A theory beyond these cases is required in order to further refine experiments on NEMS devices and especially the quantum shuttle based devices. For this reason, a first complete analytical and qualitative implementation of the quantum transport properties of a simple NEMS device and its application as a quantum shuttle device is considered in this thesis.

1.4 Theoretical implementation for quantum behaviour in nano-mechanical systems

In general, there are two different theoretical formulations that can be used to study the quantum transport in nanoscopic systems under voltage bias. Firstly, a generalized quantum master equation approach[28, 32, 37, 38, 39, 40, 41, 42, 43, 44] and secondly, the nonequilibrium Green's function formulation[45, 46, 47]. The former leads to a simple rate equation, where the coupling between the dot and the leads is considered as a weak perturbation and the electron-phonon interaction is also considered very weak. In the latter case one can consider strong leads to system and electron-phonon coupling. The nonequilibrium Green's function technique is able to deal with a very broad variety of

physical situations related to quantum transport at molecular levels[48, 49]. It can deal with strong non-equilibrium situations and very small to very large applied bias. In the early seventies, the nonequilibrium Green's function approach was applied to mesoscopic transport[50, 51, 52] by Caroli et al., where they were mainly interested in inelastic transport effects in tunneling through oxide barriers. This approach was formulated in an elegant way[53, 54, 55] by Mier et al, where they have shown an exact time dependent expression for the non-equilibrium current through mesoscopic systems. In this model an interacting and non-interacting mesoscopic system was placed between two large semi-infinite leads.

In most of the theoretical work on NEMS devices since the original proposal, the mechanical degree of freedom has been described classically/semiclassically[28, 29] or quantum mechanically[32, 37, 38, 56, 57] using the quantum master or rate equation approach. In the original proposal, the mechanical part was also treated classically, including the damped oscillator, and assuming an incoherent electron tunneling process. This approach is based on a perturbation, weak coupling and large applied bias approximations, whereas the Keldysh nonequilibrium Green's function formulation can treat the system-leads and electron-phonon coupling with strong interactions[58] for both small and large applied bias voltage. Moreover, the theories of the Jauho group[37, 38, 39], Armour[28], and Martin[56, 57] fail to explain the low bias regime. The transport properties have been described and discussed semi-classically/classically but need a complete quantum mechanical description. A theory beyond these cases is required in order to further refine experiments to investigate quantum transport properties of NEMS devices. For this reason, a first complete analytical and qualitative description of the quantum transport properties of

a simple NEMS and its application as a quantum shuttle device is performed and discussed in detail in this thesis.

We explain the technical details of implementing the Keldysh nonequilibrium Green's function formalism. The approach adopted here is somewhat pedagogical, and there are many more heuristic or intuitive explanations of this formalism in the literature. We do not go into great detail as to the nuts and bolts implementation of this formalism, as the main thrust of the thesis is to build upon this formalism in calculating quantum transport properties of NEMS devices. With these caveats, we proceed.

1.5 This thesis

This thesis contains the description and analysis of the dynamics of a quantum nanomechanical oscillator coupled to a resonant tunnel junction and its realizations as a quantum shuttle device. The models we consider describe both the mechanical and electrical degrees of freedom quantum mechanically; Firstly, a single electron transistor coupled to a quantum mechanical oscillator we extended an existing classical model proposed by Armour. Secondly, we report a first complete quantum mechanical analysis of a shuttle model proposed by Gorelik et al. To study the quantum transport properties of nanoelectromechanical systems, we have used a device consisting of a single electron transistor (a resonant tunnel junction) coupled to quantum mechanical oscillator at zero temperature. The emphasis has been to determine the quantum mechanical transport properties of a resonant tunnel junction when it measures the position of a nanomechanical oscillator. In the following we outline the contents of the thesis:

Chapter 2 reviews the exotic and novel properties of Keldysh's non-equilibrium Green's function technique in order to describes the quantum transport properties of NEMS beyond the classical and far from equilibrium. In this chapter we derive a relation for the dot population, which is equivalent to Keldysh non-equilibrium Green's function result. In the same chapter we also derive a general expression for the current.

In chapter 3 we introduce a new quantum mechanical description for the mechanical object (oscillator), which is beyond the existing experiments. Due to different coupling strength we treat the mechanical and electrical object with a nonpertubative approach. This chapter is dedicated to the application of the tools investigated in chapter 2. We have chosen to analyze the single electron transport properties of the simple NEMS model: differential conductance, average energy transferred from electrical to quantum mechanical degree of freedom, current, shot noise and the corresponding Fano factor.

Chapter 4 reports on the time dependent transport properties, including transient and steady state dynamics, using the tools investigated in chapter 2: Net current through the system, current density, equation of continuity, average energy, and Fano factor.

In chapter 5 we introduce the time dependent application of the tools investigated in chapter 2 to analyze the transport properties of a quantum shuttle device.

We give a summary of the results obtained in this thesis in chapter 6 and give an outlook for the future tasks and challenges.

Chapter 2

Green's function theory

2.1 Introduction

This chapter contains the derivation of the general time-independent and time-dependent non-equilibrium Green's function formalism[45, 46, 47, 53, 54, 55] that describes the quantum dynamics in an exact way. We start with the introduction of the time-independent single particle Green's function and then focus our attention on perturbation theory to derive a relation for the standard Dyson's Green's function. We introduce a general model: two leads, right (R) and left (L) and a single molecule such as a quantum dot. We then briefly describe the basic calculations of the time-independent retarded and advanced Green's function and the corresponding self-energy for this model. We move to introduce Langrethe's theorem and apply it to derive the time-independent lesser Green's function or the density matrix using the standard Dyson's equation. The expression of the density matrix is equivalent to the Keldysh non-equilibrium Green's function result. We derive a general time-independent expression for the current. We then move to review

the novel time-dependent Green's function and then apply it to the same model: a single quantum dot connected with two leads. Here we derive a relation for the time-dependent retarded and advanced Green's function and then the corresponding self-energy for the same model. We then derive a general equation for the time-dependent density matrix and finish the chapter with the derivation of the general expression for the time-dependent current.

2.2 Single particle Green's function

In condensed matter physics one is typically concerned about calculating physical observable from a microscopic description of the system under consideration. Such microscopic models are usually defined by writing the Hamiltonian operator, together with appropriate boundary conditions. The basic problem is the solution of the one-particle Schrödinger equation

$$(E - H)\Psi = 0 \tag{2.1}$$

where H is a single-particle Hamiltonian, E is the corresponding energy eigenvalue with the eigenstate Ψ. Of course solving this wave equation may be difficult, if possible at all. In many particle problems the systems are usually described by Hamiltonians which can't be solved exactly, and one must rely on perturbation methods. In these situations the second quantization operators and Green's functions prove to be very important techniques.

Various formulations of Green's function theory exist. For instance, in equilibrium theory there is both a zero-temperature as well as a finite-temperature (Matsubara) formalism. Here we will focus on the formulation of the more general single-particle non-

equilibrium zero-temperature theory which also applies to equilibrium as a special case. Approaches based on the non-equilibrium Green's functions (NEGF), that assume open boundaries, have been successfully utilized in the treatment of mesoscopic devices. However, the description of far-from-equilibrium situations in devices, in which the state achieved cannot be related uniquely to the initial state, poses more constraints in principle on the application of the NEGF formulation. Namely, it may be impossible to relate the far-from-equilibrium expectation values with those for the initial state, which may be, e.g., thermal equilibrium. The real power of the formulation presented here lies in providing a general approach for describing quantum behavior in the presence of interactions.

To begin, we introduce the single-particle Green's function as discussed in many standard treatments of the subject. The Hermitian operator H given in equation (2.1) obeys the following eigenvalue equation,

$$H\left|\varphi_n\right\rangle = E_n\left|\varphi_n\right\rangle, \tag{2.2}$$

where the eigenfunctions $|\varphi_n\rangle$ usually form a complete set of states:

$$completeness: \sum_n{}' \left|\varphi_n\right\rangle\left\langle\varphi_n\right|, \qquad orthonormality: \left\langle\varphi_n\right|\left.\varphi_m\right\rangle = \delta_{nm}, \tag{2.3}$$

where the symbol $\sum_n{}' = \sum_n + \int dn$ denotes that the eigenstates include both a summation over discrete states as well as integration over the continuous part of the spectrum. All eigenvalues are real due to the Hermiticity of H.

According to the above discussion of the Schrödinger equation, we may define the corresponding Green's function (operator) as

$$[E - H]G(E) = 1, \tag{2.4}$$

where the Green's function is subject to the same boundary conditions as the wave function Ψ. A formal solution of equation (2.4) may be written as

$$G(E) = [E - H]^{-1}, \tag{2.5}$$

which is defined everywhere except at the singularity, $E = E_n$.

2.3 Green's function and Perturbation Theory

In the previous section we restricted the discussion to the evaluation of the unperturbed Green's function (GF) formalism. This method is convenient because much information about the system can be extracted from the knowledge of the GF. In nonequilibrium theory we will in particular be working with the time-independent single-particle Green's function. The one-particle Hamiltonian can be separated into an unperturbed part H_0, and a perturbation ΔH as

$$H = H_0 + \Delta H \tag{2.6}$$

The eigenvalues and eigenfunctions of H_0 can be easily obtained as in the previous section. The question here is to determine the eigenvalues and eigenfunctions of the total Hamiltonian (H). It is not feasible to evaluate the total Green's function, $G(E)$ at once. Instead, one divides the Green's functions $g(E)$ and $G(E)$ corresponding to H_0 and H, respectively, as

$$g(E) = [E - H_0]^{-1} \tag{2.7}$$

and

$$G(E) = [E - H]^{-1}. \tag{2.8}$$

With the help of equation (2.1), we can now write equation (2.8) as

$$[E - H_0 - \Delta H]G(E) = 1 \tag{2.9}$$

$$[E - H_0]G(E) = 1 + \Delta H G(E) \tag{2.10}$$

$$G(E) = [E - H_0]^{-1}\{1 + \Delta H G(E)\} \tag{2.11}$$

$$G(E) = g(E) + g(E)\Delta H G(E), \tag{2.12}$$

which is the standard Dyson's equation with a single particle perturbation.

2.4 General model formulation: Time-independent

In the present case, we have two leads, right (R) and left (L) and a single molecule such as a quantum dot as shown in figure 2.1. In the tight-binding representation, the Hamiltonian of our simple system is

Figure 2.1: A quantum dot or a single molecule attached to semi-infinite leads.

$$H = H_0 + \Delta H \tag{2.13}$$

$$H_0 = \epsilon_0 c_0^\dagger c_0 + H_{\text{leads}}, \qquad \Delta H = H_{leads-dot} \tag{2.14}$$

where $\alpha = L$ or R stands for each lead and ϵ_0 is the single energy level of electrons on the dot with $c_0^\dagger, c_0$ the corresponding creation and annihilation operators. The remaining elements of the Hamiltonian are

$$H_{\text{leads}} = \sum_{j,\alpha} \epsilon_{j,\alpha} c_{j,\alpha}^\dagger c_{j,\alpha}, \tag{2.15}$$

$$H_{\text{leads-dot}} = \frac{1}{\sqrt{N}} \sum_{j,\alpha} V_\alpha \left(c_{j,\alpha}^\dagger c_0 + c_0^\dagger c_{j,\alpha} \right), \tag{2.16}$$

where N is the total number of states in the lead, j represents the channels in one of the leads $\alpha = L, R$. For the second lead the Hamiltonian can be written in the same way.

Now the Green's function on the dot due to interaction with the leads may be derived using equation (2.12). The final result is written as

$$G_{00}(E) = g_{00}(E) + \sum_{\alpha} g_{00}(E) \Delta H_{0,\alpha} G_{\alpha,0}(E), \tag{2.17}$$

where the unperturbed Green's function on the dot is g_{00} while the perturbed one on the dot due to the lead (α) is $G_{00}(E)$. With the help of

$$G_{\alpha,0}(E) = g_{\alpha,0}(E) + g_{\alpha,\alpha}(E)\Delta H_{\alpha,0}G_{00}(E)$$

one can write equation (2.17) as

$$G_{00}(E) = g_{00}(E) + \sum_{\alpha} g_{00}(E)\Delta H_{0,\alpha}\{g_{\alpha,0}(E) + g_{\alpha,\alpha}(E)\Delta H_{\alpha,0}G_{00}(E)\}. \tag{2.18}$$

Using the fact that $g_{\alpha,0}(E)$ is zero as the two sites are uncoupled, equation (2.18) is simplified to

$$G_{00}(E) = g_{00}(E) + \sum_{\alpha} g_{00}(E)\Delta H_{0,\alpha}g_{\alpha,\alpha}(E)\Delta H_{\alpha,0}G_{00}(E). \tag{2.19}$$

Using $\Sigma_{00} = \sum_{\alpha} \Delta H_{0,\alpha}g_{\alpha,\alpha}(E)\Delta H_{\alpha,0}$, the self-energy calculated in the next section, the expression (2.19) may be written as

$$G_{00}(E) = g_{00}(E) + g_{00}(E)\Sigma_{00}G_{00}(E), \tag{2.20}$$

which is similar to the standard Dyson's Green's function expression derived in the last section.

2.4.1 Retarded and advanced Green's function

The retarded and advanced Green's function differ by time order: the retarded differs from zero only for times $t > t'$, which can be used to calculate the response at time t to earlier perturbation of the system at time t' while the advanced is only finite for $t < t'$.

These two functions obey the same inhomogeneous differential equation. For the present discussion of the time independent case this implies that the energy (E) has small positive imaginary part for the retarded Green's function while negative for the advanced one.

With the help of equation (2.20), the retarded (advanced) Green's function may be written as

$$G_{00}^{r(a)}(E) = g_{00}^{r(a)}(E) + g_{00}^{r(a)}(E)\Sigma_{00}^{r(a)}G_{00}^{r(a)}(E) \tag{2.21}$$

$$[1 - g_{00}^{r(a)}(E)\Sigma_{00}^{r(a)}]G_{00}^{r(a)}(E) = g_{00}^{r(a)}(E) \tag{2.22}$$

$$G_{00}^{r(a)}(E) = \frac{g_{00}^{r(a)}}{[1 - g_{00}^{r(a)}(E)\Sigma_{00}^{r(a)}]} \tag{2.23}$$

$$G_{00}^{r(a)}(E) = \frac{1}{[[g_{00}^{r(a)}(E)]^{-1} - \Sigma_{00}^{r(a)}]}, \tag{2.24}$$

Hence, the final result is written as

$$G_{00}^{r(a)}(E) = [E - E_0 - \Sigma_{00}^{r(a)}]^{-1} \tag{2.25}$$

The $G_{00}^{r(a)}(E)$ have poles in one half-plane and are sufficient ingredients for calculating the physical response of the system. Information about the spectral properties, density of states and scattering rates are contained in these functions. $\Sigma_{00}^{r(a)}$ behaves as an exact contribution to the energy of the dot. Hence, the term "self-energy".

2.4.2 The Self-energy

The self-energy represents the contribution to the dot energy, due to interactions between the dot and the leads it is coupled to. We use the wide-band approximation where the self-energy of the dot due to each lead is considered to be energy independent. The self-energy defined in the previous section can be calculated in the following way

$$\Sigma^r_{00} = \Delta H_{0,\alpha} g^r_{\alpha,\alpha}(E) \Delta H_{\alpha,0}, \tag{2.26}$$

where

$$\begin{aligned} g^r_{\alpha,\alpha}(E) &= \frac{1}{N}\sum_j g^r_{\alpha,j}(E) \\ &= \frac{1}{N}\int_{-\infty}^{+\infty} N \frac{n_\alpha d\varepsilon_\alpha}{E-\varepsilon_\alpha} \end{aligned} \tag{2.27}$$

where $g^r_{\alpha,\alpha}(E)$is the uncoupled Green's function in the leads, $\sum_j = \int_{-\infty}^{+\infty} N n_\alpha d\varepsilon_\alpha$, j stands for every channel in each lead, and n_α is the density of states in lead α. The retarded self-energy can be rewritten as

$$\Sigma^r_{00} = \Delta H_{0,\alpha} \frac{1}{N}\int_{-\infty}^{+\infty} N \frac{n_\alpha d\varepsilon_\alpha}{E-\varepsilon_\alpha} \Delta H_{\alpha,0}, \tag{2.28}$$

which can be simplified as

$$\begin{aligned}\Sigma_{00}^{r} &= |V_{0,\alpha}|^2 \int_{-\infty}^{+\infty} \frac{n_\alpha d\varepsilon_\alpha}{E-\varepsilon_\alpha} \\ &= -|V_{0,\alpha}|^2 n_\alpha \int_{-\infty}^{+\infty} \frac{d\varepsilon_\alpha}{\varepsilon_\alpha - E} \\ &= -|V_{0,\alpha}|^2 n_\alpha \times (\pi i) \\ &= \frac{-i\Gamma_\alpha}{2},\end{aligned} \tag{2.29}$$

where $\Gamma_\alpha = 2\pi |V_{0,\alpha}|^2 n_\alpha$, and $\Sigma_\alpha^a = (\Sigma_\alpha^r)^* = \frac{i\Gamma_\alpha}{2}$ and αrepresents the L or R leads.

2.4.3 Langreth's theorem

In many-body physics, nonequilibrium Green's functions are represented in time contour while we are concerned with the time independent theory. In this case Langrethe's theorem can be applied in the same way. The general expression for a lesser function is given by

$$A^{<} = f(\varepsilon)(A^a - A^r), \tag{2.30}$$

where $f(\varepsilon)$ is the Ferm-Dirac distribution function, A^a is the advanced function and A^r represents the retarded function.

If we consider $A = BC$, then equation (2.30) can be rewritten as

$$
\begin{aligned}
(BC)^{<} &= f(\varepsilon)((BC)^{a} - (BC)^{r}) \\
&= f(\varepsilon)(BC)^{a} - f(\varepsilon)(BC)^{r} + f(\varepsilon)B^{r}C^{a} - f(\varepsilon)B^{r}C^{a} \\
&= B^{r}f(\varepsilon)(C^{a} - C^{r}) + f(\varepsilon)(B^{a} - B^{r})C^{a} \\
&= B^{r}C^{<} + B^{<}C^{a}
\end{aligned} \tag{2.31}
$$

Similarly, if $D = ABC$ then following the same approach the result for the $D^{<}$ is given as

$$
D^{<} = A^{r}B^{r}C^{<} + A^{r}B^{<}C^{a} + A^{<}B^{a}C^{a} \tag{2.32}
$$

2.4.4 Dyson's equation and the Lesser Green's function

The standard Dyson's equation derived in section 2.4 may be rewritten as

$$
G_{00}^{r(a)}(E) = g_{00}^{r(a)}(E) + g_{00}^{r(a)}(E)\Sigma_{00}^{r(a)}G_{00}^{r(a)}(E), \tag{2.33}
$$

where $G_{00}^{r}(E)$ and $G_{00}^{a}(E)$ are the retarded and advanced Green's functions respectively and are discussed in the next section.

The relation for the $G_{00}^{<}(E)$ on the dot, is

$$
G_{00}^{<}(E) = f(\varepsilon)(G_{00}^{a}(E) - G_{00}^{r}(E)), \tag{2.34}
$$

Using the expressions for the retarded and the advanced Green's function derived in equation (2.33), equation (2.34) may be written as

$$
G_{00}^{<}(E) = f(\varepsilon)\{g_{00}^{a}(E) + g_{00}^{a}(E)\Sigma_{00}^{a}G_{00}^{a}(E) - g_{00}^{r}(E) - g_{00}^{r}(E)\Sigma_{00}^{r}G_{00}^{r}(E)\} \tag{2.35}
$$

Using the Langreth's identity derived in the last section, equation (2.35) becomes

$$G^<_{00}(E) = g^<_{00}(E) + g^r_{00}(E)\Sigma^r_{00}G^<_{00}(E) + g^r_{00}(E)\Sigma^<_{00}G^a_{00}(E) + g^<_{00}(E)\Sigma^a_{00}G^a_{00}(E), \quad (2.36)$$

which can be rewritten as

$$\{1 - g^r_{00}(E)\Sigma^r_{00}\}G^<_{00}(E) = g^<_{00}(E) + g^r_{00}(E)\Sigma^<_{00}G^a_{00}(E) + g^<_{00}(E)\Sigma^a_{00}G^a_{00}(E) \quad (2.37)$$

$$\{1 - g^r_{00}(E)\Sigma^r_{00}\}G^<_{00}(E) = g^<_{00}(E)\{1 + \Sigma^a_{00}G^a_{00}(E)\} + g^r_{00}(E)\Sigma^<_{00}G^a_{00}(E) \quad (2.38)$$

$$G^<_{00}(E) = \{1 - g^r_{00}(E)\Sigma^r_{00}\}^{-1}[g^<_{00}(E)\{1 + \Sigma^a_{00}G^a_{00}(E)\} + g^r_{00}(E)\Sigma^<_{00}G^a_{00}(E)] \quad (2.39)$$

$$G^<_{00}(E) = \{1 - g^r_{00}(E)\Sigma^r_{00}\}^{-1}g^<_{00}(E)\{1 + \Sigma^a_{00}G^a_{00}(E)\} + \{1 - g^r_{00}(E)\Sigma^r_{00}\}^{-1}g^r_{00}(E)\Sigma^<_{00}G^a_{00}(E)] \quad (2.40)$$

now equation (2.40) can be further simplified by using the following relations $\{1 - g^r_{00}(E)\Sigma^r_{00}\}^{-1} = \{1 + G^r_{00}(E)\Sigma^r_{00}\}$, and $\{1 - g^r_{00}(E)\Sigma^r_{00}\}^{-1}g^r_{00}(E) = G^r_{00}(E)$. Hence, the final result is

$$G^<_{00}(E) = \{1 + G^r_{00}(E)\Sigma^r_{00}\}g^<_{00}(E)\{1 + \Sigma^a_{00}G^a_{00}(E)\} + G^r_{00}(E)\Sigma^<_{00}G^a_{00}(E). \quad (2.41)$$

For the unperturbed system, we may assume that the dot is initially empty due to which $g^<_{00}(E)$ is zero. Thus equation (2.41) can be written as

$$G_{00}^{<}(E) = G_{00}^{r}(E)\Sigma_{00}^{<}G_{00}^{a}(E), \tag{2.42}$$

This is equivalent to Keldysh's nonequilibrium Green's function result and is related to the density matrix by the following relation

$$\rho_{00} = -i\int \frac{dE}{2\pi}G_{00}^{<}(E), \tag{2.43}$$

where this is the central result of this formal development.

The lesser Green's function is called the particle propagator and the greater is called the hole propagator in which the order of the operators (creation & annihilation) is reversed. With the help of the Green's function identity ($G^r(E)-G^a(E) = G^>(E)-G^<(E)$), the greater Green's function can also be derived in the same way as

$$G^{>}(E) = -i[1 - f(\varepsilon)](G^a(E) - G^r(E)), \tag{2.44}$$

The lesser and the greater Green's functions are directly linked to physical observable and properties of the system such as dot population and current.

The lesser self-energy may be written as

$$\Sigma_{\alpha}^{<} = f(\varepsilon)[\Sigma_{\alpha}^{a} - \Sigma_{\alpha}^{r}] \tag{2.45}$$

$$\Sigma_{\alpha}^{<} = i\Gamma_{\alpha}f(\varepsilon), \tag{2.46}$$

where αrepresents the L or R leads. Similarly one can calculate the greater self-energy as

$$\Sigma_{\alpha}^{>} = -i\Gamma_{\alpha}[1 - f(\varepsilon)]. \tag{2.47}$$

2.4.5 The Current from lead α

The particle current I_α into the interacting region from the lead is given by the expectation value of the current operator, $I_\alpha = Tr(\rho\hat{I}_\alpha)$ [46, 47, 53, 54, 55], where

$$\hat{I}_\alpha = \frac{ie}{\hbar}\sum_j \{V_{0\alpha}c_0^\dagger c_{\alpha j} - c_{\alpha j}^\dagger c_0 V_{\alpha 0}\} \tag{2.48}$$

which can be written in terms of the lesser Green's function and the hopping between the dot and the leads as

$$I_\alpha = \frac{e}{\hbar}\int \frac{dE}{2\pi}\{G_{0,\alpha}^{<}(E)V_{\alpha,0} - V_{0,\alpha}G_{\alpha,0}^{<}(E)\}, \tag{2.49}$$

where in equation (2.49) we have the following relations

$$G_{o,\alpha}^{<}(E) = G_{0,0}^{r}(E)V_{0,\alpha}g_{\alpha,\alpha}^{<}(E) + G_{0,0}^{<}(E)V_{0,\alpha}g_{\alpha,\alpha}^{a}(E) \tag{2.50}$$

and

$$G_{\alpha,0}^{<}(E) = g_{\alpha,\alpha}^{r}(E)V_{\alpha,0}G_{0,0}^{<}(E) + g_{\alpha,\alpha}^{<}(E)V_{\alpha,0}G_{0,0}^{a}(E). \tag{2.51}$$

Now inserting the above two relation (2.50 & 2.51) into equation (2.49) for the current through lead α, then equation (2.49)becomes

$$\begin{aligned} I_\alpha \;=\; & \frac{e}{\hbar}\int \frac{dE}{2\pi}\{(G_{0,0}^{r}(E)V_{0,\alpha}g_{\alpha,\alpha}^{<}(E) + G_{0,0}^{<}(E)V_{0,\alpha}g_{\alpha,\alpha}^{a}(E))V_{\alpha,0} \\ & -V_{0,\alpha}(g_{\alpha,\alpha}^{r}(E)V_{\alpha,0}G_{0,0}^{<}(E) + g_{\alpha,\alpha}^{<}(E)V_{\alpha,0}G_{0,0}^{a}(E))\}. \end{aligned} \tag{2.52}$$

Here we have the fact that $\Sigma_{0,0}^{a,(r),(<)} = V_{0,\alpha} g_{\alpha,\alpha}^{a,(r),(<)}(E) V_{\alpha,0}$, where $g_{\alpha,\alpha}^{a,(r),(<)}(E)$ is the uncoupled Green's function of the leads and is given as

$$g_{\alpha,\alpha}^{r,(a),(<)}(E) = \frac{1}{N}\sum_{j} g_{\alpha,j}^{r,(a),(<)}(E) = \int_{-\infty}^{+\infty} n_\alpha d\varepsilon_\alpha g_\alpha^{r,(a),(<)}(E). \tag{2.53}$$

Using equation (2.53), we can simplify the equation (2.52) for the current as

$$I_\alpha = \frac{e}{\hbar}\int \frac{dE}{2\pi}\{G_{0,0}^r(E)\Sigma_{0,0}^< + G_{0,0}^<(E)\Sigma_{0,0}^a - \Sigma_{0,0}^r G_{0,0}^<(E) - \Sigma_{0,0}^< G_{0,0}^a(E)]\}, \tag{2.54}$$

which can be rearranged as

$$I_\alpha = \frac{e}{\hbar}\int \frac{dE}{2\pi}\{\Sigma_{0,0}^<[G_{0,0}^r(E) - G_{0,0}^a(E)] + [\Sigma_{0,0}^a - \Sigma_{0,0}^r]G_{0,0}^<(E)]\}, \tag{2.55}$$

where $\Sigma_{0,0}^< = i\Gamma_\alpha f(\varepsilon)$, and $\Sigma_\alpha^a = (\Sigma_\alpha^r)^* = \frac{i\Gamma_\alpha}{2}$. Using these relations equation (2.55) for the current is finally written as

$$I_\alpha = \frac{ie}{\hbar}\int \frac{dE}{2\pi}\{\Gamma_\alpha f(\varepsilon)(G_{0,0}^r(E) - G_{0,0}^a(E)) + \Gamma_\alpha G_{0,0}^<(E)]\}, \tag{2.56}$$

2.5 Time-dependent non-equilibrium Green's function

We review the Keldysh non-equilibrium Green's function formulation[45, 46, 47, 53, 54, 55] for the general model discussed in the last sections. This is a fully quantum mechanical and far from equilibrium formulation whose basic approximations are very transparent as this technique has been used to study a wide range of transport properties of systems. It can provide an exact analytical solution to the transport equation in the non-linear and far

from equilibrium response regime. For simplicity, we rely on the commonly used wideband approximation, where the coupling between leads and dot is taken to be independent of energy, as such provides a way to perform transient and steady state transport calculations from first principle on realistic systems, taking into account maximum information about the electronic structure of the dot and the leads. A suitable approach to deal with such systems is the Keldysh non-equilibrium Green's function method. The main characteristic of this technique is that it considers the time evolution of a quantum state along a two way path that begins in -∞ draw forward to +∞ and then backward to -∞. The Green's function is represented by two by two matrix in terms of which perturbation theory has the same structure as in equilibrium many particle systems. It is also governed by the Dyson equation that has been studied extensively in many systems and have very interesting and useful results. An advantage of this method is that it treats the infinitely extended reservoirs in an exact way in the present system, which may give a better understanding of the essential features of NEMS in a more appropriate quantum mechanical description.

2.6 Formulation for a general time-dependent model

In the present case, we have time-dependent coupling of two leads, right (R) and left (L) with a single molecule such as a quantum dot at $t = 0$. In the tight-binding representation, the H_0 is the same as in the general time-independent model but now the coupling term contains the time-dependent part of the Hamiltonian as

$$H_{\text{leads-dot}} = \frac{1}{\sqrt{N}} \sum_{j,\alpha} V_\alpha(t) \left(c^\dagger_{j,\alpha} c_0 + c^\dagger_0 c_{j,\alpha} \right), \tag{2.57}$$

where we include time-dependent hopping $V_\alpha(t)$ to enable us to connect the leads $\alpha = L, R$ to the dot at a finite time. For the time-dependent dynamics, we shall focus on sudden joining of the leads to the dot at $t = 0$, which means $V_\alpha(t) = V\theta(t)$, where $\theta(t)$ is the Heaviside unit step function. N is the total number of states in the lead, j represents the channels in one of the leads. For the second lead the Hamiltonian can be written in the same way. An advantage of this approach (joining of leads to the dot at t=0) is that it eliminates the one major criticism of the Keldysh approach, which is the lack of any clear initial conditions.

Following the standard way, we derive the Dyson equation for the retarded and advanced Green's function on the dot due to interaction with the leads,

$$G^r_{00}(t,t') = g^r_{00}(t,t') + \int dt_1 \int dt_2 g^r_{00}(t,t_1)\Sigma^r_{00}(t_1,t_2)G^r_{00}(t_2,t'), \tag{2.58}$$

$$G^a_{00}(t,t') = g^a_{00}(t,t') + \int dt_1 \int dt_2 g^a_{00}(t,t_1)\Sigma^a_{00}(t_1,t_2)G^a_{00}(t_2,t'), \tag{2.59}$$

where the $G^{r,(a)}(t_2,t')$ refers to the retarded (advanced) Green's function on the dot including the leads as

$$G^r_{00}(t_2,t') = g^r_{00}(t_2,t')\exp[-\Gamma(t_2-t')], \quad t_2 > t', \tag{2.60}$$

$$G^a_{00}(t_2,t') = g^a_{00}(t_2,t')\exp[+\Gamma(t_2-t')], \quad t' > t_2, \tag{2.61}$$

with the fact that $\Gamma = \Gamma_L = \Gamma_R$, $g^{r,(a)}(t,t_1)$ refers to the retarded (advanced) Green's function on the uncoupled dot as

$$g^r_{00}(t_2,t') = -i\theta(t_2-t')\exp[-i\epsilon_0(t_2-t')]$$

$$g^a_{00}(t_2,t') = i\theta(t'-t_2)\exp[-i\epsilon_0(t_2-t')]$$

and the retarded (advanced) self-energy is written as

$$\Sigma^{r,(a)}_{00}(t_1,t_2) = V^*_\alpha(t_1)g^{r,(a)}_{\alpha,\alpha}(t_1,t_2)V_\alpha(t_2), \tag{2.62}$$

where $g^{r,(a)}_{\alpha,\alpha}(t_1,t_2)$ refers to the unperturbed states of the leads and is given as

$$\begin{aligned} g^r_{\alpha,\alpha}(t_1,t_2) &= \frac{1}{N}\sum_j g^r_{\alpha,j}(t_1,t_2), \\ &= \int_{-\infty}^{+\infty} n_\alpha d\varepsilon_\alpha g^r_\alpha(t_1,t_2) \\ &= -in_\alpha \int_{-\infty}^{+\infty} d\varepsilon_\alpha \theta(t_1-t_2)\exp[-i\varepsilon_\alpha(t_1-t_2)], \\ &= -in_\alpha \pi\delta(t_1-t_2). \end{aligned} \tag{2.63}$$

Similarly, the advanced uncoupled Green's function in the leads is written as

$$
\begin{aligned}
g^a_{\alpha,\alpha}(t_1,t_2) &= \frac{1}{N}\sum_j g^a_{\alpha,j}(t_1,t_2) \\
&= \int_{-\infty}^{+\infty} n_\alpha d\varepsilon_\alpha g^a_\alpha(t_1,t_2) \\
&= +in_\alpha \int_{-\infty}^{+\infty} d\varepsilon_\alpha \theta(t_2-t_1)\exp[-i(\varepsilon_\alpha)(t_1-t_2)], \\
&= +in_\alpha \pi\delta(t_1-t_2).
\end{aligned}
\tag{2.64}
$$

In obtaining these results we use the wide–band approximation only for the simplicity, although the method we are using does not rely on this approximation, where the retarded self–energy of the dot due to each lead is considered to be energy independent. The retarded self-energy defined in the last section is rewritten as

$$
\Sigma^r_{0,0}(t_1,t_2) = V^*_{0,\alpha}(t_1) g^r_{\alpha,\alpha}(t_1,t_2) V_{\alpha,0}(t_2), \tag{2.65}
$$

which can be simplified as

$$
\begin{aligned}
\Sigma^r_{0,0}(t_1,t_2) &= -in_\alpha \int_{-\infty}^{+\infty} d\varepsilon_\alpha \theta(t_1-t_2) V^*_{0,\alpha}(t_1)\exp[-i\varepsilon_\alpha(t_1-t_2)]V_{\alpha,0}(t_2), \\
&= -in_\alpha V^*_{0,\alpha}(t_1)V_{\alpha,0}(t_2)\int_{-\infty}^{+\infty} d\varepsilon_\alpha \theta(t_1-t_2)\exp[-i\varepsilon_\alpha(t_1-t_2)], \\
&= -in_\alpha V^*_{0,\alpha}(t_1)V_{\alpha,0}(t_2)\times\pi\delta(t_1-t_2)
\end{aligned}
\tag{2.66}
$$

Now we use the fact that $V^*_{0,\alpha}(t_1) = |V|\times\theta(t_1), V_{\alpha,0}(t_2) = |V|\times\theta(t_2)$, then the above expression can be written as

$$\Sigma^r_{00}(t_1,t_2) = \frac{-i\Gamma_\alpha}{2}\theta(t_1)\theta(t_2)\delta(t_1-t_2) \tag{2.67}$$

where n_α is the constant number density of the leads, and $\Gamma_\alpha = 2\pi\left|V\right|^2 n_\alpha$ is the damping factor. Similarly

$$\begin{aligned}\Sigma^a_{00}(t_1,t_2) = [\Sigma^r_{00}(t_1,t_2)]^* &= \frac{+i}{2}\Gamma_\alpha \int_{-\infty}^{+\infty} \frac{d\varepsilon_\alpha}{2\pi} e^{-i\varepsilon_\alpha(t_1-t_2)} \\ &= \frac{+i}{2}\Gamma_\alpha\theta(t_1)\theta(t_2)\delta(t_1-t_2)\,.\end{aligned} \tag{2.68}$$

Inserting equation (2.68, 2.63, & 2.64) into 2.58, we arrive here

$$\begin{aligned}G^r_{00}(t,t') &= g^r_{00}(t,t') + \int_{t'}^{t} dt_1 \int_{t'}^{t} dt_2 g^r_{00}(t,t_1)\{\frac{-i\Gamma_\alpha}{2}\theta(t_1)\theta(t_2)\delta(t_1-t_2)\}G^r_{00}(t_2,t'), \\ &= -i\theta(t-t')\exp[-i\epsilon_0(t-t')] + \int_{t'}^{t} dt_1 \int_{t'}^{t} dt_2[-i\theta(t-t_1)\exp[-i\epsilon_0(t-t_1)]] \\ &\times \{\frac{-i\Gamma_\alpha}{2}\theta(t_1)\theta(t_2)\theta(t_1-t_2)\delta(t_1-t_2)\} \times \{-i\theta(t_2-t')\exp[-i(\epsilon_0-i\Gamma)(t_2-t')]\},\end{aligned} \tag{2.69}$$

With the fact that $\int_{t'}^{t} dt_2\theta(t_1)\theta(t_2)\delta(t_1-t_2) = 1$, above equation can be simplified as

$$\begin{aligned}G^r_{00}(t,t') &= -i\theta(t-t')\exp[-i\epsilon_0(t-t')] + \frac{i\Gamma_\alpha}{2}\int_{t'}^{t} dt_1 \exp[-i\epsilon_0(t-t_1)] \\ &\times \{\theta(t_1-t')\exp[-i(\epsilon_0-i\Gamma)(t_1-t')]\}, \\ &= -i\theta(t-t')\exp[-i\epsilon_0(t-t')] \\ &+ \frac{i\Gamma_\alpha}{2}\exp[-i\epsilon_0 t]\exp[+i(\epsilon_0-i\Gamma)t']\int_{t'}^{t} dt_1 \exp[-\Gamma t_1]\end{aligned}$$

After performing the time integration of the above expression, the final result may be written as

$$\begin{aligned} G^r_{00}(t,t') &= -i\theta(t-t')\exp[-i\epsilon_0(t-t')] \\ &\quad - \frac{i\Gamma_\alpha}{2\Gamma}\exp[-i\epsilon_0 t]\exp[+i(\epsilon_0 - i\Gamma)t']\{\exp[-\Gamma t] - \exp[-\Gamma t']\} \\ &= -i\theta(t-t')\exp[-i\epsilon_0(t-t')] \\ &\quad - \frac{i\Gamma_\alpha}{2\Gamma}\{\exp[-i(\epsilon_0 - i\Gamma)(t-t')] - \exp[-i\epsilon_0(t-t')]\} \end{aligned}$$

which may be finally simplified by using the fact that $\Gamma = \Gamma_L = \Gamma_R$ as

$$G^r_{00}(t,t') = -i\theta(t-t')\{\exp[-i(\epsilon_0 - i\Gamma)(t-t')]\}, \tag{2.70}$$

Similarly, the advanced Green's function can be written as

$$G^a_{00}(t,t') = +i\theta(t'-t)\{\exp[-i(\epsilon_0 + i\Gamma)(t-t')]\}, \tag{2.71}$$

2.6.1 Time-dependent density matrix $\rho(t,t)$

The density matrix is related to the lesser Green's function through $\rho(t,t) = -iG^<(t,t')$ at $t = t'$, where we can write the lesser Green's function on the dot including all the contributions from the leads as

$$G^<_{0,0}(t,t') = \int dt_1 \int dt_2 G^r_{0,0}(t,t_1)\Sigma^<_{0,0}(t_1,t_2)G^a_{0,0}(t_2,t'), \quad t \text{ and } t' > 0, \tag{2.72}$$

whereas for t and $t' < 0$, the $G^{<}_{0,0}(t,t')$ is equal to zero, and with the self-energy equation derived in last section, the retarded and advanced Green's function on the dot due to interaction with leads defined in the last section can be written as

$$G^{r}_{00}(t,t_1) = g^{r}_{00}(t,t_1)\exp[-\Gamma(t-t_1)], \qquad t_1 > 0 \tag{2.73}$$

$$G^{a}_{00}(t_2,t') = g^{a}_{00}(t_2,t')\exp[+\Gamma(t_2-t')], \qquad t_2 > 0, \tag{2.74}$$

where we have used the fact that $\Gamma_L = \Gamma_R = \Gamma$ and the Green's function on the uncoupled dot may be explicitly written as

$$g^{r}_{00}(t,t_1) = -i\theta(t-t_1)\exp[-i\epsilon_0(t-t_1)] \tag{2.75}$$

$$g^{a}_{00}(t_2,t') = i\theta(t'-t_2)\exp[-i\epsilon_0(t_2-t')] \tag{2.76}$$

and the lesser self energy is written as

$$\Sigma^{<}_{0,0}(t_1,t_2) = V^{*}_{0,\alpha}(t_1)g^{<}_{\alpha,\alpha}(t_1,t_2)V_{\alpha,0}(t_2), \tag{2.77}$$

where the lesser Green's function for the uncoupled system in the leads is

$$
\begin{aligned}
g^{<}_{\alpha,\alpha}(t_1,t_2) &= \frac{1}{N}\sum_j g^{<}_{\alpha,j}(t_1,t_2) \\
&= \int_{-\infty}^{+\infty} n_\alpha d\varepsilon g^{<}_{\alpha}(t_1,t_2), \\
&= \int_{-\infty}^{+\infty} i2n_\alpha d\varepsilon_\alpha f(\varepsilon_\alpha)\exp[-i\varepsilon_\alpha(t_1-t_2)],
\end{aligned}
\tag{2.78}
$$

where $f(\varepsilon_\alpha)$ is the Fermi-Dirac distribution function, which have different chemical potential under a voltage bias and α represents the L or R leads. The lesser self energy given in equation (2.77) may be simplified by using equation (2.78) and with the fact that $V^*_{0,\alpha}(t_1) = |V| \times \theta(t_1), V_{\alpha,0}(t_2) = |V| \times \theta(t_2)$, thus the final expression can be written as

$$
\Sigma^{<}_{0,0}(t_1,t_2) = i\Gamma_\alpha \int \frac{d\varepsilon_\alpha}{2\pi} f(\varepsilon_\alpha)\theta(t_1)\theta(t_2)e^{-i\varepsilon_\alpha(t_1-t_2)} \tag{2.79}
$$

Hence, with the help of equation (2.79), the lesser Green's function given in equation (2.72) may be rewritten as

$$
G^{<}_{0,0}(t,t') = i\int dt_1 \int dt_2 G^{r}_{0,0}(t,t_1)\{\sum_\alpha \Gamma_\alpha \int \frac{d\varepsilon_\alpha}{2\pi} f(\varepsilon_\alpha)\theta(t_1)\theta(t_2)e^{-i\varepsilon_\alpha(t_1-t_2)}\}G^{a}_{0,0}(t_2,t') \tag{2.80}
$$

Although $G^{r,(a)}_{0,0}(t_1,t_2)$ is non-zero for $t<0$, it is never required due to the way it combines with $\Sigma^{r,(a),(<)}_{0,0}(t_1,t_2)$. The electronic contributions are non-zero only when t_1 and $t_2 > 0$. This lesser Green's function is directly related to the density matrix of the total system by the following expression,

$$\rho_{0,0}(t) = -iG^{<}_{0,0}(t,t), \tag{2.81}$$

which is equivalent to the Keldysh's non-equlibrium Green's function result and is the central expression of this formal development.

2.6.2 Time-dependent Current from lead α

The particle current I_α into the interacting region from the lead is given by the expectation value of the current operator, $I_\alpha = Tr(\rho\hat{I}_\alpha)$ [46, 47, 53, 54, 55], where

$$\hat{I}_\alpha = \frac{ie}{\hbar}\sum_j \{V_{0\alpha}c^\dagger_0 c_{\alpha j} - c^\dagger_{\alpha j}c_0 V_{\alpha 0}\} \tag{2.82}$$

which may be written in terms of Green's functions as

$$I_\alpha(t) = \frac{e}{\hbar}\mathrm{Tr}\{G^{<}_{0,\alpha}(t,t)V_{\alpha,0}(t) - V^*_{0,\alpha}(t)G^{<}_{\alpha,0}(t,t)\}, \tag{2.83}$$

where we have the following relations

$$G^{<}_{o,\alpha}(t,t) = \int dt'\{G^r_{0,0}(t,t')V_{0,\alpha}(t')g^{<}_{\alpha,\alpha}(t',t) + G^{<}_{0,0}(t,t')V_{0,\alpha}(t')g^a_{\alpha,\alpha}(t',t)\} \tag{2.84}$$

and

$$G^{<}_{\alpha,0}(t,t) = \int dt'\{g^r_{\alpha,\alpha}(t,t')V_{\alpha,0}(t')G^{<}_{0,0}(t',t) + g^{<}_{\alpha,\alpha}(t,t')V_{\alpha,0}(t')G^a_{0,0}(t',t)\} \tag{2.85}$$

Now inserting equation (2.84 & 2.85) into equation (2.83), the current through lead α now reads

$$I_\alpha(t) = \frac{e}{\hbar}\int dt' \mathrm{Tr}\{(G^r_{0,0}(t,t')V^*_{0,\alpha}(t')g^<_{\alpha,\alpha}(t',t) + G^<_{0,0}(t,t')V^*_{0,\alpha}(t')g^a_{\alpha,\alpha}(t',t))V_{\alpha,0}(t) \quad (2.86)$$
$$- V^*_{0,\alpha}(g^r_{\alpha,\alpha}(t,t')V_{\alpha,0}(t')G^<_{0,0}(t',t) + g^<_{\alpha,\alpha}(t,t')V_{\alpha,0}(t')G^a_{0,0}(t',t))\},$$

where $g^{r,(a),(<)}_{\alpha,\alpha}(t,t')$ refers to the unperturbed states of the leads. Using the fact that $\Sigma^{a,(r),(<)}_{0,0}(t',t) = V^*_{0,\alpha}(t')g^{a,(r),(<)}_{\alpha,\alpha}(t',t)V_{\alpha,0}(t)$, we can simplify the above equation for the current as

$$I_\alpha(t) = \frac{e}{2\pi\hbar}\int dt' \mathrm{Tr}\{G^r_{0,0}(t,t')\Sigma^<_{0,0}(t',t) + G^<_{0,0}(t,t')\Sigma^a_{0,0}(t',t) \quad (2.87)$$
$$- \Sigma^r_{0,0}(t,t')G^<_{0,0}(t',t) - \Sigma^<_{0,0}(t,t')G^a_{0,0}(t',t)]\},$$

where the the retarded (advanced) self-energy is written as

$$\Sigma^r_{00}(t,t') = V^*_{0,\alpha}(t)g^r_{\alpha,\alpha}(t,t')V_{\alpha,0}(t'), \quad (2.88)$$
$$\Sigma^a_{00}(t',t) = V^*_{0,\alpha}(t')g^a_{\alpha,\alpha}(t',t)V_{\alpha,0}(t)$$

and the lesser self energy is written as

$$\Sigma^<_{0,0}(t,t') = V^*_{0,\alpha}(t)g^<_{\alpha,\alpha}(t,t')V_{\alpha,0}(t'), \quad (2.89)$$

where $\Sigma^{r,(a),(<)}_{0,0}(t,t')$ are non-zero only when both the times (t,t') are positive $t,t' > 0$. Although $G^{r,(a)}_{0,0}(t,t')$ is non-zero for $t < 0$, it is never required due to the way it combines with $\Sigma^{r,(a),(<)}_{0,0}(t,t')$.

Chapter 3

A Simple Model for NEMS

3.1 Introduction

In this chapter we introduce a simple model for nanoelectromechanical systems as shown in Fig.3.1[56].

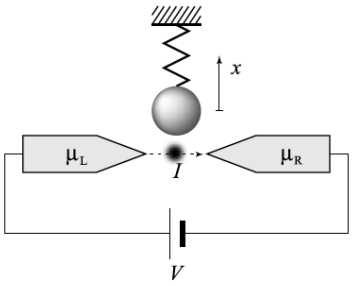


Figure 3.1: Oscillator coupled to a quantum dot. As a result of applied voltage V, electrons will tunnel from the left (L) to the right (R) electrode, with the potential energy of the dot depending on the position x of a nearby mechanical oscillator. The electromechanical coupling can be achieved by putting a net non-zero charge (or voltage) on a metallized mechanical oscillator.

This is a quantum description for both the mechanical and electrical degree of freedom in the experimental model originally proposed[10] by Knobel et al, by[17] Naik et al, and by LaHaye[14]. The theoretical techniques used by Mozyrsky and Martin[56] for the mechanical degree of freedom, and by Armour[28] et al, fail at low bias voltage and are valid only in the limit of weak electromechanical coupling. Hence, due to the nanometer scale of the system, these theories require improvement to introduce a quantum theory valid for both low and high applied bias and strong coupling. We describe the analytical calculations and numerical discussions of single particle quantum transport properties of electrons through a resonant tunnel junction coupled to a nanomechanical oscillator. By using the technique introduced in chapter 2 we calculate the transport properties of electrons on the single dot and single oscillator with strong coupling between them. An arbitrary voltage is applied to the tunnel junction and the electrons in the leads are considered to be at zero temperature. We consider the electronic state of the dot as empty/occupied (a two-level system). In the present model the system is initially in its ground state and we assume strong dissipation of the nanomechanical oscillator. This means that every independent electron which comes onto the dot finds the oscillator in its ground state. The properties of the electron-oscillator interactions on the dot are investigated using a non-perturbative approach. We consider a finite chemical potential difference between the right and left leads. In addition to the main resonant feature due to electrons on the dot, we find satellite features due to creation or annihilation of phonons. These satellite features become sharper and more significant with increasing strength of coupling between the electrons and the oscillator.

3.2 Formulation

We consider a single quantum dot connected to two identical metallic leads via tunnel junctions (SET device)[56, 57] as shown in figure 3.1. A single nanomechanical oscillator is coupled to the electrons on the dot and the applied gate voltage is used to tune the single level of the dot. This model represents a close analog of an electromechanical displacement detector[10] and contains the essential features of the recent experiments performed with a resonator, or a vibrating beam of crystal or cantilever coupled to the SET device. In most of these experiments, the motion of a resonator (nanomechanical oscillator) may be detected by capacitively coupled electrodes placed on the resonator, and biasing the electrode at a constant voltage. The dot has a small capacitance due to its small diameter (nm) and thus has charging energy. This charging energy exceeds the thermal energy in these experiments. For this reason we consider that only one excess electron may occupy the device. To ensure this condition we are working at zero temperature.

In the present simple model, both the electronic and the mechanical degrees of freedom have been treated quantum mechanically, where the nanomechanical oscillator is represented in terms of creation and annihilation operators. We neglect the spin degree of freedom and electron-electron interaction effects and consider the simplest possible model system. We also neglect the effects of finite electron temperature of the lead reservoirs and damping of the oscillator. Our model consists of the individual entities such as the single quantum dot with perpendicular oscillator on it and the left and right leads in their ground states at zero temperature. The Hamiltonian of our simple system is[59, 60, 61, 62]

$$H_0 = H_{ph-dot} + H_{leads} \tag{3.1}$$

$$H_{\text{dot-ph}} = \left[\epsilon_0 + \frac{\lambda l}{\sqrt{2}}(b^\dagger + b)\right] c_0^\dagger c_0 + H_{ph}\,, \tag{3.2}$$

$$H_{ph} = \frac{\widehat{p}^{\,2}}{2\mu} + \frac{1}{2}\mu\omega^2\widehat{x}^{\,2} = \hbar\omega(b^\dagger b + \tfrac{1}{2})\,, \tag{3.3}$$

where ϵ_0 is the single energy level of electrons on the dot with $c_0^\dagger, c_0$ the corresponding creation and annihilation operators. The parameter $\eta = \lambda l$ physically represents an effective electric field in the capacitor formed by the oscillator and the dot, which we shall call coupling strength between the oscillator and the electrons on the dot given as $\lambda l = eEl$, where e is the charge of electron, E is the strength of the electric field and $l = \sqrt{\frac{\hbar}{\mu\omega}}$ is the zero point amplitude of the oscillator with mass μ. Here we assume that the energy of the resonant level depends linearly on the oscillator coordinate. The frequency of the nanomechanical oscillator is ω and $b^\dagger$, b are the raising and lowering operator of the phonons given as

$$\widehat{x} = \frac{l}{\sqrt{2}}(b^\dagger + b), \tag{3.4}$$

and

$$\widehat{p} = \frac{i\mu\omega}{\sqrt{2}} l(b^\dagger - b), \tag{3.5}$$

The remaining elements of the Hamiltonian are

$$H_{\text{leads}} = \sum_j \epsilon_j c_j^\dagger c_j, \tag{3.6}$$

$$H_{\text{leads-dot}} = \frac{1}{\sqrt{N}} \sum_{j,\alpha} V_\alpha \left(c_{j,\alpha}^\dagger c_0 + c_0^\dagger c_{j,\alpha} \right), \tag{3.7}$$

where N is the total number of states in the lead, V_α is the hopping between the dot and the leads $\alpha = L, R$, j represents the channels in one of the leads. For the second lead the Hamiltonian can be written in the same way.

The total Hamiltonian of the system is thus $H = H_0 + \Delta H_\alpha$. We write the eigenvalues and the eigenfunctions of $H_{\text{dot-ph}}$ as

$$\epsilon = \epsilon_0 + \hbar\omega(n + \tfrac{1}{2}) - \Delta \tag{3.8}$$

$$\Psi_m(K, x_0 \neq 0) = A_m \exp[-\tfrac{l^2K^2}{2}] H_m(lK) \exp[-\mathrm{i}Kx_0] \tag{3.9}$$

$$\Psi_n(K, x_0 = 0) = A_n \exp[-\tfrac{l^2K^2}{2}] H_n(lK), \tag{3.10}$$

for the occupied, $x_0 \neq 0$ and unoccupied, $x_0 = 0$ (In eq 3.8, $\epsilon_0 = \Delta = 0$), dot respectively, where $A_n = \frac{1}{\sqrt{\sqrt{\pi} 2^n n! l}}$, $A_m = \frac{1}{\sqrt{\sqrt{\pi} 2^m m! l}}$, $\Delta = \frac{\lambda^2}{\mu\omega^2}$. $x_0 = \frac{\lambda}{\mu\omega^2}$ is the shift of the oscillator due to the coupling to the electrons on the dot, and $H_n(lK)$ are the usual Hermite polynomials. Here we have used the fact that the harmonic oscillator eigenfunctions have the same form in both real and Fourier space.

In order to transform between the representations for the occupied and unoccupied dot we require the matrix with elements

$$\Phi_{n,m} = \int \Psi_n^*(K, x_0 = 0)\Psi_m(K, x_0 \neq 0)\,\mathrm{d}K, \tag{3.11}$$

which may be simplified[63] as

$$\Phi_{n,m} = \frac{l}{\sqrt{\pi 2^{m+n} n! m!}} \int \exp\left(-l^2k^2\right) H_n^*(lK) H_m(lK) \exp\left(\mathrm{i}Kx_0\right)\,\mathrm{d}K \tag{3.12}$$

$$\Phi_{n,m} = \sqrt{\frac{2^{m-n}n!}{m!}} \exp\left(-\tfrac{1}{4}x^2\right) \left(\tfrac{1}{2}\mathrm{i}x\right)^{m-n} L_n^{m-n}\left(\tfrac{1}{2}x^2\right)$$

for $n \leq m$, where $x = \frac{x_0}{l}$ and $L_n^{m-n}(x)$ are the associated Laguerre polynomials. Note that the integrand is symmetric in m and n but the integral is only valid for $n \leq m$. Clearly the result for $n > m$ is obtained by exchanging m and n in equation (3.12) to obtain

$$\Phi_{n,m} = \sqrt{\frac{2^{|m-n|}\min[n,m]!}{\max[n,m]!}} \exp\left(-\tfrac{1}{4}x^2\right) \left(\tfrac{1}{2}\mathrm{i}x\right)^{|m-n|} L_{\min[n,m]}^{|m-n|}\left(\tfrac{1}{2}x^2\right). \tag{3.13}$$

The position of the resonant level with respect to the chemical potential in the leads is thus affected by the displacement of the nanomechanical oscillator, which in turn affects the transport properties of the junction through the device.

3.3 Green's function and quantum transport

In order to calculate the analytical results and to discuss the numerical quantum dynamics of the nanomechanical system, our focus in this section is to derive an analytical relation for the retarded self-energy. The self-energy represents the contribution to the dot energy, due to interactions between the dot and the leads it is coupled to. In obtaining these results we use the wide–band approximation where the retarded self–energy of the dot due to each lead is considered to be energy independent and is given by

$$\Sigma^r_{n_0,n_0,\alpha} = \Delta H^*_\alpha g^r_{\alpha,\alpha}(E - (n_0 + \tfrac{1}{2})\hbar\omega)\Delta H_\alpha, \tag{3.14}$$

where off-diagonal element of matrix, $\Sigma^r_{n_0,n_0',\alpha}$, are zero, and $g^r_{\alpha,\alpha}(E - (n_0 + \frac{1}{2})\hbar\omega)$ is the uncoupled Green function in the leads as

$$\begin{aligned} g^r_{\alpha,\alpha}(E - (n_0 + \tfrac{1}{2})\hbar\omega) &= \frac{1}{N}\sum_j g^r_{\alpha,j}(E - (n_0 + \tfrac{1}{2})\hbar\omega) \\ &= \frac{1}{N}\int_{-\infty}^{+\infty} \frac{N n_\alpha d\varepsilon_\alpha}{E - (n_0 + \frac{1}{2})\hbar\omega - \varepsilon_\alpha} \end{aligned} \tag{3.15}$$

where $\sum_j = \int_{-\infty}^{+\infty} N n_\alpha d\varepsilon_\alpha$, j stands for every channel in each lead, and n_α is the density of states in lead α. With the help of equation (3.15), the retarded self-energy may be written as

$$\Sigma^r_{n_0,n_0,\alpha} = \Delta H_{0,\alpha}\frac{1}{N}\int_{-\infty}^{+\infty} \frac{N n_\alpha d\varepsilon_\alpha}{E - (n_0 + \frac{1}{2})\hbar\omega - \varepsilon_\alpha}\Delta H_{\alpha,0}, \tag{3.16}$$

Equation (3.16) may be simplified as

$$\Sigma^r_{n_0,n_0,\alpha} = |V_{0,\alpha}|^2 \int_{-\infty}^{+\infty} \frac{n_\alpha d\varepsilon_\alpha}{E - (n_0 + \frac{1}{2})\hbar\omega - \varepsilon_\alpha} \tag{3.17}$$

$$= -|V_{0,\alpha}|^2 n_\alpha \int_{-\infty}^{+\infty} \frac{d\varepsilon_\alpha}{\varepsilon_\alpha - E + (n_0 + \frac{1}{2})\hbar\omega} \tag{3.18}$$

$$= -|V_{0,\alpha}|^2 n_\alpha \times (\pi i) \tag{3.19}$$

$$= \frac{-i\Gamma_\alpha}{2}, \tag{3.20}$$

where $\Gamma_\alpha = 2\pi \left|V_{0,\alpha}\right|^2 n_\alpha$, α representing the L or R leads, and the retarded self energy is now independent of the oscillator's index (n_0, n_0). Hence, it can be written as

$$\Sigma^r_{n_0 n_0,\alpha} = (\Sigma^a_{n_0,n_0,\alpha})^* = -\frac{i\Gamma_\alpha}{2} \tag{3.21}$$

The model represent the interplay between two physical time scales of the system, i.e., the oscillator frequency and the tunneling rate. This model also shows the very interesting interplay between two physical length scales of the system, i.e zero point amplitude and zero point displacement, that is actually affected by the weak and strong coupling dynamics.

We solve Dyson's equation using $\mathrm{H}_{dot-lead}$ as a perturbation. For the more general systems we aim to treat in the future, this is a reasonable small parameter. In the present case, however, we can find an exact solution. The retarded and advanced Green's functions on the dot, with the phonon states in the representation of the unoccupied dot, may be written as

$$G^{r(a)}_{nn_0}(E) = \sum_m \Phi_{n,m} g^{r(a)}_m(E) \Phi^*_{n_0,m}\,, \tag{3.22}$$

where $g^{r,(a)}_m(E)$ is the retarded (advanced) Green's function on the occupied dot,

$$g^{r,(a)}_m(E) = \left[E - \epsilon_0 - (m + \tfrac{1}{2})\hbar\omega + \Delta \pm \mathrm{i}\Gamma\right]^{-1}, \tag{3.23}$$

with the fact that $\Gamma_L = \Gamma_R = \Gamma$.

The lesser Green's function in the presence of nanomechanical oscillator including the dot and the leads and is written as

$$G^{<}_{n,n'}(E) = \sum_{n_0,n_0'} G^{r}_{n,n_0}(E)\Sigma^{<}_{n_0 n_0'} G^{a}_{n_0',n'}(E), \tag{3.24}$$

with $\Sigma^{<}_{n_0,n_0'}$ being the the lesser self energy which is given as

$$\Sigma^{<}_{n_0,n_0'} = \Sigma^{<}_{n_0,n_0',L} + \Sigma^{<}_{n_0,n_0',R}\,, \tag{3.25}$$

where the off-diagonal element of matrix, $\Sigma^{r}_{n_0,n_0',\alpha}$, are zero, and the diagonal ($n_0' = n_0$) element of the lesser self–energy may be written as

$$\begin{aligned}\Sigma^{<}_{n_0,n_0,\alpha} &= \mathrm{i}\Gamma_\alpha \int d\varepsilon_\alpha f_\alpha(\varepsilon_\alpha)\, B_{n_0}\delta(E-\varepsilon_\alpha-(n_0+\tfrac{1}{2})\hbar\omega) \\ &= \mathrm{i}\Gamma_\alpha f_\alpha(\varepsilon)\, B_{n_0},\end{aligned} \tag{3.26}$$

where $\varepsilon = E - (n_0 + \frac{1}{2})\hbar\omega$, $f_\alpha(\varepsilon_\alpha)$ and $f_\alpha(\varepsilon)$ are the Fermi distribution functions of the left ($\alpha = L$) and right ($\alpha = R$) leads, which have different chemical potentials under a voltage bias, and B_{n_0} is the Boltzmann factor for the oscillator state. Index n_0 determines the statistical occupation probability of the phonon state $|n_0\rangle$ at finite temperature, and therefore the accessibility of particular conduction channels is determined by a weight factor of the Boltzmann distribution function.

The formula for the current through each of the leads given in chapter 2 is written as

$$I_\alpha = \frac{ie}{\hbar}\sum_{n_0,n}\int \{\Sigma^{<}_{n_0,n,\alpha}(G^{r}_{n,n_0}(E) - G^{a}_{n,n_0}(E)) + (\Sigma^{a}_{n_0,n,\alpha} - \Sigma^{r}_{n_0,n,\alpha})G^{<}_{n,n_0}(E)\}dE, \tag{3.27}$$

With the help of equation (3.27), we calculate the net current through the dot and the leads with the oscillator on the dot, written as

$$I = I_L - I_R \tag{3.28}$$

$$= \frac{e}{4\pi}\sum_{n_0,n}\int \left\{ \begin{array}{c} \left[\left(\Sigma^{<}_{n_0,n,L} - \Sigma^{<}_{n_0,n,R}\right)\left(G^{r}_{n,n_0}(E) - G^{a}_{n,n_0}(E)\right)\right] \\ + \left[\left(\left(\Sigma^{a}_{n_0,n,L} - \Sigma^{r}_{n_0,n,L}\right) - \left(\Sigma^{a}_{n_0,n,R} - \Sigma^{r}_{n_0,n,R}\right)\right) G^{<}_{n,n_0}(E)\right] \end{array} \right\} \mathrm{d}E$$

The resulting expression for the net current is

$$I = \frac{e}{4\pi\hbar}\sum_{n_0,n}\int \left(\Sigma^{<}_{n_0,n,L} - \Sigma^{<}_{n_0,n,R}\right)\left(G^{r}_{n,n_0}(E) - G^{a}_{n,n_0}(E)\right) dE, \tag{3.29}$$

which is derived from equation (3.28) using the same damping factor for each lead ($\Gamma_L = \Gamma_R = \Gamma$).

For the present case of zero temperature the lesser self–energy may be recast in terms of the Heaviside step function $\theta(x)$ as

$$\Sigma^{<}_{n_0,n_0,\alpha} = \mathrm{i}\Gamma_\alpha \theta\left(\epsilon_{\mathrm{F}\alpha} + (n_0 + \tfrac{1}{2})\hbar\omega - E\right)\delta_{n_0,0}\,, \tag{3.30}$$

where $\epsilon_{\mathrm{F}\alpha}$ is the Fermi energy on lead α and the Kronecker delta, $\delta_{n_0,0}$, signifies that the nanomechanical oscillator is initially in its ground state, $n_0 = 0$.

Using the expression for the retarded and advanced Green's function and the lesser self-energy, the expression for the net current becomes

$$\begin{aligned} I &= \frac{e}{2\pi\hbar}\int \left(\begin{array}{c} \theta\left(\epsilon_{\mathrm{F}L} + \frac{1}{2}\hbar\omega - E\right) \\ -\theta\left(\epsilon_{\mathrm{F}R} + \frac{1}{2}\hbar\omega - E\right) \end{array} \right)[T_0(E)]dE, \\ &= \frac{e}{2\pi\hbar}\sum_n |\Phi_{0,n}|^2 \int_{\epsilon_{\mathrm{F}R}+\frac{1}{2}\hbar\omega}^{\epsilon_{\mathrm{F}L}+\frac{1}{2}\hbar\omega} \frac{\Gamma^2}{\left[E - \epsilon_0 - \left(n + \frac{1}{2}\right)\hbar\omega + \Delta\right]^2 + \Gamma^2} dE, \end{aligned} \tag{3.31}$$

where $T_0(E) = \Gamma[G^r_{0,0}(E)\Gamma G^a_{0,0}(E)]$.

After performing the integral in the above expression, the final result is written as

$$I = \frac{e\Gamma}{2\pi\hbar}\sum_n |\Phi_{0,n}|^2 \left[\tan^{-1}\left(\frac{\epsilon_{\mathrm{F}L} - \epsilon_0 - n\hbar\omega + \Delta}{\Gamma}\right) - \tan^{-1}\left(\frac{\epsilon_{\mathrm{F}R} - \epsilon_0 - n\hbar\omega + \Delta}{\Gamma}\right)\right], \tag{3.32}$$

where we note that the $\frac{1}{2}\hbar\omega$ terms cancel in these calculations. So, for rest of the thesis we will omit this factor.

We calculate the differential conductance by differentiating equation (3.32) with respect to $\epsilon_{\mathrm{F}L}$ and keeping $\epsilon_{\mathrm{F}R}$ constant. The final expression for the differential conductance is then

$$\frac{\mathrm{d}I}{\mathrm{d}\epsilon_{\mathrm{F}L}} = \frac{e}{2\pi\hbar}\sum_n \frac{\Gamma^2 |\Phi_{0,n}|^2}{\left[\epsilon_{\mathrm{F}L} - \epsilon_0 - n\hbar\omega + \Delta\right]^2 + \Gamma^2}\,. \tag{3.33}$$

Obviously one could have obtained the differential conductance directly from equation (3.31). without integrating and then differentiating.

3.4 Average Energy

To calculate the energy transferred from the electrons to the nanomechanical oscillator on the dot, we return to equation (3.24) and calculate the diagonal elements of the lesser Green's function at $n' = n$. The lesser Green's function is related to the density matrix through

$$\rho_{nn} = -i\int \frac{dE}{2\pi} G^{<}_{nn}(E). \tag{3.34}$$

We may therefore use the density matrix to calculate the energy transferred to the oscillator to obtain

$$E_{ph} = < n > \hbar\omega = \hbar\omega \frac{\sum_n n\rho_{n,n}}{\sum_n \rho_{n,n}}. \tag{3.35}$$

From equation (3.24) we may write the lesser Green's function in terms of the lesser self–energy and the retarded and advanced Green's functions as

$$G^{<}_{nn}(E) = G^{r}_{n,0}(E)\Sigma^{<}_{0,\alpha}G^{a}_{0,n}(E)\,, \tag{3.36}$$

where we note that, as we are working at $T = 0$, the self–energy terms are only non–zero for the zero phonon state. Hence we have the density matrix given in equation (3.34) in the following form

$$\begin{aligned}\rho_{n,n} = \frac{-i}{2\pi}\sum_{m,k,\alpha=L,R}\int_{-\infty}^{\infty}&\left[\frac{\Phi_{nm}\Phi^{*}_{0m}}{E-\epsilon_0-m\hbar\omega+\Delta+\mathrm{i}\Gamma}\right] \\ &\times\left[\mathrm{i}\Gamma\theta\left(\epsilon_{\mathrm{F}_\alpha}-E\right)\right] \\ &\times\left[\frac{\Phi_{0k}\Phi^{*}_{nk}}{E-\epsilon_0-k\hbar\omega+\Delta-\mathrm{i}\Gamma}\right]dE\,.\end{aligned} \tag{3.37}$$

With the help of the unit step function, the above expression can be simplified as

$$\begin{aligned}\rho_{n,n} &= \frac{\Gamma}{2\pi}\sum_{m,k,\alpha=L,R}\int_{-\infty}^{\epsilon_{\mathrm{F}\alpha}}\left[\frac{\Phi_{nm}\Phi^{*}_{0m}}{E-\epsilon_0-m\hbar\omega+\Delta+\mathrm{i}\Gamma}\right] \\ &\times\left[\frac{\Phi_{0k}\Phi^{*}_{nk}}{E-\epsilon_0-k\hbar\omega+\Delta-\mathrm{i}\Gamma}\right]dE \\ &= \frac{\Gamma}{2\pi}\sum_{m,k,\alpha=L,R}\frac{\Phi_{n,m}\Phi^{*}_{0,m}\Phi_{0,k}\Phi^{*}_{n,k}}{(k-m)\hbar\omega+2\mathrm{i}\Gamma} \\ &\times\int_{-\infty}^{\epsilon_{\mathrm{F}\alpha}}\left[\frac{1}{E-\epsilon_0-k\hbar\omega+\Delta-\mathrm{i}\Gamma}-\frac{1}{E-\epsilon_0-m\hbar\omega+\Delta+\mathrm{i}\Gamma}\right]dE\end{aligned} \tag{3.38}$$

After integrating the above expression[64], we arrive at the final result

$$\rho_{n,n} = \frac{\Gamma}{2\pi}\sum_{m,k}\frac{\Phi_{n,m}\Phi^{*}_{0,m}\Phi_{0,k}\Phi^{*}_{n,k}}{(k-m)\hbar\omega + 2\mathrm{i}\Gamma} \tag{3.39}$$

$$\times\left\{\begin{array}{c} \frac{1}{2}\ln\left[\frac{(\epsilon_{\mathrm{F}L}-\epsilon_0-k\hbar\omega+\Delta)^2+\Gamma^2}{(\epsilon_{\mathrm{F}L}-\epsilon_0-m\hbar\omega+\Delta)^2+\Gamma^2}\right] \\ +i\left(\tan^{-1}[\frac{\epsilon_{\mathrm{F}L}-\epsilon_0-m\hbar\omega+\Delta}{\Gamma}]+\tan^{-1}[\frac{\epsilon_{\mathrm{F}L}-\epsilon_0-k\hbar\omega+\Delta}{\Gamma}]+\pi\right) \\ +\frac{1}{2}\ln\left[\frac{(\epsilon_{\mathrm{F}R}-\epsilon_0-k\hbar\omega+\Delta)^2+\Gamma^2}{(\epsilon_{\mathrm{F}R}-\epsilon_0-m\hbar\omega+\Delta)^2+\Gamma^2}\right] \\ +i\left(\tan^{-1}[\frac{\epsilon_{FR}-\epsilon_0-m\hbar\omega+\Delta}{\Gamma}]+\tan^{-1}[\frac{\epsilon_{\mathrm{F}R}-\epsilon_0-k\hbar\omega+\Delta}{\Gamma}]+\pi\right) \end{array}\right\}.$$

Hence, the average energy transferred to the oscillator may be calculated using equation (3.34).

3.5 Current noise and Fano factor

In recent years, there has been a great interest in the measurement of current noise near the quantum limit[10, 13, 14, 15, 16, 17] of displacement sensitivity using single electron transistors (SET) and nanomechanical oscillators. Current noise[65, 66, 67, 68] is the non-equilibrium fluctuation which is caused by the discreteness of charged carriers. When the size of an electromechanical system reaches the nanometer scale, the current noise problem becomes a very interesting aspect of the NEMS based devices. In NEMS devices it is a fundamental physical signature, which can provide us additional information regarding quantum transport, in addition to differential conductance and current voltage characteristics. The electrons traveling through the device become correlated in the same channel and the same probe, as well as in different channels and different probes. For a mesoscopic system, the electrons are correlated due to coherent transport, and they are governed by the Fermi distribution and Pauli principle. Noise is caused by the randomness

of electron scattering and it has been extensively studied in different types of mesoscopic structures. For uncorrelated electrons travelling through a macroscopic conductor, shot noise $S(0)$ at zero frequency is given by the Poisson value

$$S(0) = 2eI,$$

where I is the net average current flowing through the system. However, for a mesoscopic system, electrical current correlations are dominated by the Pauli principle, and a Fermi distribution can lead to the deviation of shot noise from a Poissonian (F=1) form. An important parameter for describing this type of shot noise is the Fano factor F= $S(0)/2eI$, using which the shot noise can be classified as sub-Poissonian (F < 1) or super-Poissonian (F > 1).

The zero frequency shot-noise has been derived and applied successfully in many examples of the transport dynamics of nanoscopic systems[59, 69, 70]. This is given as

$$\begin{aligned} S(0) = \frac{e^2}{\pi\hbar}\int dE\{&[f_L(\varepsilon)(1-f_L(\varepsilon)) + f_R(\varepsilon)(1-f_R(\varepsilon))][T_0(E)] \\ &+ (f_L(\varepsilon) - f_R(\varepsilon))^2[(1-T_0(E))T_0(E)]\}, \end{aligned} \tag{3.40}$$

Using the values of transmission coefficients ($T_0(E)$) from equation (3.31) at zero temperature, the above expression can be simplified as

$$S(0) = \frac{e^2}{\pi\hbar}\int_{\epsilon_{\mathrm{F}R}}^{\varepsilon_{F_L}} dE[(1-T_0(E))T_0(E)] \tag{3.41}$$
$$= \frac{e^2}{\pi\hbar}\int_{\epsilon_{\mathrm{F}R}}^{\epsilon_{\mathrm{F}L}} \left\{ \begin{array}{c} \sum_n \frac{|\Phi_{0,n}|^2\Gamma^2}{\left[E-\epsilon_0-\left(n+\frac{1}{2}\right)\hbar\omega+\Delta\right]^2+\Gamma^2} \\ -\left(\sum_n \frac{|\Phi_{0,n}|^2\Gamma^2}{\left[E-\epsilon_0-\left(n+\frac{1}{2}\right)\hbar\omega+\Delta\right]^2+\Gamma^2}\right)^2 \end{array} \right\} dE,$$

After integrating the above expression, we arrive at the final result

$$S(0) = \frac{e^2\Gamma}{\pi\hbar}\left\{\sum_n S_n(0) + \sum_{n>m} S_{n,m}(0)\right\}, \tag{3.42}$$

where $S_n(0)$ and $S_{n,m}(0)$ are defined as

$$S_n(0) = |\Phi_{0,n}|^2 \left\{ \begin{array}{c} \tan^{-1}\left(\frac{\epsilon_{\mathrm{F}L}-\epsilon_0-n\hbar\omega+\Delta}{\Gamma}\right) - \tan^{-1}\left(\frac{\epsilon_{\mathrm{F}R}-\epsilon_0-n\hbar\omega+\Delta}{\Gamma}\right) \\ \sum_n \frac{|\Phi_{0,n}|^2}{2}\{\frac{\Gamma(\epsilon_{\mathrm{F}L}-\epsilon_0-n\hbar\omega+\Delta)}{((\epsilon_{\mathrm{F}L}-\epsilon_0-n\hbar\omega+\Delta)^2+\Gamma^2)} + \tan^{-1}[\frac{\epsilon_{\mathrm{F}L}-\epsilon_0-n\hbar\omega+\Delta}{\Gamma}]\} \\ -\sum_n \frac{|\Phi_{0,n}|^2}{2}\{\frac{\Gamma(\epsilon_{\mathrm{F}R}-\epsilon_0-n\hbar\omega+\Delta)}{((\epsilon_{\mathrm{F}R}-\epsilon_0-n\hbar\omega+\Delta)^2+\Gamma^2)} - \tan^{-1}[\frac{\epsilon_{\mathrm{F}R}-\epsilon_0-n\hbar\omega+\Delta}{\Gamma}]\} \end{array} \right\}$$

$$S_{n,m}(0) = \left\{ \begin{array}{c} +\frac{|\Phi_{0,n}|^2|\Phi_{0,m}|^2\Gamma^2}{i((n-m)\hbar\omega)((n-m)\hbar\omega+2i\Gamma)} \left(\begin{array}{c} \frac{1}{2}\ln\left[\frac{(\epsilon_{\mathrm{F}L}-\epsilon_0-n\hbar\omega+\Delta)^2+\Gamma^2}{(\epsilon_{\mathrm{F}R}-\epsilon_0-n\hbar\omega+\Delta)^2+\Gamma^2}\right] \\ +i(\tan^{-1}[\frac{\epsilon_{\mathrm{F}L}-\epsilon_0-n\hbar\omega+\Delta}{\Gamma}] - \tan^{-1}[\frac{\epsilon_{\mathrm{F}R}-\epsilon_0-n\hbar\omega+\Delta}{\Gamma}] \end{array} \right) \\ +\frac{|\Phi_{0,n}|^2|\Phi_{0,m}|^2\Gamma^2}{i((m-n)\hbar\omega)((m-n)\hbar\omega+2i\Gamma)} \left(\begin{array}{c} \frac{1}{2}\ln\left[\frac{(\epsilon_{\mathrm{F}L}-\epsilon_0-m\hbar\omega+\Delta)^2+\Gamma^2}{(\epsilon_{\mathrm{F}R}-\epsilon_0-m\hbar\omega+\Delta)^2+\Gamma^2}\right] \\ +i(\tan^{-1}[\frac{\epsilon_{\mathrm{F}L}-\epsilon_0-m\hbar\omega+\Delta}{\Gamma}] - \tan^{-1}[\frac{\epsilon_{\mathrm{F}R}-\epsilon_0-m\hbar\omega+\Delta}{\Gamma}] \end{array} \right) \end{array} \right\}$$

The corresponding Fano factor can be calculated from the zero frequency noise and the net current flowing through the system, which is defined as

$$F = \frac{S(0)}{2eI}$$

3.6 Discussion of results

The differential conductance is shown graphically in figure 3.2 as a function of applied voltage for different values of coupling strength, using the same parameters[10, 14, 16, 28, 56, 57, 61, 62] as: the single energy level of the dot $\epsilon_0 = 0.5$, the characteristic frequency of the oscillator $\hbar\omega = 0.3$, the damping factor $\Gamma = 0.3\hbar\omega$ and the chemical potentials $0 \leq \epsilon_{\mathrm{F}L} \leq 1$ and $\epsilon_{\mathrm{F}R} = 0$.

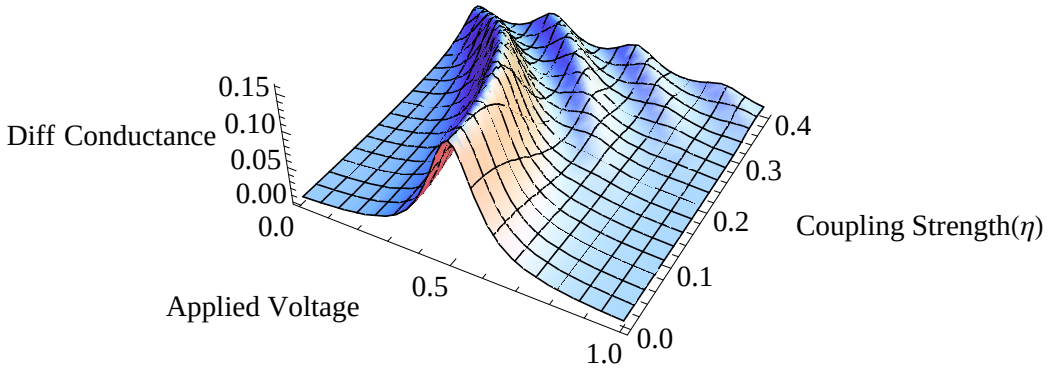


Figure 3.2: Differential conductance (dimensionless) as a function of applied voltage ϵ_{FL} (in arbitrary units) and coupling strength η. Gate voltage $\epsilon_0 = 0.5$, oscillator energy $\hbar\omega = 0.3$, self-energy $\Gamma = 0.3\hbar\omega$.

These are chosen to illustrate the physics of such systems rather than to represent a specific implementation. The oscillator induced resonance effects are clearly visible in the numerical results. It must be noted that we have obtained these results in the regime of strong and zero or weak coupling of the oscillator with the electrons on the dot. The coupling between the leads and the dot is considered to be symmetric and we assume that the electrons in the leads are at zero temperature and the leads have constant density of

states. With increasing coupling strength, the number of satellite peaks also increases while for zero or weak coupling we find only the basic resonance. This confirms the effect of the coupling between the electrons on the dot and the single oscillator mode where higher energy electrons are able to drop to the dot energy by creation of phonons. Transport processes involving creation or annihilation of phonons are a common feature of NEMS.

Closer analytical examination of the expression for the differential conductance (3.33) shows that the main resonance peaks occur when the applied voltage, ϵ_{FL} is equal to the energy eigenvalues of the coupled dot electron and oscillator. The main peak ($n = 0$) is given by the Lorentzian form with its center at the $\epsilon_{FL} = \epsilon_0 - \Delta$, known as a Breit-Wigner resonance[71, 72, 73, 74, 75, 76, 77]. The satellite peaks due to the emission of phonons can be seen on the positive energy side with $\epsilon_{FL} = \epsilon_0 - \Delta + n\hbar\omega$ where ω is the characteristic frequency of the oscillator.

The main or basic resonance peak is the elastic or zero phonon transition. The amplitude of the satellite peaks or steps is much smaller than the basic resonance peak. The electrons that tunnel onto the dot can only excite the oscillator mode as at zero temperature there are no phonons available to be absorbed. Moreover, we have seen that with increasing coupling strength, the number and intensity of the satellite peaks increases but their intensity always remains much smaller than the main peak. The peaks or steps in the current characteristics vanish if the upper electrochemical potential is smaller than the dot energy plus the oscillator energy.

The differential conductance as a function of gate voltage, ϵ_0, is shown in fig.3.3 for various coupling strengths at $T = 0$[70]. The main peak at $\epsilon_0 = \epsilon_{\mathrm{F}L} + \Delta$ corresponds to

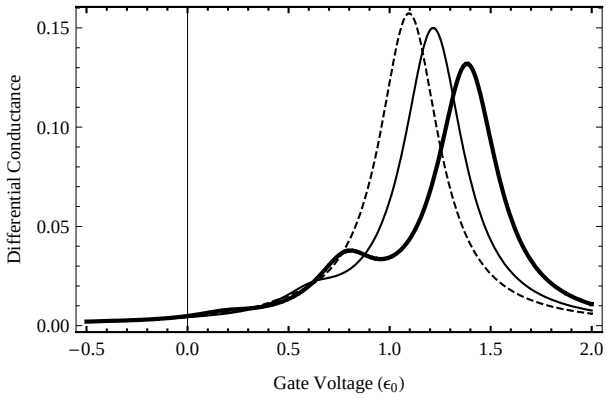


Figure 3.3: Differential conductance (dimensionless) as a function of gate voltage ϵ_0, with applied voltage ϵ_{FL} (in arbitrary units)=1, oscillator energy $\hbar\omega = 0.6$, self-energy $\Gamma = 0.3\hbar\omega$, and coupling strength $\eta = 0.4\hbar\omega$ (dotted line), $0.6\hbar\omega$ (light solid line), and $0.8\hbar\omega$ (bold solid line)

the elastic or zero–phonon transition and the satellites peaks are due to emission of phonons corresponding to $n = 1, 2, 3, 4, \ldots$. This shows more and more satellites corresponding to every multiple of $\hbar\omega$.

With increasing coupling strength while keeping the temperature zero, we see that the energy transferred to the oscillator increases with increasing coupling strength, while the amplitude of the satellite peaks is much smaller than the main peak which is shifted toward the right by a factor Δ. The amplitude of the main peak is also affected: its magnitude decreases with increasing coupling strength.

In fig. 3.4 & 3.5, we plot the average energy transferred to the oscillator per transmitted electron as a function of applied bias and gate voltage. Due to Coulomb blockade only one electron is allowed to occupy the dot at once.

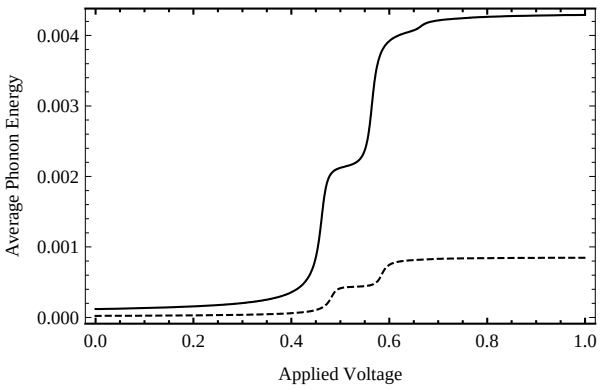


Figure 3.4: Average energy (dimensionless) transferred to the oscillator as a function of applied voltage ϵ_{FL} (in arbitrary units) with gate voltage $\epsilon_0 = 0.5$, oscillator energy $\hbar\omega = 0.1$, self-energy $\Gamma = 0.1\hbar\omega$, and coupling strength $\eta = 0.4\hbar\omega$ (dotted line), and $\eta = 0.6\hbar\omega$ (solid line).

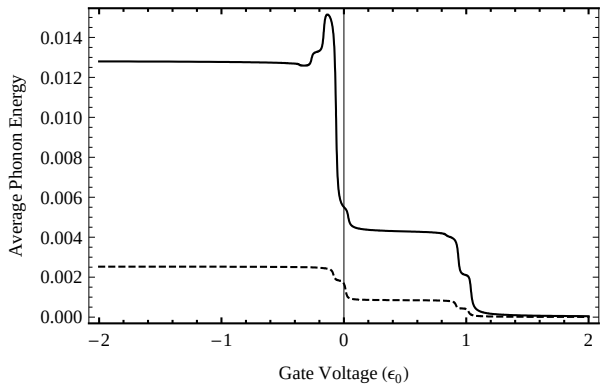


Figure 3.5: Average energy (dimensionless) transferred to the oscillator as a function of gate voltage ϵ_0 with applied voltage ϵ_{FL} (in arbitrary units)=1, oscillator energy $\hbar\omega = 0.1$, self-energy $\Gamma = 0.1\hbar\omega$, and coupling strength $\eta = 0.4\hbar\omega$ (dotted line), and $\eta = 0.6\hbar\omega$ (solid line).

As we are considering strong relaxation of the nanomechanical oscillator, we assume the oscillator has to return to its ground state before the next electron arrives. Therefore at zero temperature we only consider the energy gained by the oscillator from single

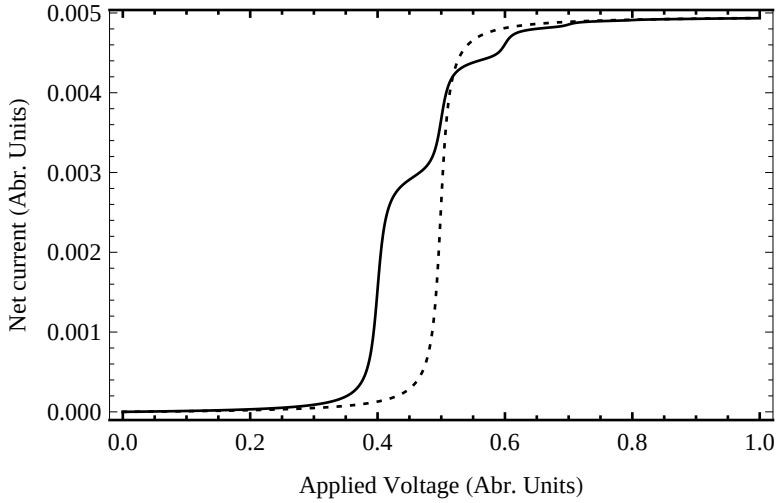


Figure 3.6: Current-voltage characteristics (dimensionless) as a function of applied voltage ϵ_{FL} (in arbitrary units), coupling strength $\eta = 0.1\hbar\omega$(dotted line), and $1\hbar\omega$ (solid line). Gate voltage $\epsilon_0 = 0.5$, oscillator energy $\hbar\omega = 0.1$, self-energy $\Gamma = 0.1\hbar\omega$.

electron process and ignore any cumulative effect due to passage of multiple electrons. We note that there is some structure as individual phonons are excited but there is also a saturation level $\propto \eta^4$. The peak just below $\epsilon_0 \approx \epsilon_{\mathrm{F}R}$ in figure 3.5 is due to the fact that there is no elastic transmission in this regime and *all* transmitted electrons result in the creation of phonons. Note that this is the average energy transferred when the system starts in its ground state and should not be confused with the energy transferred after many electrons have interacted with the oscillator. Moreover, the phonon energy of the oscillator on the dot and the level width are both typically larger than the experimental temperature.

We have shown the I-V characteristics of the NEMS device against applied bias for different values of the coupling strength in Fig. 3.6. The main resonance step is the elastic or zero phonon transition. The amplitude of the additional steps is much smaller than the basic resonance step. The electrons that tunnel onto the dot can only excite the oscillator mode as at zero temperature there are no phonons available to be absorbed.

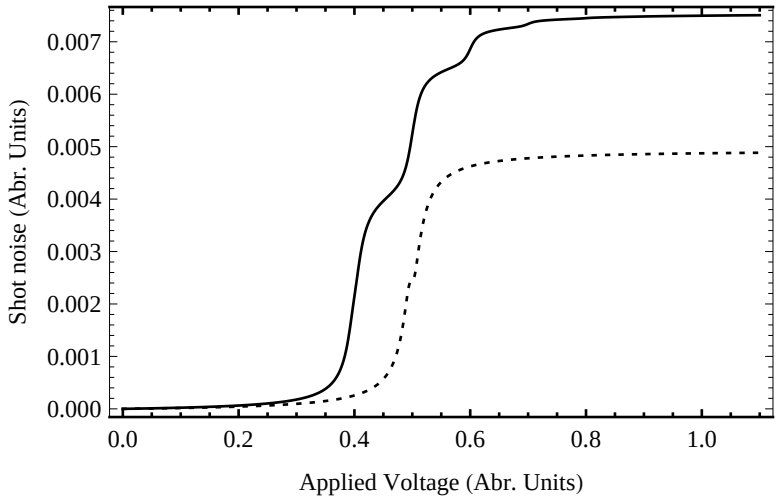


Figure 3.7: Shot noise (dimensionless) as a function of applied voltage ϵ_{FL} (in arbitrary units), with gate voltage ϵ_0=0.5, oscillator energy $\hbar\omega = 0.1$, self-energy $\Gamma = 0.1\hbar\omega$, and coupling strength $\eta = 0.1\hbar\omega$ (dotted line), and $1\hbar\omega$ (light solid line).

Moreover, we have seen that with increasing coupling strength, the number and intensity of the additional steps increases but their intensity always remains much smaller than the main step. The steps in the current characteristics vanish if the upper electrochemical potential is smaller than the dot energy plus the oscillator energy. Next, we have shown the shot noise as a function of applied bias in Fig. 3.7, which exhibits the single step in the presence of weak or zero electron-oscillator coupling while the number of additional steps increases with increasing coupling strength. Obviously, the shape of the shot noise curve is similar to that of the net current, as shown in Fig. 3.6. The only difference is associated with their behavior above resonance point, where noise power for the strong coupling case can exceed shot noise for zero phonon case. We also show the differential shot noise against applied bias for different values of the coupling strength(in Fig. 3.8). In the absence of phonons, when transport is coherent, the shot noise spectrum exhibits two peaks separated by antiresonance and located symmetrically around the position where

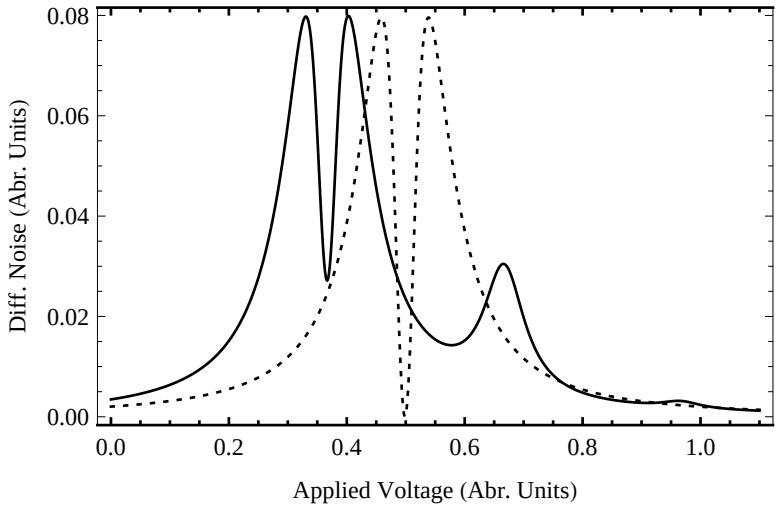


Figure 3.8: Differential shot noise (dimensionless) as a function of applied voltage ϵ_{FL} (in arbitrary units) with gate voltage $\epsilon_0 = 0.5$, oscillator energy $\hbar\omega = 0.3$, self-energy $\Gamma = 0.3\hbar\omega$, and coupling strength $\eta = 0.1\hbar\omega$ (dotted line), and $\eta = 2\hbar\omega$ (solid line).

the current step associated with the single level of the dot is located. The origin of such antiresonance in the noise spectrum is associated with the fact that no noise is generated when the transmission via the dot state is perfect T = 1 or zero. Due to the presence of the nanomechanical oscillator, the main resonance peaks are shifted by Δ due to the oscillator effect. Meanwhile, the sharp peaks are now accompanied by a set of additional peaks. We notice that the separation between the differential shot noise peaks is set by the frequency of the oscillator. This phenomena can be explained on the basis of phonons emission during electron-phonon coupling, indicating that a new channel has opened and participates in contributing to the resonant tunneling process.

Finally, we have shown the Fano factor against applied bias for different values of the coupling strength. Information about the statistical properties of the electrons is included into the Fano factor, which is plotted in Fig. 3.9. Since in our model all the interactions between the current carriers are neglected, such electron correlations are as-

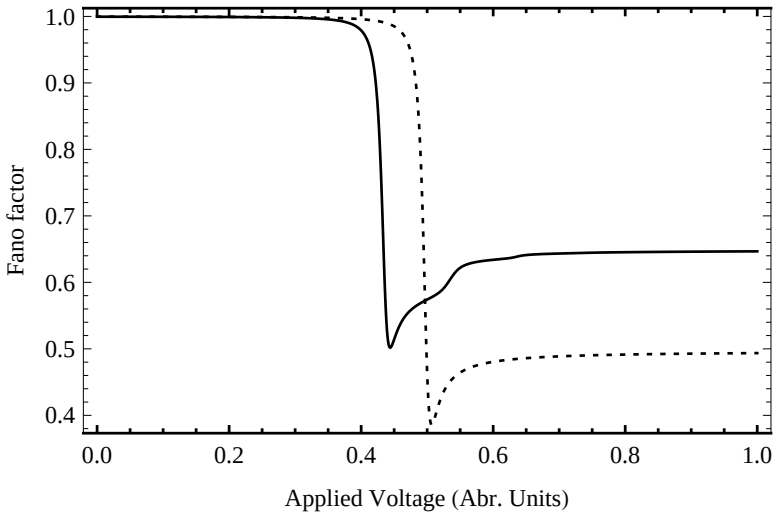


Figure 3.9: Fano factor as a function of applied voltage ϵ_{FL} (in arbitrary units) with gate voltage ϵ_0=0.5, oscillator energy $\hbar\omega = 0.1$, self-energy $\Gamma = 0.1\hbar\omega$, and coupling strength $\eta = 0.1\hbar\omega$ (dotted line), and $\eta = 1\hbar\omega$ (solid line).

sociated only with the Pauli principle. This exclusion rule is related to the fact that one electron feels the presence of the others, since it cannot occupy the state on the dot already occupied by the electron. The crossover in the shot noise power from Poissonian limit (F =1) to sub-Poissonian region (F<1) is always observed after the first step in the current voltage dependence. This implies that electrons tunnel in a correlated way in NEMS device. The important thing is significant enhancement of Fano factor due to the phonon effects, observed for $\epsilon_{FL} > \epsilon_0 - \Delta + n\hbar\omega$, where the multi-channel process reduces electron correlations in comparison with the single channel one. Moreover, the shift, Δ can also be easily recognized in Fig. 3.9.

3.7 Conclusions

In this chapter, we analyzed the single electron transport dynamics of a nanomechanical oscillator coupled to a resonant tunnel junction by using the Green's function approach without treating the electron phonon coupling as a perturbation. We have derived an expression for the current and differential conductance and discuss it in detail for different values of the coupling strength. We have found steps/peaks in the current spectrum as a function of the chemical potential difference in addition to the main resonant step, due to the transfer of energy from electrons on the dot to the oscillator. We have also studied the effect of gate voltage. We derive an expression for the average energy transferred from the electrons to the oscillator. We also derive an analytical relation for the shot noise and the corresponding Fano factor. We have shown that the steps grow with increasing coupling strength of electrons on the dot and the oscillator. This confirms that the additional satellite peaks or steps in the spectrum of numerical results are due to the transfer of energy from the electrons to the oscillator.

Chapter 4

Time-dependent dynamics of simple NEMS model

4.1 Introduction

In this chapter we introduce the time-dependent dynamics of the same model discussed in chapter 3. Here, we present a theoretical study of time-dependent quantum transport in a resonant tunnel junction coupled to a nanomechanical oscillator within the non-equilibrium Green's function technique discussed in chapter 2. In this system, we include the time-dependent hopping between the dot and the leads to enable us to connect the leads to the dot at a finite time. An advantage of the time-dependent non-equilibrium Green's function approach considered in this chapter is that it eliminates the one major criticism of the Keldysh approach, which is the lack of any clear initial conditions. We assume strong dissipation of the nanomechanical oscillator. We describe the electronic state

of the dot as a two-state system (empty/occupied). The electrons in the leads are considered to be at zero temperature. We consider an arbitrary finite chemical potential difference between the right and left leads. The transient and the steady state behavior of the system is considered here in order to explore the quantum dynamics of the oscillator as a function of time. The properties of the phonon distribution of the nanomechanical oscillator strongly coupled to the electrons on the dot are investigated using a non-perturbative approach. We consider both the energy transferred from the electrons to the oscillator and the Fano factor as a function of time. We discuss the quantum dynamics of the nanomechanical oscillator in terms of pure and superposition states. We have found a significant difference between a quantum and a classical oscillator. In particular, the energy of a classical oscillator will always be dissipated by the electrons whereas the quantum oscillator remains in an excited state. This will provide useful insight for the design of experiments aimed at studying the quantum behavior of an oscillator.

4.2 Model calculations

The Hamiltonian, eigenvalues and eigenfunctions for the following discussion are same except the hopping term, which is now time-dependent and is written as[46, 47, 53, 54, 55]

$$H_{\text{leads-dot}} = \frac{1}{\sqrt{N}} \sum_{j,\alpha} V_\alpha(t) \left(c^\dagger_{j,\alpha} c_0 + c^\dagger_0 c_{j,\alpha} \right), \tag{4.1}$$

where we include time-dependent hopping $V_\alpha(t)$ to enable us to connect the leads $\alpha = L, R$ to the dot at a finite time. For the time-dependent dynamics, we shall focus on sudden joining of the leads to the dot at $t = 0$, which means $V_\alpha(t) = V\theta(t)$, where $\theta(t)$ is the

Heaviside unit step function. N is the total number of states in the lead, and j represents the channels in one of the leads. For the second lead the Hamiltonian can be written in the same way.

In order to calculate the analytical solutions and to discuss the numerical results of the transient and steady state dynamics of the nanomechanical systems, our focus in this section is to derive an analytical relation for the time dependent effective self-energy and the Green's functions. In obtaining these results we use the wide–band approximation only for simplicity, although the method we are using does not rely on this approximation, where the retarded self–energy of the dot due to each lead is given by[46, 53, 54, 55]

$$\Sigma^r_\alpha(t_1,t_2) = V^*_\alpha(t_1) g^r_{\alpha,\alpha}(t_1,t_2) V_\alpha(t_2), \tag{4.2}$$

where $\alpha = L, R$ represent the left and right leads and the Green's function in the leads for the uncoupled system is

$$g^r_{\alpha,\alpha}(t_1,t_2) = \frac{1}{N}\sum_j g^r_{\alpha,j}(t_1,t_2) = -in_\alpha\theta(t_1-t_2)\int_{-\infty}^{+\infty} d\varepsilon_\alpha \exp[-i(\varepsilon_\alpha + m\hbar\omega)(t_1-t_2)], \tag{4.3}$$

with the fact that $\sum_j = \int_{-\infty}^{+\infty} N n_\alpha d\varepsilon_\alpha$, where j stands for every channel in each lead and n_α is the constant number density of the leads.

Now using the uncoupled Green's function in equation (4.2), the retarded self energy may be written as

$$\begin{aligned}\Sigma^r_\alpha(t_1,t_2) &= -in_\alpha\theta(t_1-t_2)\int_{-\infty}^{+\infty} d\varepsilon_\alpha V^*_\alpha(t_1)\exp[-i(\varepsilon_\alpha + m\hbar\omega)(t_1-t_2)]V_\alpha(t_2), \\ &= -in_\alpha V^*_\alpha(t_1)V_\alpha(t_2)\theta(t_1-t_2)\int_{-\infty}^{+\infty} d\varepsilon_\alpha \exp[-i(\varepsilon_\alpha + m\hbar\omega)(t_1-t_2)],\end{aligned} \tag{4.4}$$

After performing the integral, the final result is written as

$$\Sigma^r_\alpha(t_1,t_2) = -in_\alpha V^*_\alpha(t_1)V_\alpha(t_2)\theta(t_1-t_2)\times\pi\delta(t_1-t_2), \tag{4.5}$$

Now we use the fact that $V_\alpha(t_1) = |V|\times\theta(t_1), V_\alpha(t_2) = |V|\times\theta(t_2)$. Then the above expression can be written as

$$\Sigma^r_\alpha(t_1,t_2) = \frac{-i\Gamma_\alpha}{2}\theta(t_2)\delta(t_1-t_2) \tag{4.6}$$

where $\Gamma_\alpha = 2\pi|V|^2 n_\alpha$ is the damping factor ($\Gamma_L = \Gamma_R = \Gamma$). Similarly $\Sigma^a_\alpha(t_1,t_2) = [\Sigma^r_\alpha(t_1,t_2)]^* = +\mathrm{i}\frac{1}{2}\Gamma_\alpha\ \theta(t_2)\delta(t_1-t_2)$.

We solve Dyson's equation using $H_{\text{dot-leads}}$, as a perturbation. In the presence of the oscillator, the retarded and advanced Green's functions on the dot, with the phonon states in the representation of the unoccupied dot, may be written as

$$G^r_{n,n'}(t,t_1) = \sum_m \Phi_{n,m}g^r_m(t,t_1)\Phi^*_{n',m}\,,\ G^a_{n,n'}(t_2,t') = \sum_k \Phi_{n,k}g^a_k(t_2,t')\Phi^*_{n',k} \tag{4.7}$$

where $g^{r(a)}_{m(k)}$ is the retarded (advanced) Green's function on the occupied dot coupled to the leads may be written as,

$$g^r_m(t,t_1) = -i\theta(t-t_1)\times\exp[-i(\varepsilon_m - i\Gamma)(t-t_1)],\ t_1>0 \tag{4.8}$$

and

$$g^a_k(t_2,t') = i\theta(t'-t_2)\times\exp[-i(\varepsilon_k + i\Gamma)(t_2-t')],\quad t_2>0 \tag{4.9}$$

with $\varepsilon_m = \epsilon_0 + m\hbar\omega - \Delta$, $\varepsilon_k = \epsilon_0 + k\hbar\omega - \Delta$, and $\Delta = \lambda^2/\mu\omega^2$.

The above Eqs. (4.6), (4.7), (4.8) and (4.9) will be the starting point of our examination of the time-dependent response of the coupled system. These functions are the

essential ingredients for theoretical considerations of such diverse problems as low and high voltage, coupling of electron and phonons, transient and steady state phenomena.

4.3 Time-dependent dot population $\rho(t)$

The density matrix is related to the dot population through $\rho(t) = \sum_n \rho_{n,n}(t,t)$, where the density matrix $\rho_{n,n}(t,t) = -i\ G^<_{n,n'}(t,t')$ for $t = t'$ and $n = n'$, here $G^<_{n,n'}(t,t')$ is the lesser Green's function[45, 46, 53, 54, 55] on the dot including all the contributions from the leads. The lesser Green's function for the dot in the presence of the nanomechanical oscillator is given by

$$G^<_{n,n'}(t,t') = \sum_{n_0,n_0',\alpha} \int\int dt_1 dt_2 G^r_{n,n_0}(t,t_1)\Sigma^<_{n_0,n_0',\alpha}(t_1,t_2)G^a_{n_0',n'}(t_2,t'), \quad t, \text{ and } t' > 0 \tag{4.10}$$

whereas for t, and $t' < 0$, the $G^<_{n,n'}(t,t')$ is equal to zero, and $G^<_{n,n'}(t,t')$ includes all the information of the nanomechanical oscillator and electronic leads of the system, and n_0, n_0', n, n' are the oscillator indices. The lesser self-energy, $\Sigma^<_{n_0,n_0',\alpha}(t_1,t_2)$, contains electronic and oscillator contributions. The electronic contributions are non-zero only when t_1 and $t_2 > 0$. As the oscillator is initially in its ground state, only the $n_0 = n_0' = 0$ term gives a non-zero contribution to the lesser self-energy. The lesser self–energy for the dot may be written as

$$\Sigma^<_{0,0,\alpha}(t_1,t_2) = V^*_\alpha(t_1) g^<_{\alpha,\alpha}(t_1,t_2) V_\alpha(t_2), \tag{4.11}$$

with

$$g^<_{\alpha,\alpha}(t_1,t_2) = \frac{1}{N}\sum_j g^<_{\alpha,j}(t_1,t_2) = \int_{-\infty}^{+\infty} d\varepsilon_\alpha f(\varepsilon_\alpha) 2i n_\alpha B_m \exp[-i(\varepsilon_\alpha + m\hbar\omega)(t_1 - t_2)], \tag{4.12}$$

where B_m is the Boltzmann factor. We are going to consider that temperature is zero in the leads. So, we assume, when the oscillator appears in the leads it will always be in its ground state such that $m = 0$ ($B_m = \delta_{m,0}$) and the Fermi distribution function can be replaced with the theta function which in turn limits the integral. $f(\varepsilon_\alpha)$ is the Fermi distribution functions of the left and right leads, which have different chemical potentials under a voltage bias. For the present case of zero temperature the lesser self–energy may be recast in terms of the Heaviside step function $\theta(x)$ as

$$\Sigma^{<}_{0,0,\alpha}(t_1,t_2) = \mathrm{i}\Gamma_\alpha \int_{-\infty}^{+\infty} \frac{d\varepsilon_\alpha}{2\pi} \theta\left(\epsilon_{\mathrm{F}\alpha} - \varepsilon_\alpha\right) \theta(t_1)\theta(t_2) \exp[-i\varepsilon_\alpha(t_1 - t_2)]\,, \tag{4.13}$$

where $\Sigma^{r,(a),(<)}_{0,0,\alpha}(t_1,t_2)$ all are non-zero only when both the times (t_1,t_2) are positive $t_1, t_2 > 0$ and $\epsilon_{\mathrm{F}\alpha}$ is the Fermi energy on each of leads. Similarly one can calculate the greater self–energy as $\Sigma^{>}_{0,0,\alpha}(t_1,t_2) = -\mathrm{i}\Gamma_\alpha \int \frac{d\varepsilon_\alpha}{2\pi} \theta(t_1)\theta(t_2) \exp[-i\varepsilon_\alpha(t_1 - t_2)][1 - f(\varepsilon_\alpha)]\,.$

The density matrix $\rho_{n,n}(t,t)$ can be calculated by using Eqs. (4.6), (4.7), (4.8), (4.9) and (4.13) into Eq. (4.10) at $t = t'$ and $n = n'$ as

$$\begin{aligned}\rho_{n,n}(t,t) = -i \sum_{\alpha,m,k} \int_0^t \int_0^t dt_1 dt_2 \Phi_{n,m}\Phi^*_{0,m} \exp[-i(\varepsilon_m - i\Gamma)(t - t_1)] \\ \times \{\mathrm{i}\Gamma \int_{-\infty}^{\epsilon_{F\alpha}} \frac{d\varepsilon_\alpha}{2\pi} \exp[-i\varepsilon_\alpha(t_1 - t_2)\,\}\Phi_{0,k}\Phi^*_{n,k} \exp[-i(\varepsilon_k + i\Gamma)(t_2 - t)],\end{aligned} \tag{4.14}$$

Although $g^{r,(a)}(t_1,t_2)$ is non-zero for $t < 0$, it is never required due to the way it combines with $\Sigma^{r,(a),(<)}_{0,0,\alpha}(t_1,t_2)$. By carrying out the time integrations, the resulting expression is written as

$$\rho_{n,n}(t,t) = \frac{\Gamma}{2\pi}\sum_{\alpha,m,k}\int_{-\infty}^{\epsilon_{F\alpha}} d\varepsilon_\alpha \frac{\Phi_{n,m}\Phi^*_{0,m}\Phi_{0,k}\Phi^*_{n,k}}{(\varepsilon_\alpha - \varepsilon_k - i\Gamma)(\varepsilon_\alpha - \varepsilon_m + i\Gamma)} \tag{4.15}$$

$$\times \{1 + \exp[i(\varepsilon_k - \varepsilon_m + 2i\Gamma)t] - \exp[-i(\varepsilon_\alpha - \varepsilon_k - i\Gamma)t] - \exp[i(\varepsilon_\alpha - \varepsilon_m + i\Gamma)t]\}$$

The integral over the energy in the above equation is carried out[78]. The final result for the density matrix is written as

$$\rho_{n,n}(t,t) = \frac{\Gamma}{2\pi}\sum_{m,k}\frac{\Phi_{n,m}\Phi^*_{m,0}\Phi_{0,k}\Phi^*_{n,k}}{\varepsilon_k - \varepsilon_m + 2i\Gamma}[Y_L + Y_R + Z_L + Z_R], \tag{4.16}$$

where we have added the contribution from the right and the left leads, which can be written in terms of α as

$$Y_\alpha = (1 + \exp[i(\varepsilon_k - \varepsilon_m + 2i\Gamma)t])\,\{\frac{1}{2}\frac{\ln[(\epsilon_{\mathrm{F}\alpha} - \varepsilon_k)^2 + \Gamma^2]}{\ln[(\epsilon_{\mathrm{F}\alpha} - \varepsilon_m)^2 + \Gamma^2]}$$

$$+ i[\tan^{-1}[\frac{\varepsilon_{F\alpha} - \varepsilon_k}{\Gamma}] + \tan^{-1}[\frac{\varepsilon_{F\alpha} - \varepsilon_m}{\Gamma}] + \pi]\},$$

and

$$Z_\alpha = \{\exp[i(\varepsilon_k - \varepsilon_m + 2i\Gamma)t](-\,\mathrm{Ei}[it(\epsilon_{\mathrm{F}\alpha} - \varepsilon_k - i\Gamma)] + \mathrm{Ei}[-it(\epsilon_{\mathrm{F}\alpha} - \varepsilon_m + i\Gamma)])$$

$$+ \mathrm{Ei}[it(\epsilon_{\mathrm{F}\alpha} - \varepsilon_m + i\Gamma)] - \mathrm{Ei}[-it(\epsilon_{\mathrm{F}\alpha} - \varepsilon_k - i\Gamma)]\},$$

with $\epsilon_{\mathrm{F}\alpha}$ being the right and the left Fermi levels and Ei (x) the exponential integral function. Special care is required in evaluating the Ei(x) to choose the correct Riemann sheets in order to make sure that these functions are consistent with the initial conditions $\rho(0) = 0$ and are continuous functions of time and chemical potential.

Now using equation (4.16), the dot population may be written as

$$\rho(t) = \sum_n \rho_{n,n}(t,t) = \frac{\Gamma}{2\pi} \sum_{m,k} \frac{\Phi_{n,m}\Phi^*_{m,0}\Phi_{0,k}\Phi^*_{n,k}}{\varepsilon_k - \varepsilon_m + 2i\Gamma}[Y_L + Y_R + Z_L + Z_R]. \tag{4.17}$$

4.4 Time-dependent Current from lead α

The particle current I_α into the interacting region from the lead is given by the expectation value of the current operator, $I_\alpha = Tr(\rho \hat{I}_\alpha)$ [46, 47, 53, 54, 55], where

$$\hat{I}_\alpha = \frac{ie}{\hbar} \sum_j \{V_{0\alpha} c_0^\dagger c_{\alpha j} - c_{\alpha j}^\dagger c_0 V_{\alpha 0}\} \tag{4.18}$$

and the final result for the current through each of the leads is written as (See Appendix A)

$$I_\alpha(t) = \frac{e\Gamma}{2\pi\hbar} \sum_m \Phi_{0,m}\Phi^*_{0,m}\{I_{1,\alpha} + I_{2,L} + I_{2,R}\}, \tag{4.19}$$

$$I_{1,\alpha} = [(2\tan^{-1}[\frac{\epsilon_{\mathrm{F}\alpha} - \varepsilon_m}{\Gamma}] + \frac{\pi}{2}) - i\{\mathrm{Ei}[it(\epsilon_{\mathrm{F}\alpha} - \varepsilon_m + i\Gamma)] - \mathrm{Ei}[-it(\epsilon_{\mathrm{F}\alpha} - \varepsilon_m - i\Gamma)]\}],$$

$$\begin{aligned} I_{2,\alpha} = \{&-(1 + \exp[-2\Gamma t])\,(\tan^{-1}[\frac{\varepsilon_{F\alpha} - \varepsilon_m}{\Gamma}] + \frac{\pi}{2}) \\ &+ \frac{i}{2}\exp[-2\Gamma t](-\mathrm{Ei}[it(\epsilon_{\mathrm{F}\alpha} - \varepsilon_m - i\Gamma)] + \mathrm{Ei}[-it(\epsilon_{\mathrm{F}\alpha} - \varepsilon_m + i\Gamma)]) \\ &+ \frac{i}{2}(\mathrm{Ei}[it(\epsilon_{\mathrm{F}\alpha} - \varepsilon_m + i\Gamma)] - \mathrm{Ei}[-it(\epsilon_{\mathrm{F}\alpha} - \varepsilon_m - i\Gamma)])\}, \end{aligned}$$

where in calculating the left current we need $I_{1,L}$ and both the contributions $I_{2,L}, I_{2,R}$ and for the right current we need $I_{1,R}$ and both $(I_{2,L}, I_{2,R})$. As before, special care is required in

evaluating the Ei(x) to choose the correct Riemann sheets in order to make sure that these functions are consistent with the initial conditions $I_\alpha(t) = 0$ and are continuous functions of time and chemical potential.

4.5 Average energy and the Fano factor

To calculate the energy transferred from the electrons to the nanomechanical oscillator, we return to the density matrix ($\rho_{n,n}(t,t)$) given in Eq. (4.16). We may therefore use the lesser Green's function or density matrix to calculate the energy transferred to the oscillator as

$$E_{ph} =< n\hbar\omega >= \frac{\sum\limits_n n\hbar\omega\rho_{n,n}(t,t)}{\sum\limits_n \rho_{n,n}(t,t)}. \tag{4.20}$$

In order to further characterize the state of the nanomechanical oscillator we investigate the Fano factor for the change of average occupation number, $< n >$, as a function of time. The corresponding relation for the Fano factor[79, 80] is given by

$$F_n = \frac{\langle n^2\rangle - \langle n\rangle^2}{\langle n\rangle}, \tag{4.21}$$

where $< n >= \frac{\sum\limits_n n\rho_{n,n}(t,t)}{\sum\limits_n \rho_{n,n}(t,t)}$, and $< n^2 >= \frac{\sum\limits_n n^2\rho_{n,n}(t,t)}{\sum\limits_n \rho_{n,n}(t,t)}$, with the average evaluated using the diagonal element of the density matrix on the quantum dot.

4.6 Discussion of Results

The dot population, net current through the system, total current into the system, average energy and Fano factor of a resonant tunnel junction coupled to a nanomechanical

oscillator are shown graphically as a function of time for different values of coupling strength, tunneling rate, and voltage bias. The following parameters[10, 14, 16, 28, 56, 57, 61, 62] were employed: the single energy level of the dot $\epsilon_0 = 0.5$, and the characteristic frequency of the oscillator $\hbar\omega = 0.1$. These parameters will remain fixed for all further discussions and have same dimension as of $\hbar\omega$. We are interested in small and large values of tunneling from the leads, different values of the coupling strength between the electrons and the nanomechanical oscillator, and of the left chemical potential $0 \leq \epsilon_{\mathrm{F}L} \leq 1$. The nanomechanical oscillator induced resonance effects are clearly visible in the numerical results. It must be noted that we have obtained these results in the regime of both strong and zero or weak coupling between the nanomechanical oscillator and the electrons on the dot. The tunneling of electrons between the leads and the dot is considered to be symmetric ($\Gamma_R = \Gamma_L$) and we assume that the leads have constant density of states. The dot population is shown in Fig. 4.1, as a function of time in order to see the transient and steady state dynamics of the system. We consider here empty, half full and occupied states of the system for fixed values of $\Gamma = 0.1$, $\eta = 0.05$, by choosing the right and the left Fermi levels pairs (0, 0), (0, 1) and (1, 1) respectively. Firstly, when both the Fermi levels are below the dot energy then the dot population rises initially for a short time and for long times settles at a small but finite value. This is not quite empty because the finite Γ allows some tunneling onto the dot. Secondly, when the left Fermi level is above the dot energy then the dot population settles in a partially full (half full) state. Thirdly, when both the Fermi levels are above the dot energy, it is almost full for long time but not quite full, again due to the dot coupling with the leads. These results are consistent with the particle-hole symmetry of the system

as the empty state of the system is not empty and the occupied state is not completely full, while the partially full is roughly half full.

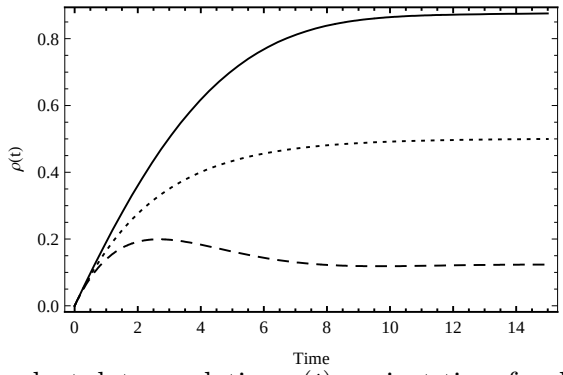


Figure 4.1: Time-dependent dot population $\rho(t)$ against time for different pairs of the right and the left Fermi energies (0,0) (empty), (0,1)(half full), (1,1)(partially full). Parameters: $\epsilon_0 = 0.5, \hbar\omega = 0.1, \Gamma = 0.1, \eta = 0.05$. Units: all the parameters have the same dimension as $\hbar\omega$.

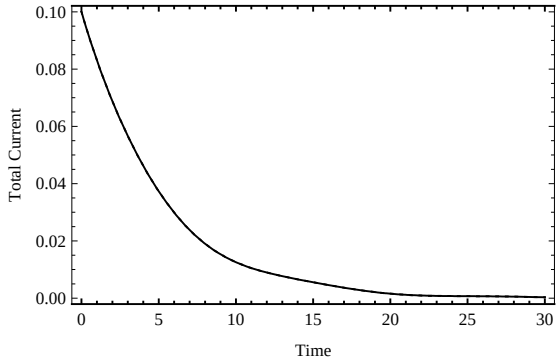


Figure 4.2: Total current $(I_L(t) + I_R(t))$ flowing onto the dot as a function of time for fixed values of $\epsilon_0 = 0.5, \hbar\omega = 0.1, \Gamma = 0.1, \eta = 0.05, \epsilon_{FR} = 0, \epsilon_{FL} = 1$.This current (solid line) is equivalent to the rate of change of dot population $\frac{d}{dt}\rho(t)$ (dashed line) as a function of time for the same parameters as the current. In this figure, solid and dashed lines have same values at all points. Units: all the parameters have the same dimension as $\hbar\omega$.

In Fig. 4.2, we have shown the total current flowing onto the dot as a function of time for fixed values of $\Gamma = 0.1, \eta = 0.05, \epsilon_{\mathrm{F}R} = 0$, and of the left Fermi level 1. This current (solid line) is equivalent to the rate of change of the dot population (dashed line) for the same parameters. In this figure, we can not distinguish the solid and the dashed

line. This confirms that our analytical results are consistent with the equation of continuity, $I_L(t) + I_R(t) = \frac{d}{dt}\rho(t)$, and hence, with the conservation laws for all parameters.

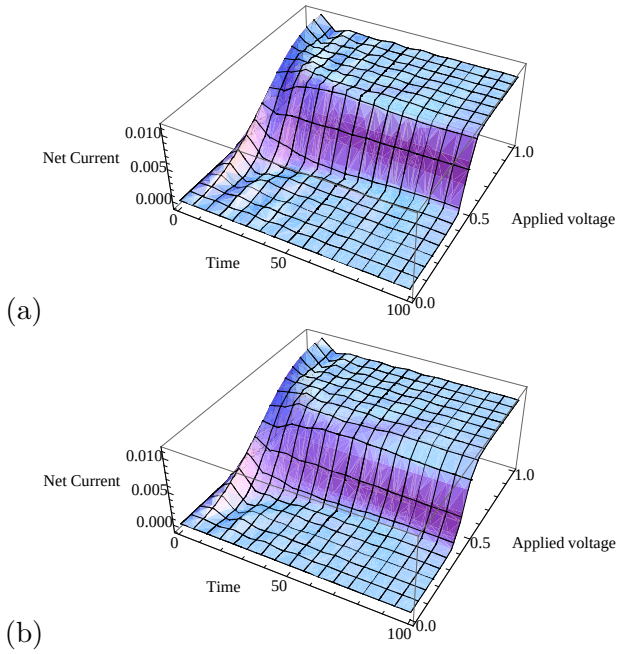
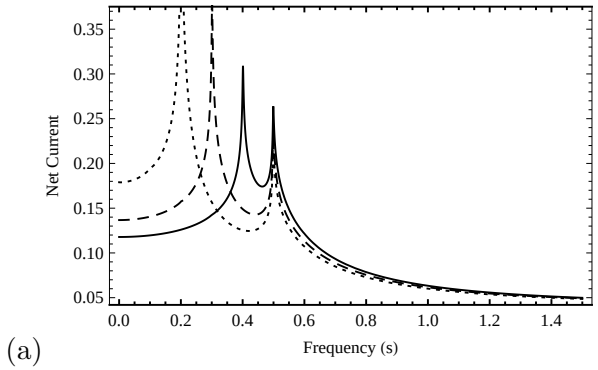


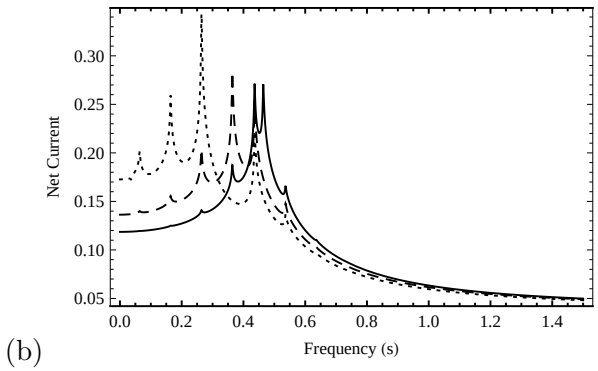
Figure 4.3: Net current $(I_L(t) - I_R(t))$ flowing through the system as a function of both time and of the left Fermi level for two different values of coupling strength: $\eta = 0.02$ (a) and $\eta = 0.1$ (b). Parameters: $\epsilon_0 = 0.5, \epsilon_{FR} = 0, \epsilon_{FL} = 1, \hbar\omega = 0.1, \Gamma = 0.01$. Units: all the parameters have the same dimension as $\hbar\omega$.

In fig. 4.3 a & b we have shown the net current $(I_L(t) - I_R(t))$ flowing through the system as a function of both time and of the left Fermi level for two different values of coupling strength: $\eta = 0.02$ and $\eta = 0.08$ and for fixed value of Γ. We observe simple oscillations in the net current flowing through the system for weak coupling strength and weak tunneling. With increasing coupling strength the structure of the oscillations becomes more complicated as shown in fig. 4.3b. In order to interpret this complicated structure, we have a two step discussion: firstly, we have plotted the net current as a function of time in Fig. 4.5 with fixed values of the Fermi level, $\epsilon_{\mathrm{F}L} = 1$, $\epsilon_{\mathrm{F}R} = 0$, tunneling energy,

$\Gamma = 0.01$ and for different values of coupling strength: $\eta = 0.02$ and $\eta = 0.08$. In this figure, in the limit of weak coupling the oscillations are again simple while for the strong coupling limit, there is a beating pattern in the oscillations. We note that the frequency of the simple oscillations is $(|\epsilon_{\mathrm{F}L} - \epsilon_0|)$ and these oscillations are present even in the limit of weak coupling. We conclude that this is a purely electronic process (plasmon oscillations). In order to gain a better understanding of the oscillations we consider the Fourier/Laplace transform of the current, $\tilde{I}(s) = \int_0^\infty \mathrm{e}^{\mathrm{i}st} I(t)\,\mathrm{d}t$, where $I(t) = I_L(t) - I_R(t)$.



(a)



(b)

Figure 4.4: Fourier/Laplace transform of the net current $\left|s\left[\tilde{I}_L(s) - \tilde{I}_R(s)\right]\right|^2$ flowing through the system as a function of frequency s for three different values of the left Fermi level $\epsilon_{\mathrm{F}L} = 0.7(\text{dotted line}), 0.8(\text{dashed line}), 0.9(\text{solid line})$ and coupling strength, $\eta = 0.01$ (fig. 4.4a) and $\eta = 0.08$ (fig. 4.4b). Parameters: $\epsilon_0 = 0.5, \epsilon_{FR} = 0, \hbar\omega = 0.1, \Gamma = 0.001$. Units: all the parameters have the same dimensions as $\hbar\omega$.

Here we have plotted $\left|s\tilde{I}(s)\right|^2$, which has the advantages that it suppresses a strong peak at s=0 while making it easier to relate the $s \to 0$ and $s \to \infty$ limits to $t \to \infty$ and $t \to 0$ respectively. We expect to see a peak at any frequency where there is an oscillation in $I(t)$, independently of the phase of that oscillation.

From fig. 4.4a, for weak coupling, we see 2 peaks, which are easily associated with electron and hole oscillations with frequencies $s = |\epsilon_{\rm F} - (\epsilon_0 - \Delta)|$. With increased coupling, fig. 4.4b, we observe additional features at multiples of ω to the left of the electron peak and to the right of the hole peak, which we can associate with the creation of phonons. The corresponding "anti-Stokes" features are absent as we are working at $T = 0$. Hence we may conclude that the beats in fig.4.5 are only indirectly due to the oscillator, through Δ: the beating is due to the difference between the electron and hole oscillations. Secondly, in Fig. 4.6, we have plotted the net current for fixed values of $\epsilon_{{\rm F}L} = 1$, $\epsilon_{{\rm F}R} = 0$, tunneling energy, $\Gamma = \hbar\omega$ and for different values of coupling strength: $\eta = 0.02$ and $\eta = 0.08$. We have found that in the regime ($\Gamma \geq \hbar\omega$), the effects of the oscillator are not apparent and the period of the nanomechanical oscillator can not be resolved. Why can the period of the oscillator not be resolved by the electrons in this limit? In this regime, electrons spend less time on the dot than the period of the oscillator. Therefore, electrons do not resolve the period of the nanomechanical oscillator. Now we will focus only in the regime of small tunneling $\Gamma < \hbar\omega$, for further discussion in order to analyze the dynamics of the nanomechanical oscillator and the effects of coupling between the electrons and the nanomechanical oscillator.

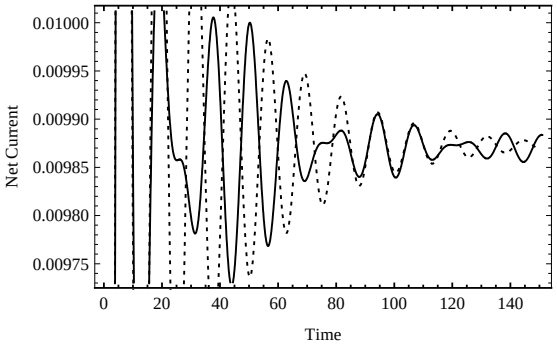


Figure 4.5: Net current $(I_L(t) - I_R(t))$ flowing through the system as a function of time for two different values of coupling strength: $\eta = 0.02$ (dotted line), and 0.08 (solid line). Parameters: $\epsilon_0 = 0.5, \epsilon_{FR} = 0, \epsilon_{FL} = 1, \hbar\omega = 0.1, \Gamma = 0.01$. Units: all the parameters have the same dimension as $\hbar\omega$.

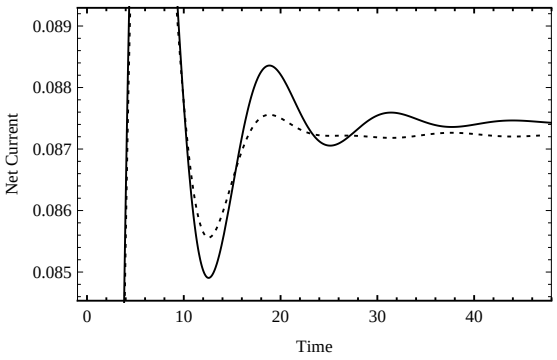


Figure 4.6: Net current $(I_L(t) - I_R(t))$ flowing through the system as a function of time for two different values of coupling strength: $\eta = 0.02$ (dotted line), and 0.08 (solid line), and $\Gamma = 0.1$. All the parameters are the same as in FIG.4.5 and have the same dimension as $\hbar\omega$.

Next we have shown the average energy of the nanomechanical oscillator as a function of time and of the left Fermi energy in Fig. 4.7 & 4.8 for fixed values of tunneling $\Gamma = 0.01$, $\epsilon_{\mathrm{F}R} = 0$, and for different values of coupling strength $\eta = 0.02$, $\eta = 0.08$.

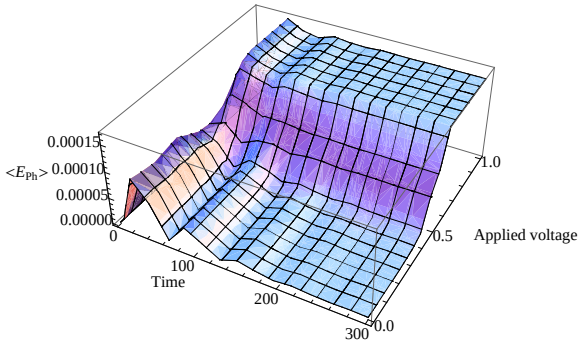


Figure 4.7: Average energy transferred to the oscillator as a function of time and left Fermi level for fixed values of $\epsilon_0 = 0.5, \epsilon_{FR} = 0, \Gamma = 0.01$ and for different values of coupling strength: $\eta = 0.02$. Units: all the parameters have the same dimension as $\hbar\omega$.

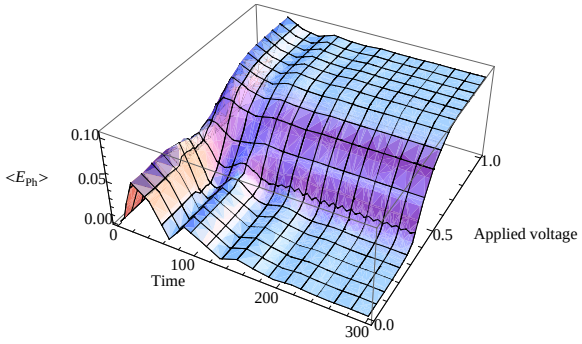


Figure 4.8: Average energy transferred to the oscillator as a function of time and left Fermi level for fixed values of $\epsilon_0 = 0.5, \epsilon_{FR} = 0, \Gamma = 0.01$ and for different values of coupling strength: $\eta = 0.08$. Units: all the parameters have the same dimension as $\hbar\omega$.

We found damped oscillations for short times and constant energy for long times. This constant average energy increases with increasing Fermi level. Why have we found this particular type of structure? We know that the nanomechanical oscillator potential seen by the electrons on the dot is independent of time when the oscillator is in any of its pure eigenstates. Otherwise, when the oscillator is not in a pure state, the potential seen by the electrons is time dependent. In the former case, the electrons are scattered elastically

by the time independent potential and in the latter case the scattering process is inelastic because the time dependent potential allow the transfer of energy between the two. We observe that the constant average energy also has steps as a function of the left Fermi level which become more pronounced with increasing coupling strength. Hence, the oscillatory part of the behavior of the mechanical oscillator is damped by coupling with the electrons on the dot but the constant part is not. The damping mechanism in the transient dynamics is due to transfer of energy from the nanomechanical oscillator to the electrons on the dot while when the oscillator is in any of the pure eigenstates then there is no mechanism for the transfer of energy between the two. This same physical phenomenon also applies to the net current flowing through the dot as well. This appears to be a specifically new quantum phenomenon in the study of nanomechanical systems.

Can we compare this quantum phenomena with the classical mechanical oscillator[28]? Yes, the nanomechanical oscillator has to enter the classical regime in the limit of small $\hbar$. For this, we study the dynamics of the quantum oscillator in the classical limit, in which $\hbar \to \hbar'$ in the mechanical oscillator part of the Hamiltonian given in Eq. (3.2) goes to zero, where $\hbar'\omega < \Gamma$. To see this, we have plotted the average energy as a function of $Y = \frac{\hbar'}{\hbar}$ in the nanomechanical part of the system in Fig. 4.9 for fixed values of tunneling $\Gamma = 1$, $\epsilon_{\mathrm{F}R} = 0, \epsilon_{\mathrm{F}L} = 1$ and coupling strength $\eta = 0.05$. We found that the average energy of the quantum nanomechanical oscillator scales as $\hbar^2$. We set the average energy in the limit $\hbar' \to 0$ to see what happen to the system for long time. It implies that in this limit, the energy transferred to the nanomechanical oscillator is zero for long time. Hence, we conclude that the long time dynamics of the classical mechanical oscillator is always zero.

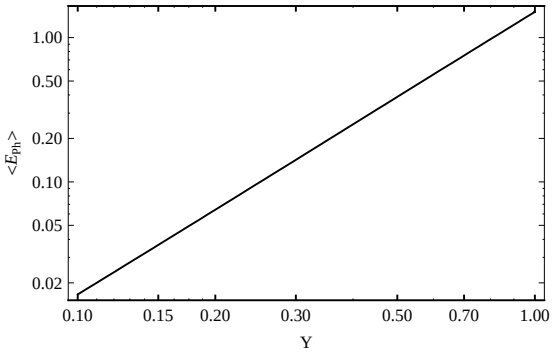


Figure 4.9: Average energy transferred to the oscillator as a function of $\frac{\hbar'}{\hbar}$ and for fixed values of $\epsilon_0 = 0.5, t = 1000, \epsilon_{FR} = 0, \epsilon_{FL} = 1, \Gamma = 1$ and $\eta = 0.02$. Units: all the parameters have the same dimension as $\hbar\omega$.

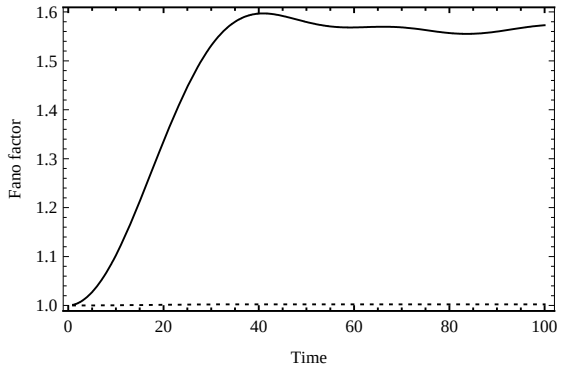


Figure 4.10: Fano factor as a function of time for two different values of coupling strength: $\eta = 0.02$ (dotted line), and 0.08 (solid line). Parameters: $\epsilon_0 = 0.5, \epsilon_{FR} = 0, \epsilon_{FL} = 1, \hbar\omega = 0.1, \Gamma = 0.01$. Units: all the parameters have the same dimension as $\hbar\omega$.

Finally, we have shown the Fano factor as a function of time in figure 4.10 for two different values of $\eta = 0.02, \eta = 0.08$ and for fixed values of $\Gamma = 0.01, \epsilon_{\mathrm{F}R} = 0, \epsilon_{\mathrm{F}L} = 1$. In the limit of weak coupling, the nanomechanical oscillator shows thermal like behavior and poissonian statistics while in the limit of strong coupling its dynamics is non-thermal which leads to super-poissonian statistics. In this figure, the short time behavior is always

thermal, but this is trivial as the nanomechanical oscillator is initially in its ground state.

In conclusion, we have found pure and superposition states in our results which confirm the quantum dynamics of our model with the following justifications: in a classical mechanical oscillator model[28] all states give rise to a time dependent potential. Hence, all states of the classical mechanical oscillator are damped. Thus, we confirm the new quantum dynamics of the nanomechanical oscillator that will be helpful for further experiments beyond the classical limit to develop better understanding of NEMS devices.

4.7 Conclusions

In this chapter, we analyzed the time-dependent quantum transport of a resonant tunnel junction coupled to a nanomechanical oscillator by using the nonequilibrium Green's function approach without treating the electron phonon coupling as a perturbation. We have derived an expression for the full density matrix or the dot population and discuss it in detail for different values of the coupling strength and the tunneling rate. We derive an expression for the current to see the effects of the coupling of the electrons to the oscillator on the dot and the tunneling rate of electrons to resolve the dynamics of the nanomechanical oscillator. This confirms that electrons resolve the dynamics of nanomechanical oscillator in the regime $\tau_e > \tau_{Osc}$ while they do not in the opposite case $\tau_e < \tau_{Osc}$. Furthermore, we discuss the average energy transferred to oscillator as a function of time. We also discuss the Fano factor as a function of time, which shows thermal behavior and poissonian to non-thermal and super-poissonian behavior. We have found new dynamics of the nanomechanical oscillator: pure and superposition states, which are never present in a classical oscillator. These results

suggest further experiments for NEMS to go beyond the classical dynamics.

Chapter 5

Time-dependent transport via a quantum shuttle

5.1 Introduction

We introduce an interesting application of NEMS devices in this chapter, where an oscillating mechanical object transfer an electron per cycle between two leads. We present a theoretical study of time-dependent transport via a quantum shuttle within the non-equilibrium Green's function technique discussed in chapter 2. An arbitrary voltage is applied to the tunnel junction and electrons in the leads are considered to be at zero temperature. The transient and the steady state behavior of the system is considered here in order to explore the quantum dynamics of the shuttle device as a function of time and applied bias. The properties of the phonon distribution of the oscillating dot coupled to the electrons are investigated using a non-perturbative approach. We derive a relation for the

oscillator momentum charge density correlation function which is an interesting physical example for the visualization of shuttling phenomenon. We consider the crossover between the tunneling and shuttling regimes for different values of the key parameters as a function of applied bias and time. We also consider the energy transferred from the electrons to the oscillating dot as a function of time. This will provide useful insight for the design of experiments aimed at studying the quantum behavior of a shuttling device.

5.2 Formulation

The model consists of a moveable quantum dot suspended between the right and the left semi-infinite leads[16, 32, 38]. This model is a close analogue to the dot attached to the tip of a cantilever or connected to the leads by some soft material or embedded into an elastic matrix. In this model the center of mass of the nanoparticle is confined to a harmonic potential. In the most recent experimental realizations[31] of a quantum dot shuttle (QDS) at room temperature, due to its small diameter, the quantum dot has a very small capacitance and thus has a charging energy that exceeds the thermal energy k_BT. Due to Coulomb blockade[30] we consider only one excess electron can occupy the device. We consider the electronic state of the central quantum dot as empty or charged (a two level system). The tunneling amplitude of the electrons depends exponentially on the position of the central island and thus electrons can tunnel between the leads and the quantum dot. This is due to the exponentially decreasing/increasing overlapping of the electronic wave functions.

The coupled system is described by a single electronic level of energy ϵ_0 and a

nanomechanical oscillator with frequency ω and mass μ. An electrostatic force (eE) acts on the mechanical grain when the quantum dot is charged and gives the electrical influence on the nanomechanical dynamics of the system. The electric field E is generated by the voltage drop between the left and the right leads. In our model, though, it is kept as an external parameter. The quantum dynamics of the nanomechanical oscillator is represented in terms of position and momentum operators. In terms of creation and annihilation operators for the nanomechanical oscillator excitations the Hamiltonian of our simple system is same as in chapter 3 except the hopping term, which is now position and time dependent and is written as[28, 32, 37, 38, 39, 40]

$$H_{\text{leads-dot}} = \frac{1}{\sqrt{N}} \sum_{j,\alpha} V_\alpha(t) \left(c^\dagger_{j,\alpha} c_0 + c^\dagger_0 c_{j,\alpha} \right), \tag{5.1}$$

where N is the total number of states in the lead, $\alpha = L, R$, and j represents the channels in one of the leads. We include the time-dependent hopping $V_\alpha(t)$ to enable us to connect the leads α to the moving dot at a finite time. An advantage of this approach (joining of leads to the dot at t=0) is that it eliminates the one major criticism of Keldysh approach, namely the lack of any clear initial conditions. $V_\alpha(t)$ is written as

$$V_\alpha(t) = V_0(t) e^{\mp \xi \hat{X}} \tag{5.2}$$

where $\xi = \frac{1}{\zeta}$ is the inverse tunneling length (ζ), $-$ stands for $V_L(t) = V_0(t) e^{-\xi \hat{X}}$ and $+$ stands for $V_R(t) = V_0(t) e^{+\xi \hat{X}}$. For the time-dependent dynamics, we shall focus on sudden joining of the leads to the moving dot at $t = 0$, which means $V_0(t) = V\theta(t)$, where $\theta(t)$ is the Heaviside unit step function. The displacement operator is given as

$$\hat{X} = \frac{l(b^\dagger + b)}{\sqrt{2}} \tag{5.3}$$

5.3 The self-energy and the Green's function

In order to calculate the analytical solutions and to discuss the numerical results of the transient and steady state quantum dynamics of the nanomechanical shuttle device, our focus in this section is to derive an analytical relation for the time-dependent effective self energy and the corresponding Green's function. The effective self-energy represents the contribution to the moving dot energy, due to interactions between the oscillating dot and the leads it is coupled to. In obtaining these results we use the wide-band approximation only for the simplicity, although the method we are using does not rely on this approximation. The retarded self-energy of the oscillating dot due to each lead is given by (see Appendix B)

$$\mathbf{\Sigma}^r(t,t_1) = -\frac{i\Gamma_\alpha}{2}\theta(t_2)\delta(t-t_1)\mathbf{\Sigma}^r(\mp) \tag{5.4}$$

with the matrix $\mathbf{\Sigma}^r(\mp)$

$$\begin{aligned}\mathbf{\Sigma}^r(\mp) &\equiv \Sigma^r_{n_0,n_0'}(\mp) \qquad (5.5)\\ &= \exp[(\gamma \mp x)^2 - x^2]\sqrt{\frac{2^{|n_0'-n_0|}\min[n_0,n_0']!}{\max[n_0,n_0']!}}(\mp\gamma)^{|n_0'-n_0|}L^{|n_0'-n_0|}_{\min[n_0,n_0']}(-2\gamma^2),\end{aligned}$$

where $\mathbf{\Sigma}^a(t,t_1) = (\mathbf{\Sigma}^r(t,t_1))^*$ with α representing the L or R leads, the dimensionless tunneling length $\gamma = \frac{\xi l}{\sqrt{2}}$, $x = \frac{x_0}{l}$, and the $-,+$ signs stands for the left and the right leads respectively. In the present representation, the effective self energy is given in terms of a matrix due to the position dependence of the tunneling matrix elements.

The final result for the lesser self energy matrix may be written as

$$\begin{aligned}\mathbf{\Sigma}^{<}(t_1,t_2) &= i\Gamma_\alpha\theta(t_1)\theta(t_2)\times\mathbf{\Sigma}^{<}(\mp) \\ &\times\int_{-\infty}^{\epsilon_{F\alpha}}\frac{d\varepsilon_\alpha}{2\pi}\exp[-i\varepsilon_\alpha(t_1-t_2)],\end{aligned} \tag{5.6}$$

where the matrix element of the lesser self-energy is written as

$$\mathbf{\Sigma}^{<}(\mp) = \mathbf{V}^{<}(\mp)[\mathbf{V}^{<}(\mp)]^{\intercal}, \tag{5.7}$$

where $\mathbf{V}^{<}(\mp)\equiv V_n^{<}(\mp)=\frac{\exp[\frac{-x^2}{2}+(\frac{\gamma\mp x}{2})^2]}{\sqrt{n!}}[\mp(\frac{\gamma\pm x}{2})]^n$.

This model represent the interplay between two physical time scales of the system, i.e., the oscillator frequency (ω), and the tunneling rate (Γ_α). The model also shows very interesting interplay between three physical length scales of the system, i.e., dimensionless tunneling length (γ), zero point amplitude (l) and the displaced oscillator equilibrium position to the zero point amplitude of the oscillator (x), which are actually affected by the weak and strong coupling dynamics and small and large tunneling rate.

We solve Dyson's equation using $H_{\text{dot-leads}}$, as a perturbation in terms of matrix representation. In the presence of the oscillator, the matrix of the retarded, $\mathbf{G}^r(t,t_1)$ and advanced, $\mathbf{G}^a(t_2,t')$ Green's functions on the dot, with the phonon states may be written as

$$\begin{aligned}\mathbf{G}^r(t,t_1) &= -i\theta(t-t_1)\exp[-i(\mathbf{M})(t-t_1)],\quad t_1>0 \\ &\equiv G^r_{m,n_0}(t,t_1)\end{aligned} \tag{5.8}$$

where $\mathbf{G}^r$ and $\mathbf{M}$ are matrices in nanomechanical oscillator space with indices m, n_0, and

the matrix $\mathbf{M}$ may be written as

$$\mathbf{M} \equiv (E_m \delta_{m,n_0} + \Sigma^r_{m,n_0}), \qquad E_m = \epsilon_0 + m\hbar\omega - \Delta, \tag{5.9}$$

$$\begin{aligned} \mathbf{G}^a(t_2,t') = (\mathbf{G}^r(t',t_2))^* &= +i\theta(t'-t_2)\exp[-i(\mathbf{M}^*)(t_2-t')], \quad t_2 > 0 \\ &\equiv G^a_{n_1,k}(t_2,t') \end{aligned} \tag{5.10}$$

The above Eqs. (5.4), (5.6), (5.8), and (5.10) will be the starting point of our examination of the time-dependent response of the coupled system. These functions are the essential ingredients for theoretical consideration of such diverse problems as low and high voltage, coupling of electron and phonons, transient and steady state phenomena.

5.4 The Density matrix $\rho_{n,n'}(t,t)$ and the correlation function

The density matrix is related to the lesser Green's function through $\rho_{n,n'}(t,t) = -iG^<_{n,n'}(t,t')$ at $t' = t$, where the $G^<_{n,n'}(t,t')$ is the lesser Green's function on the oscillating dot including all the contribution from the leads. The lesser Green's function[46, 47, 53, 54, 55] for the dot in the presence of the nanomechanical oscillator on the dot, with phonon states in the representation of the unoccupied dot, may be written as

$$\begin{aligned} G^<_{n,n'}(t,t') &= \sum_{m,n_0,n_1,k} \int_0^t \int_0^{t'} dt_1 dt_2 \Phi_{n,m} G^r_{m,n_0}(t,t_1) \Sigma^<_{n_0,n_1}(t_1,t_2) G^a_{n_1,k}(t_2,t') \Phi^*_{n',k}, \quad t \text{ and } t' > 0, \\ &\equiv \int_0^t \int_0^{t'} dt_1 dt_2 \mathbf{\Phi} \mathbf{G}^r(t,t_1) \mathbf{\Sigma}^<(t_1,t_2) \mathbf{G}^a(t_2,t') \mathbf{\Phi}^\dagger \end{aligned} \tag{5.11}$$

whereas for t and $t' < 0$, the $G^<_{n,n'}(t,t')$ is equal to zero and $\mathbf{\Phi} \equiv \Phi_{n,m}$. $G^<_{n,n'}(t,t')$ includes all the information for the nanomechanical oscillator and electronic leads of the system, and

m, k, n_0, n_1, n, n' are the oscillator indices. The lesser self-energy, $\Sigma^{<}_{n_0,n_1}(t_1, t_2)$, contains electronic and oscillator contributions. The electronic contributions are non-zero only when t_1 and $t_2 > 0$. The retarded Green's function, $G^r_{m,n_0}(t, t_1)$, is represented as

$$\mathbf{G}^r(t, t_1) = -i\theta(t - t_1)\exp[-i(\mathbf{M})(t - t_1)], \tag{5.12}$$

Using the eigenvalues and eigenfunctions of $\mathbf{M}$, the retarded Green's function may be written as

$$\mathbf{G}^r(t, t_1) = \mathbf{U}\mathbf{g}^r(t, t_1)\mathbf{U}^{\intercal}, \tag{5.13}$$

with eigenvectors $\mathbf{U}$ and its inverse such that $\mathbf{U}\mathbf{U}^{\intercal} = \mathbf{I}$ (not $\mathbf{U}\mathbf{U}^{\dagger} = \mathbf{I}$), and

$$\mathbf{g}^r(t, t_1) \equiv g^r_i(t, t_1) = -i\theta(t - t_1)\exp[-i(\epsilon_i - i\zeta_i)(t - t_1)]\delta_{i,j}, \tag{5.14}$$

where ϵ_i, ζ_i are the real and imaginary parts of the ith eigenvalue of the matrix $\mathbf{M}$. The advanced Green's function, $G^a_{n_1,k}(t_2, t)$, is written as

$$\mathbf{G}^a(t_2, t') = +i\theta(t' - t_2)\exp[-i(\mathbf{M}^*)(t_2 - t')], \tag{5.15}$$

In terms of eigenvalues and eigenfunctions, the advanced Green's function is written as

$$\mathbf{G}^a(t_2, t') = \mathbf{U}^*\mathbf{g}^a(t_2, t')\mathbf{U}^{\dagger}, \tag{5.16}$$

with eigenvectors $\mathbf{U}^*$ and its inverse such that $\mathbf{U}^*\mathbf{U}^{\dagger} = \mathbf{I}$, and

$$\mathbf{g}^a(t_2, t') \equiv g^a_i(t_2, t') = +i\theta(t' - t_2)\exp[-i(\epsilon_i + i\zeta_i)(t_2 - t')]\delta_{i,j}, \tag{5.17}$$

The lesser self-energy, $\mathbf{\Sigma}^{<}(t_1, t_2)$, in matrix space of the oscillator was derived in the previous section.

The lesser Green's function can be calculated by using Eqs. (5.6, 5.13 & 5.16) in equation (5.11) at $t = t'$ as

$$\begin{aligned} G^{<}_{n,n'}(t,t) &\equiv \int_0^t \int_0^t dt_1 dt_2 \mathbf{\Phi U} \mathbf{g}^r(t,t_1) \mathbf{U}^\intercal \mathbf{\Sigma}^{<}(t_1,t_2) \mathbf{U}^* \mathbf{g}^a(t_2,t) \mathbf{U}^\dagger \mathbf{\Phi}^\dagger, \\ &= \int_0^t \int_0^t dt_1 dt_2 \sum_{g,b,\alpha} [\mathbf{\Phi U}]_{n,g} \mathbf{g}^r(t,t_1) \mathbf{U}^\intercal \mathbf{\Sigma}^{<}(\mp) \Sigma^{<}_{\alpha}(t_1,t_2) \mathbf{U}^* \mathbf{g}^a(t_2,t) [\mathbf{\Phi U}]^\dagger_{b,n'}, \\ &= \sum_{g,b,\alpha} [\mathbf{\Phi U}]_{n,g} [\mathbf{U}^\intercal \mathbf{\Sigma}^{<}(\mp) \mathbf{U}^*]_{g,b} \chi^{\alpha}_{g,b}(t) [\mathbf{\Phi U}]^\dagger_{b,n'}, \end{aligned} \tag{5.18}$$

where the function $\chi^{\alpha}_{g,b}(t)$ is written as

$$\chi^{\alpha}_{g,b}(t) = \int_0^t \int_0^t dt_1 dt_2 g^r_g(t,t_1) \Sigma^{<}_{\alpha}(t_1,t_2) g^a_b(t_2,t) \tag{5.19}$$

which can be written as

$$\begin{aligned} \chi^{\alpha}_{g,b}(t) = \int_0^t \int_0^t dt_1 dt_2 \exp[-i(\epsilon_g - i\zeta_g)(t-t_1)] \\ \times \{\mathrm{i}\Gamma_\alpha \int_{-\infty}^{\epsilon_{F\alpha}} \frac{d\varepsilon_\alpha}{2\pi} \exp[-i\varepsilon_\alpha(t_1 - t_2)\,\} \exp[-i(\epsilon_b + i\zeta_b)(t_2 - t)], \end{aligned} \tag{5.20}$$

Although $\mathbf{G}^{r(a)}(t,t')$ is non-zero for $t < 0$, it is never required due to the way it combines with $\mathbf{\Sigma}^{r,(a),(<)}_{\alpha}(t,t')$. By carrying out the time integrations, the resulting expression is written as

$$\begin{aligned} \chi^{\alpha}_{g,b}(t) = \frac{i\Gamma_\alpha}{2\pi} \int_{-\infty}^{\epsilon_{F\alpha}} d\varepsilon_\alpha \frac{1}{(\varepsilon_\alpha - \epsilon_b - i\zeta_b)(\varepsilon_\alpha - \epsilon_g + i\zeta_g)} \\ \times \{1 + \exp[i(\epsilon_b - \epsilon_g + i(\zeta_b + \zeta_g))t] - \exp[-i(\varepsilon_\alpha - \varepsilon_b - i\zeta_b)t] - \exp[i(\varepsilon_\alpha - \varepsilon_g + i\zeta_g)t]\} \end{aligned} \tag{5.21}$$

For all values of b, g,and α, $\chi^{\alpha}_{g,b}(t=0)$ must be equal to zero. The integral over the energy in the above equation is carried out[78]. The final result for the above expression is written as

$$\chi^{\alpha}_{g,b}(t) = \frac{i\Gamma_{\alpha}}{2\pi}\{\frac{1}{\varepsilon_b - \varepsilon_g + i(\zeta_b + \zeta_g)}\}[Y^{\alpha}_{g,b} + Z^{\alpha}_{g,b}], \tag{5.22}$$

where we have added the contribution from the right and the left leads, which can be written in terms of α as

$$Y^{\alpha}_{g,b} = \left(1 + \exp[i(\varepsilon_b - \varepsilon_g + i(\zeta_b + \zeta_g))t]\right)\{\frac{1}{2}\frac{\ln[(\epsilon_{\mathrm{F}\alpha} - \varepsilon_b)^2 + \zeta_b^2]}{\ln[(\epsilon_{\mathrm{F}\alpha} - \varepsilon_g)^2 + \zeta_g^2]}$$
$$+ i[\tan^{-1}[\frac{\varepsilon_{F\alpha} - \varepsilon_b}{\zeta_b}] + \tan^{-1}[\frac{\varepsilon_{F\alpha} - \varepsilon_g}{\zeta_g}] + \pi]\},$$

and

$$Z^{\alpha}_{g,b} = \{\exp[i(\varepsilon_b - \varepsilon_g + i(\zeta_b + \zeta_g))t](-\operatorname{Ei}[it(\epsilon_{\mathrm{F}\alpha} - \varepsilon_b - i\zeta_b)] + \operatorname{Ei}[-it(\epsilon_{\mathrm{F}\alpha} - \varepsilon_g + i\zeta_g)])$$
$$+ \operatorname{Ei}[it(\epsilon_{\mathrm{F}\alpha} - \varepsilon_g + i\zeta_g)] - \operatorname{Ei}[-it(\epsilon_{\mathrm{F}\alpha} - \varepsilon_b - i\zeta_b)]\},$$

with $\epsilon_{\mathrm{F}\alpha}$ being the right and the left Fermi levels and $\operatorname{Ei}(x)$ the exponential integral function. Special care is required in evaluating the $\operatorname{Ei}(x)$ to choose the correct Riemann sheets in order to make sure that these functions are consistent with the initial conditions $\chi^{\alpha}_{g,b}(t=0) = 0$ and are continuous functions of time and chemical potential for each value of b,g, and α.

Now using equation (5.18), the dot population may be written as

$$\rho(t) = \sum_n \rho_{n,n}(t,t) = \sum_n -iG^{<}_{n,n}(t,t), \tag{5.23}$$

Next we derive a relation for the oscillator momentum charge density correlation function which is an interesting physical quantity to see the shuttling dynamics of the system. With the help of equation (5.18) the correlation function $\mathrm{Tr}< \widehat{p}\mathbf{G}^{<}(t,t) >$, where $\widehat{p} = \frac{il\mu\omega}{\sqrt{2}}(b^{\dagger} - b)$

is the momentum operator of the oscillator, may be written as

$$\mathrm{Tr}\left\langle \frac{il\mu\omega}{\sqrt{2}}(b^\dagger - b)\mathbf{G}^<(t,t)\right\rangle = \sum_n \left\langle \frac{il\mu\omega\sqrt{n}}{\sqrt{2}}\{G^<_{n-1,n}(t,t) - G^<_{n,n-1}(t,t)\}\right\rangle, \tag{5.24}$$

which we expect to be finite in case of shuttling as the dot should be occupied for positive momentum while zero for unoccupied dot. We note that the momentum correlation function depends on off-diagonal elements of the lesser Green's function, which can only be finite when the nanomechanical oscillator is in a mixed quantum state rather than in a simple eigenstate.

5.5 Time-dependent Current from lead α

The particle current I_α into the interacting region from the lead is given by the expectation value of the current operator, $I_\alpha = Tr(\rho\hat{I}_\alpha)$ [46, 47, 53, 54, 55], where

$$\hat{I}_\alpha = \frac{ie}{\hbar}\sum_j \{V_{0\alpha}c_0^\dagger c_{\alpha j} - c_{\alpha j}^\dagger c_0 V_{\alpha 0}\} \tag{5.25}$$

and the final result for the current through each of the leads is written as (See Ref. 51 for detail) as

$$\begin{aligned} I_\alpha(t) = \frac{e}{\hbar}\int_0^t dt_1 \mathrm{Tr}\{&\mathbf{G}^r(t,t_1)\mathbf{\Sigma}^<(t_1,t) + \mathbf{G}^<(t,t_1)\mathbf{\Sigma}^a(t_1,t) \\ &- \mathbf{\Sigma}^r(t,t_1)\mathbf{G}^<(t_1,t) - \mathbf{\Sigma}^<(t,t_1)\mathbf{G}^a(t_1,t)]\}, \\ &= \frac{e}{\hbar}(Z_1^\alpha + Z_2^\alpha) \end{aligned} \tag{5.26}$$

where Z_1^α is defined as

$$Z_1^\alpha \equiv \int_0^t dt_1 \mathrm{Tr}\{\mathbf{G}^r(t,t_1)\mathbf{\Sigma}^<(t_1,t) - \mathbf{\Sigma}^<(t,t_1)\mathbf{G}^a(t_1,t)\} \tag{5.27}$$

$$= \int_0^t dt_1 \mathrm{Tr}\{\mathbf{U}\mathbf{g}^r(t,t_1)\mathbf{U}^\intercal\mathbf{\Sigma}^<(\mp)\Sigma_\alpha^<(t_1,t) - \mathbf{\Sigma}^<(\mp)\Sigma_\alpha^<(t,t_1)\mathbf{U}^*\mathbf{g}^a(t_1,t)\mathbf{U}^\dagger\}$$

$$= [\sum_g \{[\mathbf{U}^\intercal\mathbf{\Sigma}^<(\mp)\mathbf{U}]_{g,g}\chi_g^\alpha(t) - \sum_g [\mathbf{U}^\dagger\mathbf{\Sigma}^<(\mp)\mathbf{U}^*]_{g,g}\left(\chi_g^\alpha(t)\right)^*\},$$

where $\chi_g^\alpha(t)$ is defined as

$$\chi_g^\alpha(t) = \int_0^t dt_1 g_g^r(t,t_1)\Sigma_\alpha^<(t_1,t) \tag{5.28}$$

$$= \frac{-i\theta(t-t_1)}{2\pi}\int_0^t dt_1 \exp[-i(\epsilon_g - i\zeta_g)(t-t_1)]i\Gamma_\alpha \int_{-\infty}^{\epsilon_{F\alpha}} d\varepsilon_\alpha \exp[-i\varepsilon_\alpha(t_1-t)$$

$$= \frac{i\Gamma_\alpha}{2\pi}\int_{-\infty}^{\epsilon_{F\alpha}} d\varepsilon_\alpha \frac{(1-\exp[-i(\varepsilon_\alpha - \epsilon_g + i\zeta_g)t])}{\varepsilon_\alpha - \epsilon_g + i\zeta_g}$$

$$= \frac{i\Gamma_\alpha}{2\pi}\{\ln[(\epsilon_{\mathrm{F}\alpha} - \varepsilon_g) + i\zeta_g] - \mathrm{Ei}[it(\epsilon_{\mathrm{F}\alpha} - \varepsilon_g + i\zeta_g)]\}$$

Hence, final result for Z_1^α is written as

$$Z_1^\alpha = \frac{i\Gamma_\alpha}{2\pi}\left\{\begin{array}{c} \sum_g [[\mathbf{U}^\intercal\mathbf{\Sigma}^<(\mp)\mathbf{U}]_{g,g}\{\frac{1}{2}\ln[(\epsilon_{\mathrm{F}\alpha} - \varepsilon_g) + i\zeta_g] - \mathrm{Ei}[it(\epsilon_{\mathrm{F}\alpha} - \varepsilon_g + i\zeta_g)]\}] \\ -\sum_b [\mathbf{U}^\dagger\mathbf{\Sigma}^<(\mp)\mathbf{U}^*]_{b,b}\{\frac{1}{2}\ln[(\epsilon_{\mathrm{F}\alpha} - \varepsilon_b) - i\zeta_b] - \mathrm{Ei}[-it(\epsilon_{\mathrm{F}\alpha} - \varepsilon_b - i\zeta_b)]\}] \end{array}\right\} \tag{5.29}$$

and Z_2^α is written as

$$
\begin{aligned}
Z_2^\alpha &\equiv \int dt_1 \mathrm{Tr}\{\mathbf{G}^<(t,t_1)\mathbf{\Sigma}^a(t_1,t) - \mathbf{\Sigma}^r(t,t_1)\mathbf{G}^<(t_1,t)\} \qquad (5.30)\\
&= \int dt_1 \mathrm{Tr}\left\{\mathbf{G}^<(t,t_1)\mathbf{\Sigma}^a(\mp)\frac{i\Gamma_\alpha}{2}\theta(t_1)\delta(t-t_1) + \mathbf{\Sigma}^r(\mp)\frac{i\Gamma_\alpha}{2}\theta(t_1)\delta(t-t_1)\mathbf{G}^<(t_1,t)\right\}\\
&= \mathrm{Tr}\left\{\frac{i\Gamma_\alpha}{2}\mathbf{G}^<(t,t)\mathbf{\Sigma}^a(\mp) + \frac{i\Gamma_\alpha}{2}\mathbf{\Sigma}^r(\mp)\mathbf{G}^<(t,t)\right\}\\
&= i\Gamma_\alpha \int_0^t\int_0^t dt_2 dt_3 \mathrm{Tr}\{\mathbf{G}^r(t,t_3)\mathbf{\Sigma}^<(\mp)\Sigma_\alpha^<(t_3,t_2)\mathbf{G}^a(t_2,t)\mathbf{\Sigma}^a(\mp)\}\\
&= i\Gamma_\alpha \int_0^t\int_0^t dt_2 dt_3 \mathrm{Tr}\{\mathbf{U}\mathbf{g}^r(t,t_3)\mathbf{U}^\intercal\mathbf{\Sigma}^<(\mp)\Sigma_\alpha^<(t_3,t_2)\mathbf{U}^*\mathbf{g}^a(t_2,t)\mathbf{U}^\dagger\mathbf{\Sigma}^a(\mp)\}\\
&= i\Gamma_\alpha\{\sum_{g,b,\alpha}[[\mathbf{U}^\dagger\mathbf{\Sigma}^a(\mp)\mathbf{U}]_{b,g}[\mathbf{U}^\intercal\mathbf{\Sigma}^<(\mp)\mathbf{U}^*]_{g,b}\chi_{g,b}^\alpha(t)\},
\end{aligned}
$$

where $\chi_{g,b}^\alpha(t)$ as in (5.22).

Now using Eqs. (5.22, 5.29 & 5.30) in equation (5.26), we arrive at the final result for the current through lead α as

$$
I_\alpha(t) = \frac{e}{\hbar}(Z_1^\alpha + Z_2^L + Z_2^R), \qquad (5.31)
$$

where in calculating the left current we need Z_1^L and both the contributions Z_2^L and Z_2^R and for the right current Z_1^L is replaced by Z_1^R. As before, special care is required in evaluating the $\ln(x)$ and $\mathrm{Ei}(x)$ to choose the correct Riemann sheets in order to make sure that these functions are consistent with the initial conditions $I_\alpha(t) = 0$ and are continuous functions of time and chemical potential.

5.6 Average energy

To calculate the energy transferred from the electrons to the nanomechanical oscillator, we return to the density matrix $\rho_{n,n}(t,t)$ given in Eq. (5.23). We may use the lesser Green's function or density matrix to calculate the energy transferred to the oscillator as

$$E_{Ph} =< n > \hbar\omega = \frac{\hbar\omega \sum_n n\rho_{n,n}(t,t)}{\sum_n \rho_{n,n}(t,t)} \tag{5.32}$$

where the average evaluated using the diagonal element of the density matrix on the oscillating quantum dot. Note that the normalization in equation (5.32) is required as the bare density matrix contains both electronic and oscillator contributions. The trace eliminates the oscillator part, leaving the electronic part.

5.7 Discussion of Results

The net $(I_L(t) - I_R(t))$ average current through the system, the oscillator momentum charge density correlation function $< \widehat{p}G^<(t,t) >$, total $(I_L(t) + I_R(t))$ average current into the system, and the average energy of an oscillating dot between the leads have been calculated as a function of time $(2\pi/\omega)$ for different values of tunneling length, tunneling rate, and voltage bias. The following parameters[10, 14, 16, 28, 56, 57, 61, 62] were employed: the single energy level of the dot $\epsilon_0 = 0.5$ and $\epsilon_{\mathrm{F}R} = 0$. These parameters will remain fixed for all further discussions and have same dimension as $\hbar\omega$. We are interested in small and large values of tunneling rates $(\Gamma_{L/R})$ from the leads, different values of the tunneling length (ζ) between the oscillating dot and the electrons, and of the left chemical potential $0 \leq \epsilon_{\mathrm{F}L} \leq 2$. The oscillating dot induced resonance effects are clearly visible in

the numerical results. The tunneling rate of the electrons between the leads and the dot is considered to be asymmetric ($\Gamma_R = \Gamma_L \exp[-\gamma x]$) and we assume that the leads have constant density of states. The values of the tunneling rates has been chosen such that when the dot is occupied and the zero point has moved to x_0, these values are reversed.

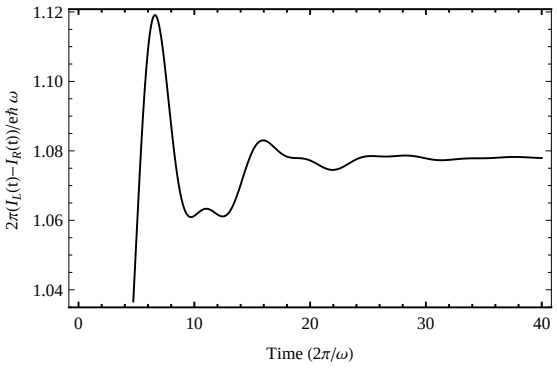


Figure 5.1: Time-dependent net average current $2\pi(I_L(t) - I_R(t))/e\hbar\omega, \epsilon_0 = 0.5, \epsilon_{FR} = 0, \epsilon_{FL} = 2, x_0 = 0.2l, \hbar\omega = 0.63, \Gamma_L = \hbar\omega/2\pi$, $\Gamma_R = \Gamma_L \exp[-\gamma x])$ and $\gamma = 0.5$. The electron per cycle behavior in this figure corresponds to the shuttling mechanism. Units: all the parameters have the same dimension as $\hbar\omega$.

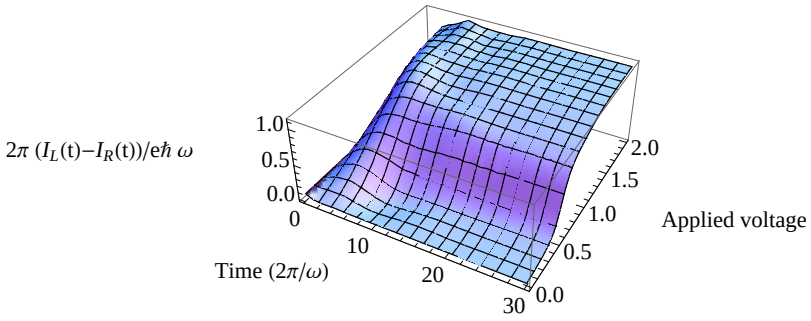


Figure 5.2: Net average current $(2\pi(I_L(t) - I_R(t))/e\hbar\omega)$ flowing through the system as a function of both time $(2\pi/\omega)$ and of the left Fermi level for same values of the parameters as in fig.5.1.

In Fig. 5.1 & 5.2 we have shown the net average current $2\pi(I_L(t) - I_R(t))/e\hbar\omega$ flowing through the system as a function of time $(2\pi/\omega)$ for fixed values of the Fermi

level, $\epsilon_{\mathrm{F}L} = 2$, $\epsilon_{\mathrm{F}R} = 0$, tunneling energy, $\Gamma_L = \hbar\omega/2\pi$, the characteristic energy of the oscillator $\hbar\omega = 0.63$, $\Gamma_R = \Gamma_L \exp[-\gamma x]$, $x_0 = 0.3l$ and finite $\gamma = 0.5$. This ($\gamma = 0.5$) is the physical condition for shuttling in the quantum regime: when the zero point amplitude of the nanomechanical oscillator is half of the tunneling length ($\zeta = \xi^{-1}$). In this figure, in which the oscillator period is comparable with the left bare tunneling rate ($\Gamma_L = \hbar\omega/2\pi$), the average current saturates at one electron per mechanical cycle (corresponding to average current $2\pi(I_L(t) - I_R(t))/e\hbar\omega = 1$) as the electrons are shuttled one by one from the source to the drain by the oscillating dot. We get the following physical picture: every time an electron jumps onto the dot when $\Gamma_L = \hbar\omega/2\pi$, the dot is near the source lead and subject to the electrostatic force eE that accelerates it towards the drain lead. Energy is pumped into the nanomechanical oscillator and the dot starts to oscillate between the leads. When the right tunneling time is high compared to the left tunnelling time, the oscillator dissipates this energy into the environment before the next event occurs. This continuously drives the oscillator away from equilibrium and a stationary state is reached only when the energy pumped per cycle into the system is dissipated during the same cycle in the environment. With this setup, the system will be in the shuttle regime. We note that the frequency of the short period weak oscillations in fig 5.1 is ($|\epsilon_{\mathrm{F}L} - \epsilon_0|$) and these oscillations are present even in the limit of small but finite γ. We conclude that this is a purely electronic process (plasmon oscillations). It is clear from the figure that in the strong tunneling case, it contains two beating frequencies, therefore we interpret this as due to a mixture of electronic and hole frequencies. In Fig. 5.2 the long time behavior of the net average current has steps as function of the left Fermi energy which become more

pronounced with increasing γ. In contrast, when both the bare tunneling rates are equal and smaller than the mechanical frequency, and $\gamma << 1$, the dynamics of the system is similar to a double barrier resonant tunneling system, since the dot is static and far from both the leads. The tunneling dynamics of the net average current is shown in Fig. 5.3 for fixed values of $\Gamma_L = \Gamma_R = 0.1\hbar\omega/2\pi, x_0 = 0.1l$ and the oscillator energy $\hbar\omega$ =0.63. This confirms the tunneling behavior of the system oscillating with beating frequency which is due to mixture of electronic and hole degrees of freedom and is consistent with previous studies.

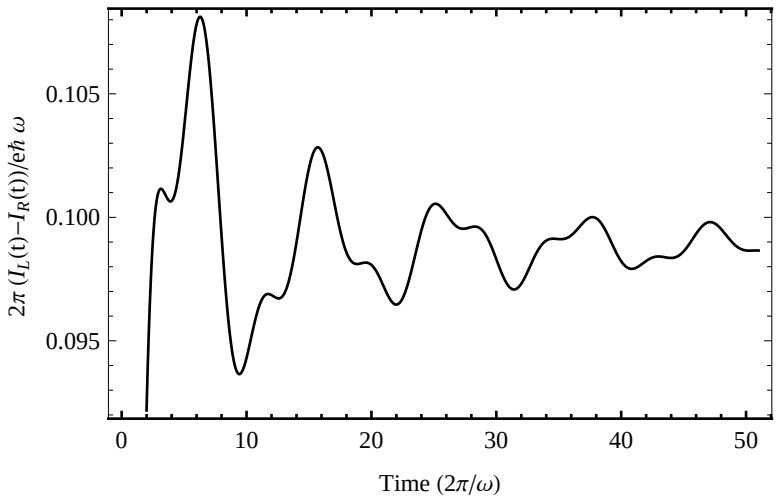


Figure 5.3: Net average current $(2\pi(I_L(t) - I_R(t))/e\hbar\omega)$ flowing through the system as a function of time $(2\pi/\omega)$ for fixed values of the parameters in the case of the tunneling mechanism: $\epsilon_0 = 0.5, \epsilon_{FR} = 0, \epsilon_{FL} = 2, \hbar\omega = 0.63, \Gamma_L = \Gamma_R = 0.1\hbar\omega/2\pi, x_0 = 0.1l$ and $\gamma = 0.001$. Units: all the parameters have the same dimension as $\hbar\omega$.

The oscillator momentum charge density correlation function is shown in Fig. 5.4 & 5.5, as a function of time $(2\pi/\omega)$ and left Fermi energy for fixed values of tunneling length $\zeta = 2l$, $x_0 = 0.5l$, $\hbar\omega = 0.63$ and tunneling rates $\Gamma_L = \hbar\omega/2\pi$, $\Gamma_R = \Gamma_L \exp[-\gamma x]$.

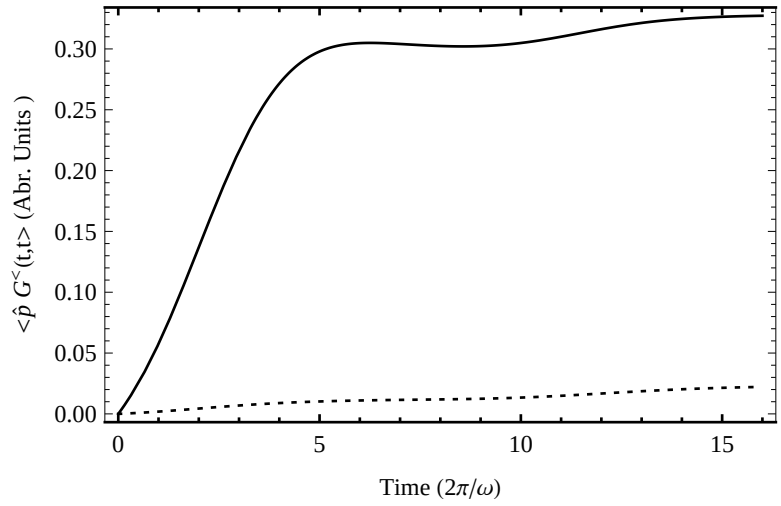


Figure 5.4: The oscillator momentum charge density correlation function as a function of time $(2\pi/\omega)$ showing the shuttling (solid line) and the tunneling (dotted line) behavior. Parameters for the shuttling are $\epsilon_0 = 0.5, \hbar\omega = 0.63, \Gamma_L = \hbar\omega/2\pi, x_0 = 0.2l$, $\Gamma_R = \Gamma_L \exp[-\gamma x])$ and $\gamma = 0.5$, and for the tunneling are $\epsilon_0 = 0.5, \epsilon_{FR} = 0, \epsilon_{FL} = 2, \hbar\omega = 0.63, \Gamma_L = \Gamma_R = 0.1\hbar\omega/2\pi, x_0 = 0.1l$ and $\gamma = 0.001$. All the parameters have the same dimension as $\hbar\omega$.

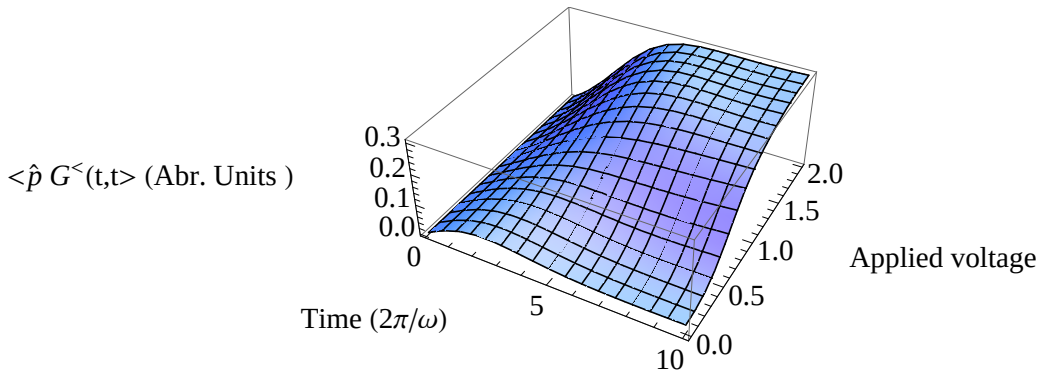


Figure 5.5: The oscillator momentum charge density correlation function as a function of time $(2\pi/\omega)$ and left Fermi energy showing the shuttling behavior. Parameters for the shuttling are $\epsilon_0 = 0.5, \hbar\omega = 0.63, \Gamma_L = \hbar\omega/2\pi, x_0 = 0.2l$, $\Gamma_R = \Gamma_L \exp[-\gamma x])$ and $\gamma = 1$. All the parameters have the same dimension as $\hbar\omega$.

We distinguish between the shuttling and tunneling dynamics of the system for

long time for different tunneling rates and γ: For shuttling (solid line) $\Gamma_L = \hbar\omega/2\pi$, $\Gamma_R = \Gamma_L \exp[-\gamma x]$, $\gamma = 0.5$, and for tunneling (dotted line) $\Gamma_L = \Gamma_R = 0.1\hbar\omega/2\pi$, $x_0 = 0.1l$, and $\gamma = 0.001$. Why have we found this particular type of structure? We know that, in the ideal shuttling regime, we expect the dot to be occupied when the momentum is positive and unoccupied when the momentum is negative. Hence, the correlation function is positive. In contrast, when the transport is independent of the mechanical oscillator, the correlation function is zero as

$$< \widehat{p} G^{<}(t,t) >=< \widehat{p} >< G^{<}(t,t) >= 0.$$

In figure 5.5, we have shown the long time value of the oscillator momentum correlation function as a function of the left Fermi level.

Next, we have shown the total average current $(I_L(t) + I_R(t))$ flowing onto the oscillating dot in Fig. 5.6 as a function of time $(2\pi/\omega)$ for fixed values of $\Gamma_L = \Gamma_R = 0.1\hbar\omega/2\pi$, $\hbar\omega = 0.63, \epsilon_{\mathrm{F}R} = 0$, $\epsilon_{\mathrm{F}L} = 2$, and finite value of the tunneling length $\gamma = 0.1$.

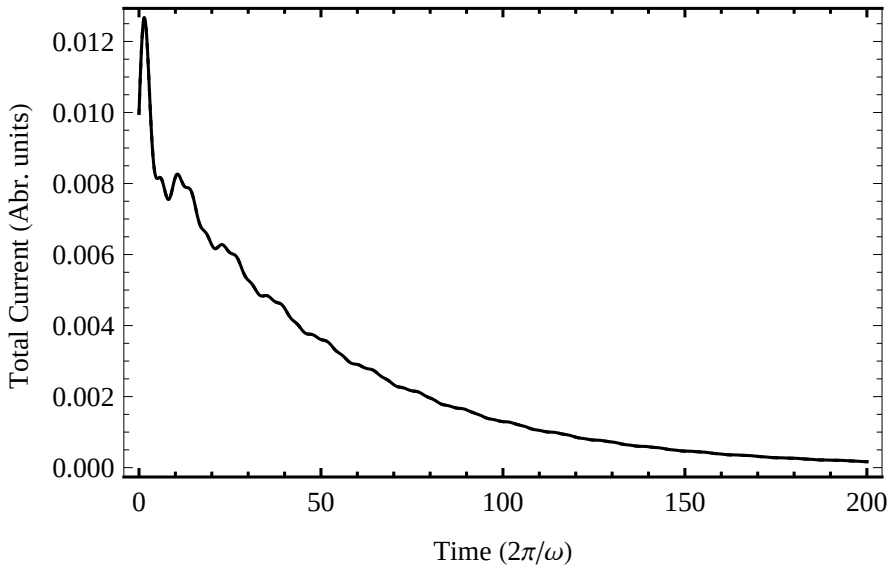


Figure 5.6: Total average current $(I_L(t) + I_R(t))$ flowing onto the dot as a function of time $(2\pi/\omega)$ for fixed values of $\epsilon_0 = 0.5, \epsilon_{FR} = 0, \epsilon_{FL} = 2, \hbar\omega = 0.63, \Gamma_L = \Gamma_R = 0.1\hbar\omega/2\pi, x_0 = 0.2l$ and $\gamma = 0.1$. All the parameters have same dimension as $\hbar\omega$. This current (solid line) is equivalent to the rate of change of dot population $\frac{d}{dt}\rho(t)$ (dashed line) as a function of time for the same parameters as for the current. In this figure, solid and dashed lines have same values at all points. Units: all the parameters have the same dimension as $\hbar\omega$.

This current (solid line) is equivalent to the rate of change of the dot population (dashed line) for the same parameters. In this figure, we can not distinguish the solid and the dashed line. This confirms that our analytical results are consistent with the equation of continuity, $I_L(t) + I_R(t) = \frac{d}{dt}\rho(t)$, and hence, with the conservation laws for all parameters. We interpret the long period oscillations as a function of time $(2\pi/\omega)$ is the mechanical frequency of the system and short period weak oscillations with the electronic frequency $(|\epsilon_{\mathrm{F}L} - \epsilon_0|)$, which is consistent with the net average current results as well.

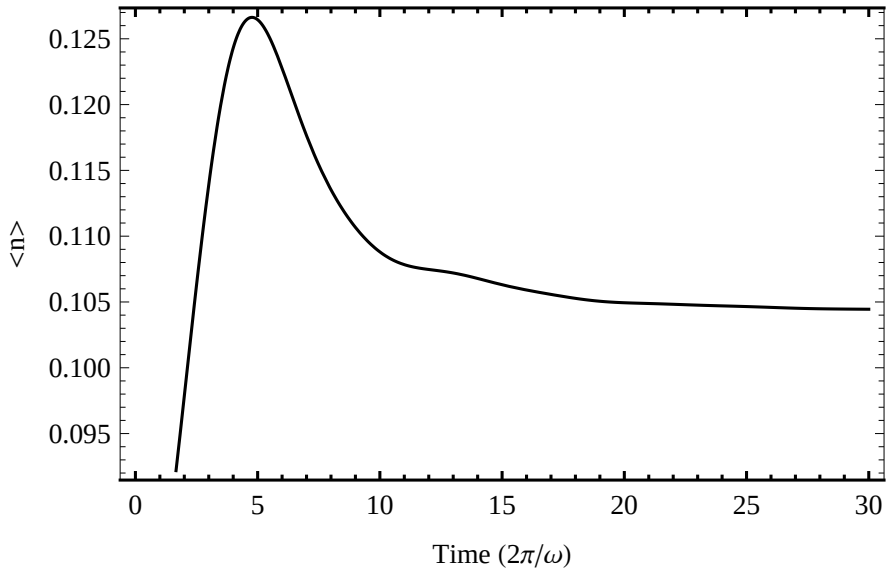


Figure 5.7: Average energy transferred to the oscillator as a function of time $(2\pi/\omega)$ for fixed values of $\hbar\omega = 0.63, \Gamma_L = \hbar\omega/2\pi, x_0 = 0.5l$, $\Gamma_R = \Gamma_L \exp[-\gamma x])$ and $\gamma = 1$. Units: all the parameters have the same dimension as $\hbar\omega$.

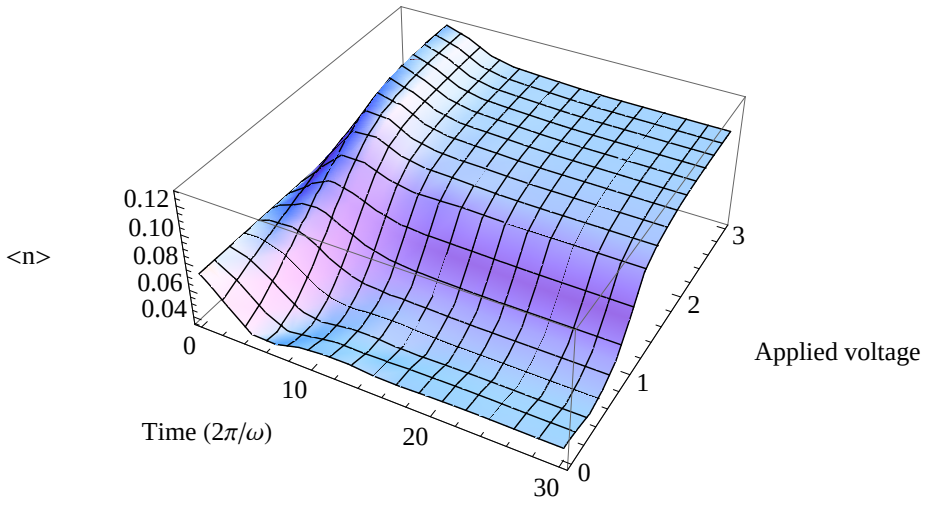


Figure 5.8: Average energy transferred to the oscillator as a function of time $(2\pi/\omega)$ and left Fermi energy for all the parameters as in fig. 5.7.

Finally we have shown the average energy of the nanomechanical oscillator as a

function of time $(2\pi/\omega)$ and of the left Fermi energy in Fig. 5.7 & 5.8 for fixed values of tunneling rates $\Gamma_L = 0.1$, $\Gamma_R = \Gamma_L \exp[-\gamma x], \epsilon_{\mathrm{F}R} = 0$, $x_0 = 0.3l$ and tunneling length $\gamma = 0.5$. These parameters correspond to the shuttling regime of the system. We found constant average energy of the nanomechanical oscillator for long time. This constant average energy increases with increasing Fermi level as shown in fig. 5.8. We consider two possible interpretations of this structure. One is presented in the previous chapter: that the oscillator is in any of its pure states and therefore the potential seen by the electrons is time independent. Secondly, this is an average over several time-dependent processes with different phases such that any Rabi like features cancel. Hence, we note that only the second interpretation is consistent with the correlation function. For the case of the tunneling regime of the system, the average energy of the nanomechanical oscillator is shown in Fig. 5.9 as a function of time $(2\pi/\omega)$ for fixed values $\Gamma_L = \Gamma_R = 0.1\hbar\omega/2\pi$, $\hbar\omega = 0.63, \epsilon_{\mathrm{F}R} = 0$, $\epsilon_{\mathrm{F}L} = 2$, and for very small value of the tunneling length $l = 0.001\zeta$. The structure of average energy of the nanomechanical oscillator in this figure with zero or very small tunneling length is consistent with that discussed in chapter 4.

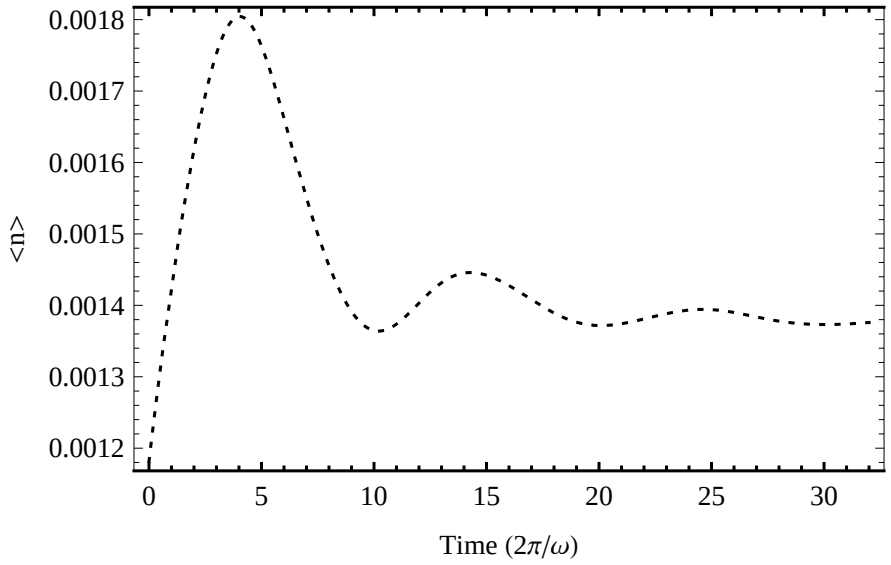


Figure 5.9: Average energy transferred to the oscillator as a function of time $(2\pi/\omega)$ for fixed values of $\epsilon_0 = 0.5, \epsilon_{FR} = 0, \epsilon_{FL} = 1, \hbar\omega = 0.63, \Gamma_L = \Gamma_R = 0.1\hbar\omega/2\pi, x_0 = 0.5l$ and $\gamma = 0.001$. Units: all the parameters have the same dimension as $\hbar\omega$.

In Fig. 5.7, 5.8 & 5.9 it appears that the oscillator is not in its ground state at t=0. However, if we look at the structure of the lesser self-energy, the quantity in the middle refers to the state of the oscillator when the dot is empty and the oscillator is in its ground state. Whereas the whole self-energy refers to the state of the oscillator when an electron has passed through the barrier onto the dot. At this point the oscillator is not necessarily in its ground state. When the electron is in the leads, the oscillator is in its ground state but when the electron is on the dot two things happen: the representation of the lesser self-energy is changed and the other is the effect of the $\exp[\mp\gamma x]$ operator which kicks the oscillator out of its ground state. This comes back into a saturated state for long time with finite value of average energy. This could be a mixed or a thermal state. When taken with the finite correlation function for the same parameters, we conclude that the

long time average energy of the nanomechanical oscillator corresponds to the mixed state.

5.8 Conclusions

In this chapter, we analyzed the time-dependent transport via a quantum shuttle by using the nonequilibrium Green's function approach without treating the electron phonon coupling as a perturbation. We have derived an expression for the full density matrix and discuss it in detail for different values of the tunneling length and the tunneling rate. Using the full density matrix calculation we have shown the oscillator momentum charge density correlation function which distinguishes the shuttling and the tunneling regime of the system. We derive an expression for the current to see the effects of the coupling of the electrons to the oscillator on the dot and the tunneling rate of electrons to resolve the dynamics of the nanomechanical oscillator. We found a positive correlation function for the nanomechanical oscillator in the shuttling regime and zero in the case of the tunneling regime. The shuttling regime will occur when the electron left jump rate introduces kicks the nanomechanical oscillator on the island. This happens when the left jump rate is close to the oscillation frequency of the island $\Gamma_L = \hbar\omega/2\pi$. By setting an appropriate ejection rate ($\Gamma_R = \Gamma_L \exp[-\gamma x]$) and $l = 0.5\zeta$, there exists a condition where the island will keep oscillating between the leads. In contrast, in the limit of equal bare tunneling rates, smaller than the mechanical frequency, and when $\gamma << 1$, the dynamics of the system is similar to a double barrier resonant tunneling system, where we found periodic oscillations as a function of time ($2\pi/\omega$), which corresponds to the mechanical frequency of the system. Furthermore, we discuss the average energy transferred to oscillator as a function of time. We have found

a mixed or a thermal state shown in the average energy of the nanomechanical oscillator for long time which is consistent with the finite correlation function for the same parameters. These results suggest further experiments for NEMS to go beyond the classical dynamics of a shuttle device.

Chapter 6

Summary and outlook

We summarize in this chapter the main results presented in the thesis. We introduced a new non-perturbative approach for modelling the quantum transport in nanomechanical systems using the nonequilibrium Green's function formulation. The general motivation was the future prospects of NEMS based electronic devices for which a detailed understanding of quantum transport at low or high bias in the presence of strong electron-phonon coupling will certainly be cardinal. The richness of this new non-perturbative quantum model still leaves many open questions in the description and understanding of the quantum dynamics of NEMS. We close the chapter with some open questions that could encourage a continuation of this work.

6.1 Summary

In this thesis we analyzed the quantum dynamics of two different models: a simple quantum device and a charge shuttle. These devices are nanoelectromechanical systems

(NEMS) in which an oscillator is strongly coupled to the quantum dot between the source and drain leads. The dynamics of such devices is the result of strong interplay between the electrical and mechanical degrees of freedom at an applied bias. As the size of the system is small, the quantum effects become important in nano physics. Due to this reason, we introduced a new non-perturbative quantum approach for the coupling of electrical and mechanical degree of freedom. In this way we have considered the strong coupling limit for the interaction of the electrical and the mechanical part of the system at low or high applied bias, which is the essential element of the present method of non-perturbative electron-phonon coupling.

Among the different theoretical approaches for the description of the quantum dynamics of a nanosize system we choose the nonequilibrium Green's function technique. With this technique we have considered strong coupling both between the system and the leads and between the oscillator and the dot electrons. This is a fully quantum mechanical formulation whose basic approximations are very transparent. The nonequilibrium Green's function technique is able to deal with a very broad variety of physical situations related to quantum transport at molecular levels. It can deal with strong non-equilibrium situations and very small to very large applied bias. An advantage of the time-dependent non-equilibrium Green's function approach considered in this thesis is that it eliminates the one major criticism of the Keldysh approach, which is the lack of any clear initial conditions. This provided a way to perform transient and steady state quantum transport calculations from first principles while retaining the essential physics of the electronic structure of the dot and the leads. Another advantage of this method is that it treats the infinitely extended

reservoirs in an exact way in the present system, which gave a better understanding of the essential features of NEMS in a more appropriate quantum mechanical picture.

With this technique we first investigated the quantum transport properties of a simple NEMS model. We considered the average over single particle properties, implicitly assuming strong damping of the mechanical oscillator. Simply averaging over a single particle expression is a valid description of a many particle problem, as long as any excitation caused by one electron has been dissipated before the next electron arrives. This is the strong dissipation regime. The main exciting contribution of this work is: we included a range from very small to very large chemical potential difference between the leads. In our calculation inclusion of the oscillator is not perturbative as the recent experiments are beyond the perturbation theory. Hence, our work provides an exact analytical solution to the current–voltage, conductance, average energy, shot noise, coupling of leads with the system, very small chemical potential difference and includes both the right and left Fermi level response regimes. We have found satellite peaks in the differential conductance spectrum as a function of the chemical potential difference in addition to the main resonant peak, due to the transfer of energy from electrons on the dot to the oscillator. We found that the side-bands grow with increasing the coupling strength between the nanomechanical oscillator and the dot electrons. We have found that when there is no coupling of oscillator with electrons on the single dot then there are no additional satellite peaks and no energy transfer. We have derived an analytical expression for the net current flowing through the system and for the shot noise. This enables us to see the effects of the weak or zero and strong coupling of the electrons to the oscillator on the dot and the tunneling rate of

electrons. We have found additional steps or peaks due to coupling of single phonon mode which are absent for very weak or no coupling strength. We also discuss the corresponding Fano factor as a function of applied bias which shows thermal or poissonian behavior to non-thermal or sub-poissonian behavior. This confirms that the additional satellite peaks or steps in the spectrum of numerical results at zero temperature are only due to the transfer of energy from the electrons to the oscillator.

We then investigated the time evolution of a quantum dot coupled to a nanomechanical oscillator as a reaction to a sudden joining to the leads. We employed the nonequilibrium Green's function method in order to discuss the transient and steady state dynamics of NEMS. Hence, our work provides an exact analytical solution to the dot population, current–voltage characteristics, and the average energy as a function of time including coupling of leads with the system, very small chemical potential difference and both the right and left Fermi level response regimes. Here we considered the time dependent transport properties of simple NEMS model, where we discussed the quantum dynamics of the nanomechanical oscillator in terms of pure and superposition states. We have found a significant difference between a quantum mechanical and a classical oscillator. In particular, the energy of a classical oscillator was always dissipated by the electrons whereas the quantum oscillator remained in an excited state.

Finally, we investigated a special kind of application of NEMS, which is transport via a quantum shuttle where we have considered the time evolution of an oscillating quantum dot as a reaction to a sudden joining to the leads. We employed the nonequilibrium Green's function method in order to discuss the transport properties of a quantum shuttle device. In

this model, we include the time-dependent hopping between the oscillating dot and the leads to enable us to connect the leads to the dot at a finite time. We assume strong dissipation of the oscillating dot, where we consider the average over single particle properties, implicitly assuming strong damping of the mechanical oscillator. We describe the electronic state of the dot as a two-state system (empty/occupied). The electrons in the leads are considered to be at zero temperature. We consider an arbitrary finite chemical potential difference between the right and left leads. The transient and the steady state behavior of the system is considered here in order to explore the quantum dynamics of the shuttle device as a function of time. In our calculation inclusion of the oscillator is not perturbative. As the recent studies are beyond the perturbation theory, a non-perturbative approach is required beyond the quantum master equation or linear response. Hence, our work provides an exact analytical solution to the current–voltage, correlation functions, average energy, coupling of leads with the system, very small chemical potential difference and includes both the right and left Fermi level response regimes. We have shown the dynamics of a shuttle device as a function of time, which exhibits electron per cycle behavior in average current characteristics. We have found a pure state of the nanomechanical oscillator shown in the average energy for long time which is also consistent with the correlation function.

6.2 Technique modified

In this work we have not explicitly included the dissipation of the mechanical object of the system in order to introduce the simplest possible model. Hence, the technique developed in this thesis will have to modified by including the damping of the mechanical

oscillator to explore the weak, intermediate and strong damping effects of the mechanical part of the NEMS device.

This model can be further improved by including the spin effects which will be helpful in theoretical understanding of spin-dependent NEMS devices. In the present work we have disregarded the spin effects.

The effects of time dependent gate voltage or alternating potential in the leads should be taken into account in order to explore the full dynamics of NEMS.

Furthermore, the technique could be improved by replacing the sudden joining of leads with a sudden change of chemical potential from equilibrium, which is a more physical realistic discussion of NEMS.

6.3 Future outlook

During the development of the present work many questions arose about possible phenomena to investigate in different NEMS devices. These questions could be of interest for example in understanding or proposing future experiments. We list them here as a possible continuation of the present work.

We have developed a technique where we have two leads and an oscillator connected with the dot. Simply we can say that in this system we have a device connected between a source and a drain leads. This system is closely related to a single molecule connected between two leads, which lead directly to the calculation of the sudden joining process.

Furthermore, we have an oscillator coupled strongly with the dot electrons where we have introduced a new non-pertubative approach for their interactions. There are some

general class of problems where there is strong interaction between both the electrons and the oscillator, and the system and the leads we can apply this method too. So that this technique can be generalized to a more complex device in between two leads such as; Single molecule like diphenol and free standing nanotubes. Can we understand some thing new from this quantum treatment for the molecular devices in the presence of strong vibrational effects?

Appendix A

Time dependent current

The particle current I_α into the interacting region from the lead is given by the expectation value of the current operator, $I_\alpha = Tr(\rho \hat{I}_\alpha)$ [46, 47, 53, 54, 55], where

$$\hat{I}_\alpha = \frac{ie}{\hbar} \sum_j \{V_{0\alpha} c_0^\dagger c_{\alpha j} - c_{\alpha j}^\dagger c_0 V_{\alpha 0}\} \tag{A.1}$$

$$I_\alpha(t) = \frac{e}{\hbar} \{G_{0,\alpha}^<(t,t) V_{\alpha,0}(t) - V_{0,\alpha}^*(t) G_{\alpha,0}^<(t,t)\}, \tag{A.2}$$

where we have the following relations

$$G_{o,\alpha}^<(t,t) = \int dt' \{G_{0,0}^r(t,t') V_{0,\alpha}(t') g_{\alpha,\alpha}^<(t',t) + G_{0,0}^<(t,t') V_{0,\alpha}(t') g_{\alpha,\alpha}^a(t',t)\} \tag{A.3}$$

and

$$G_{\alpha,0}^<(t,t) = \int dt' \{g_{\alpha,\alpha}^r(t,t') V_{\alpha,0}(t') G_{0,0}^<(t',t) + g_{\alpha,\alpha}^<(t,t') V_{\alpha,0}(t') G_{0,0}^a(t',t)\}, \tag{A.4}$$

where $g_{\alpha,\alpha}^{r,(a),(<)}(t,t')$ refers to the unperturbed states of the leads and is given as

$$g^r_{\alpha,\alpha}(t,t') = \frac{1}{N}\sum_j g^r_{\alpha,j}(t,t') = -in_\alpha\theta(t-t')\int_{-\infty}^{+\infty} d\varepsilon_\alpha \exp[-i\varepsilon_\alpha(t-t')],$$

with the fact that $\sum_j = \int_{-\infty}^{+\infty} Nn_\alpha d\varepsilon_\alpha$ with n_α being the constant number density of the leads and other uncoupled Green's function in the leads are

$$g^a_{\alpha,\alpha}(t,t') = \frac{1}{N}\sum_j g^a_{\alpha,j}(t,t') = +in_\alpha\theta(t'-t)\int_{-\infty}^{+\infty} d\varepsilon_\alpha \exp[-i(\varepsilon_\alpha)(t-t')],$$

$$g^<_{\alpha,\alpha}(t,t') = \frac{1}{N}\sum_j f_\alpha(\varepsilon_\alpha) g^<_{\alpha,j}(t,t') = \int_{-\infty}^{+\infty} d\varepsilon_\alpha f_\alpha(\varepsilon_\alpha) in_\alpha \exp[-i\varepsilon_\alpha(t-t')],$$

Now using equations (A3 & A4) in the equation (A2) of current through lead α as

$$\begin{aligned} I_\alpha(t) = \frac{e}{\hbar}\int dt' \mathrm{Tr}\{&(G^r_{0,0}(t,t')V_{0,\alpha}(t')g^<_{\alpha,\alpha}(t',t) + G^<_{0,0}(t,t')V_{0,\alpha}(t')g^a_{\alpha,\alpha}(t',t))V_{\alpha,0}(t) \\ &- V^*_{0,\alpha}(g^r_{\alpha,\alpha}(t,t')V_{\alpha,0}(t')G^<_{0,0}(t',t) + g^<_{\alpha,\alpha}(t,t')V_{\alpha,0}(t')G^a_{0,0}(t',t))\}, \end{aligned} \tag{A.5}$$

Using the fact that $\Sigma^{r,(a),(<)}_{0,0,\alpha}(t',t) = V^*_{0,\alpha}(t')g^{r,(a),(<)}_{\alpha,\alpha}(t',t)V_{\alpha,0}(t)$, we can simplify the above equation as

$$\begin{aligned} I_\alpha(t) = \frac{e}{\hbar}\int dt' \mathrm{Tr}\{&G^r_{0,0}(t,t')\Sigma^<_{0,0,\alpha}(t',t) + G^<_{0,0}(t,t')\Sigma^a_{0,0,\alpha}(t',t) \\ &- \Sigma^r_{0,0,\alpha}(t,t')G^<_{0,0}(t',t) - \Sigma^<_{0,0,\alpha}(t,t')G^a_{0,0}(t',t)]\}, \end{aligned} \tag{A.6}$$

where $\Sigma^{r,(a),(<)}_{0,0,\alpha}(t,t')$ are non-zero only when both the times (t,t') are positive $t,t' > 0$. Although $g^{r,(a)}(t,t')$ is non-zero for $t < 0$, it is never required due to the way it combines

with $\Sigma^{r,(a),(<)}_{0,0,\alpha}(t,t')$. Here we note that we require $g^{r,(a)}(t,t')$ from Eq. (4.8 & 4.9) for positive times only ($t > 0$).The first integral on right hand side of Eq. (A6) may be solved by using Eq. (4.7, 4.8 & 4.13) as

$$\mathrm{Tr}\int_0^t dt' G^r_{0,0}(t,t')\Sigma^<_{0,0,\alpha}(t',t) = \frac{-\Gamma}{2\pi}\sum_{\alpha,m}\int_{-\infty}^{\epsilon_{F\alpha}} d\varepsilon_\alpha \int_0^t dt' \Phi_{0,m}\Phi^*_{0,m} \times \exp[-i(\varepsilon_m - i\Gamma)(t-t')] \times \exp[-i\varepsilon_\alpha(t'-t)],$$

$$= \frac{i\Gamma}{2\pi}\sum_{\alpha,m}\Phi_{0,m}\Phi^*_{0,m}\int_{-\infty}^{\epsilon_{F\alpha}} \frac{d\varepsilon_\alpha[1-\exp[i(\varepsilon_\alpha - \varepsilon_m + i\Gamma)t]}{(\varepsilon_\alpha - \varepsilon_m + i\Gamma)},$$

Using the standard integral[78], the final result is written as

$$\mathrm{Tr}\int_0^t dt' G^r_{0,0}(t,t')\Sigma^<_{0,0,\alpha}(t',t) = \frac{i\Gamma}{2\pi}\sum_{\alpha,m}\Phi_{0,m}\Phi^*_{0,m}\{\frac{1}{2}\ln[(\epsilon_{\mathrm{F}\alpha} - \varepsilon_m)^2 + \Gamma^2] - i\left(\tan^{-1}[\frac{\epsilon_{\mathrm{F}\alpha} - \varepsilon_m}{\Gamma}] + \frac{\pi}{2}\right) - \mathrm{Ei}[it(\epsilon_{\mathrm{F}\alpha} - \varepsilon_m + i\Gamma)]\}, \quad \text{(A.7)}$$

where we note that special care is required in evaluating the Ei(x) to choose the correct Riemann sheets in order to make sure that these functions are consistent with the initial conditions and are continuous functions of time and chemical potential. This statement will apply to all further discussions also.

The second & third integral on right hand side of Eq. (A6) are written as

$$\mathrm{Tr}\int_0^t dt'\{G^<_{0,0}(t,t')\Sigma^a_{0,0,\alpha}(t',t) - \Sigma^r_{0,0,\alpha}(t,t')G^<_{0,0}(t',t)\} = i\Gamma\mathrm{Tr}G^<_{n,n'}(t,t)\delta_{n,n'},$$

This integral can be solved in the same way as the dot population, and the final result is written as

$$i\Gamma \mathrm{Tr} G^{<}_{n,n'}(t,t)\delta_{n,n'} = \frac{\Gamma}{2\pi}\sum_{\alpha,m}\Phi_{0,m}\Phi^{*}_{0,m}\{-\left(1+\exp[-2\Gamma t]\right)\left(\tan^{-1}[\frac{\varepsilon_{F\alpha}-\varepsilon_m}{\Gamma}]+\frac{\pi}{2}\right)$$
$$+\frac{i}{2}\exp[-2\Gamma t](-\,\mathrm{Ei}[it(\epsilon_{\mathrm{F}\alpha}-\varepsilon_m-i\Gamma)]+\mathrm{Ei}[-it(\epsilon_{\mathrm{F}\alpha}-\varepsilon_m+i\Gamma)])$$
$$+\frac{i}{2}(\mathrm{Ei}[it(\epsilon_{\mathrm{F}\alpha}-\varepsilon_m+i\Gamma)]-\mathrm{Ei}[-it(\epsilon_{\mathrm{F}\alpha}-\varepsilon_m-i\Gamma)])\}, \tag{A.8}$$

and the fourth integral on right hand side of equation (A6) can be solved[78] by using Eq. (4.7, 4.9 & 4.13) as

$$-\mathrm{Tr}\int_0^t dt'\Sigma^{<}_{0,0,\alpha}(t,t')G^{a}_{0,0}(t',t)] = \frac{\Gamma}{2\pi}\sum_{\alpha,m}\int_{-\infty}^{\epsilon_{FL}}d\varepsilon_\alpha\int_0^t dt'\Phi_{0,m}\Phi^{*}_{0,m}$$
$$\times\exp[-i(\varepsilon_m+i\Gamma)(t'-t)]\times\exp[-i\varepsilon_\alpha(t-t')],$$

$$=\frac{-i\Gamma}{2\pi}\sum_{\alpha,m}\Phi_{0,m}\Phi^{*}_{0,m}\int_{-\infty}^{\epsilon_{F\alpha}}\frac{d\varepsilon_\alpha[1-\exp[-i(\varepsilon_\alpha-\varepsilon_m-i\Gamma)t]}{(\varepsilon_\alpha-\varepsilon_m-i\Gamma)},$$

$$=\frac{-i\Gamma}{2\pi}\sum_{\alpha,m}\Phi_{0,m}\Phi^{*}_{0,m}\begin{bmatrix}\frac{1}{2}\ln[(\epsilon_{\mathrm{F}\alpha}-\varepsilon_m)^2+\Gamma^2]\\ +i\left(\tan^{-1}[\frac{\epsilon_{\mathrm{F}\alpha}-\varepsilon_m}{\Gamma}]+\frac{\pi}{2}\right)-\mathrm{Ei}[-it(\epsilon_{\mathrm{F}\alpha}-\varepsilon_m-i\Gamma)]\end{bmatrix} \tag{A.9}$$

Using equation (A7), (A8 & (A9) into Eq. (A6), the final expression for the current is written as

$$I_\alpha(t)=\frac{e\Gamma}{2\pi\hbar}\sum_m\Phi_{0,m}\Phi^{*}_{0,m}\{I_{1,\alpha}+I_{2,L}+I_{2,R}\}, \tag{A.10}$$

where components of current are written as

$$I_{1,\alpha} = [(2\tan^{-1}[\frac{\epsilon_{\mathrm{F}\alpha} - \varepsilon_m}{\Gamma}] + \frac{\pi}{2}) - i\{\mathrm{Ei}[it(\epsilon_{\mathrm{F}\alpha} - \varepsilon_m + i\Gamma)] - \mathrm{Ei}[-it(\epsilon_{\mathrm{F}\alpha} - \varepsilon_m - i\Gamma)]\}],$$

$$\begin{aligned} I_{2,\alpha} = \{&- (1 + \exp[-2\Gamma t])\,(\tan^{-1}[\frac{\varepsilon_{F\alpha} - \varepsilon_m}{\Gamma}] + \frac{\pi}{2}) \\ &+ \frac{i}{2}\exp[-2\Gamma t](-\mathrm{Ei}[it(\epsilon_{\mathrm{F}\alpha} - \varepsilon_m - i\Gamma)] + \mathrm{Ei}[-it(\epsilon_{\mathrm{F}\alpha} - \varepsilon_m + i\Gamma)]) \\ &+ \frac{i}{2}(\mathrm{Ei}[it(\epsilon_{\mathrm{F}\alpha} - \varepsilon_m + i\Gamma)] - \mathrm{Ei}[-it(\epsilon_{\mathrm{F}\alpha} - \varepsilon_m - i\Gamma)])\}, \end{aligned}$$

where in calculating the left current we need $I_{1,L}$ and together with $I_{2,L}, I_{2,R}$ and for the right current we need $I_{1,R}$ and both $I_{2,L}, I_{2,R}$.

Appendix B

Self-energy

In this appendix we derive an analytical relation for the time-dependent self-energy. The effective self-energy represents the contribution to the moving dot energy, due to interactions between the oscillating dot and the leads it is coupled to. The retarded self-energy of the oscillating dot due to lead α is given by

$$\Sigma^r_{n_0,n_0'}(t,t_1) = \phi_{n_0,m}(t) g^r_{\alpha,\alpha}(t,t_1) \phi^*_{n_0',m}(t_1), \tag{B.1}$$

where the uncoupled Green's function $g^r_{\alpha,\alpha}(t,t_1)$ in the leads is

$$\begin{aligned} g^r_{\alpha,\alpha}(t,t_1) = \frac{1}{N}\sum_j g^r_{\alpha,j}(t,t_1) &= \int_{-\infty}^{+\infty} n_\alpha d\varepsilon_\alpha g^r_\alpha(t,t_1) \\ &= -i\theta(t-t_1)\int_{-\infty}^{+\infty} d\varepsilon_\alpha n_\alpha \exp[-i(\varepsilon_\alpha + m\hbar\omega)(t-t_1)], \end{aligned} \tag{B.2}$$

and $\sum_j \Rightarrow \int_{-\infty}^{+\infty} N n_\alpha d\varepsilon_\alpha$, where j stands for every channel in each lead, n_α is the density of states in lead α, $g^r_{\alpha,j}(t,t_1)$ is the uncoupled Green's function for every channel in the leads.

The tunneling matrix $\phi_{n_0,m}(t)$ is written as

$$\begin{aligned}\phi_{n_0,m}(t) &=< V_0(t)e^{\mp\xi\hat{X}} > \\ &= \int dX A^*_{n_0} e^{-\frac{(X-x_0)^2}{2l^2}} H_{n_0}(\frac{X-x_0}{l}) V_0(t) e^{\mp\xi\hat{X}} A_m e^{-\frac{(X)^2}{2l^2}} H_m(\frac{X}{l}),\end{aligned} \tag{B.3}$$

where X is the coordinate of the oscillator, ξ being the inverse tunneling length.

Using the expressions of the tunneling matrix and the uncoupled retarded Green's function in equation (B1), the retarded self-energy may be written as

$$\begin{aligned}\Sigma^r_{n_0,n_0'}(t,t_1) = \sum_m -i\theta(t-t_1) \int_{-\infty}^{+\infty} N d\varepsilon_\alpha \frac{|V|^2 \theta(t)\theta(t_1)}{N} n_\alpha \exp[-i(\varepsilon_\alpha + m\hbar\omega)(t-t_1)] \\ \times \int\int dX dX' A_{n_0} e^{-\frac{(X-x_0)^2}{2l^2}} H_{n_0}(\frac{X-x_0}{l}) V_0 e^{\mp\xi\hat{X}} A^*_m e^{-\frac{(X)^2}{2l^2}} \\ \times H_m(\frac{X}{l}) A^*_{n_0'} e^{-\frac{(X'-x_0)^2}{2l^2}} H_{n_0'}(\frac{X'-x_0}{l}) V_0 e^{\mp\xi\hat{X}'} A_m e^{-\frac{(X')^2}{2l^2}} H_m(\frac{X'}{l}),\end{aligned} \tag{B.4}$$

The the above expression (B4) can be rewritten as

$$\begin{aligned}\Sigma^r_{n_0,n_0'}(t,t_1) = \sum_m -i\theta(t-t_1) |V|^2 \theta(t)\theta(t_1) n_\alpha \\ \times \int_{-\infty}^{+\infty} \exp[-i(\varepsilon_\alpha + m\hbar\omega)(t-t_1)] d\varepsilon_\alpha \\ \times \int\int dX dX' A_{n_0} e^{-\frac{(X-x_0)^2}{2l^2}} H_{n_0}(\frac{X-x_0}{l}) V_0 e^{\mp\xi\hat{X}} A^*_m e^{-\frac{(X)^2}{2l^2}} \\ \times H_m(\frac{X}{l}) A^*_{n_0'} e^{-\frac{(X'-x_0)^2}{2l^2}} H_{n_0'}(\frac{X'-x_0}{l}) V_0 e^{\mp\xi\hat{X}'} A_m e^{-\frac{(X')^2}{2l^2}} H_m(\frac{X'}{l}),\end{aligned} \tag{B.5}$$

After performing the time integral, equation (B5) can be simplified as

$$\begin{aligned}= -in_\alpha |V|^2 \theta(t)\theta(t_1)\theta(t-t_1)\pi\delta(t-t_1) \\ \times \sum_m \int\int dX dX' A_{n_0} e^{-\frac{(X-x_0)^2}{2l^2}} H_{n_0}(\frac{X-x_0}{l}) V_0 e^{\mp\xi\hat{X}} A^*_m e^{-\frac{(X)^2}{2l^2}} \\ \times H_m(\frac{X}{l}) A^*_{n_0'} e^{-\frac{(X'-x_0)^2}{2l^2}} H_{n_0'}(\frac{X'-x_0}{l}) V_0 e^{\mp\xi X'} A_m e^{-\frac{(X')^2}{2l^2}} H_m(\frac{X'}{l}),\end{aligned} \tag{B.6}$$

where Γ_α=$2\pi\left|V\right|^2 n_\alpha$.

Using the completeness identity,

$$\sum_m A_m^* e^{-\frac{(X)^2}{2l^2}} H_m(\frac{X}{l}) A_m e^{-\frac{(X')^2}{2l^2}} H_m(\frac{X'}{l}) = \delta(X - X')$$

equation (B6) can be written as

$$\Sigma^r_{n_0,n_0'}(t,t_1) = -\frac{i\Gamma_\alpha}{2}\theta(t_1)\delta(t-t_1) \tag{B.7}$$
$$\times \int dX' A_{n_0} e^{-\frac{(X'-x_0)^2}{l^2}} H_{n_0}(\frac{X'-x_0}{l}) V_0 e^{\mp 2\xi \hat{X}'} A^*_{n_0'} e^{-\frac{(X'-x_0)^2}{2l^2}} H_{n_0'}(\frac{X'-x_0}{l}),$$

After integrating[63] the above expression, we arrive at the following final result for the retarded self-energy,

$$\Sigma^r_{n_0,n_0'}(t,t_1) = -\frac{i\Gamma_\alpha}{2}\theta(t_1)\delta(t-t_1)\mathbf{\Sigma}^r(\mp), \tag{B.8}$$
$$= \Sigma^r_\alpha(t,t_1)\mathbf{\Sigma}^r(\mp) \equiv \mathbf{\Sigma}^r(t,t_1)$$

with

$$\mathbf{\Sigma}^r(\mp) \equiv \psi^{\mp}_{n_0,n_0'} \exp[(\gamma \mp x)^2 - x^2] \tag{B.9}$$

where $\Sigma^a_\alpha(t,t_1) = (\Sigma^r_\alpha(t,t_1))^*$ with α represents the L or R leads, and the matrices $\psi_{n_0,n_0'}$ is given as

$$\psi^{\mp}_{n_0,n_0'} = \sqrt{\frac{2^{|n_0'-n_0|}\min[n_0,n_0']!}{\max[n_0,n_0']!}}(\mp\gamma)^{|n_0'-n_0|} L^{|n_0'-n_0|}_{\min[n_0,n_0']}(-2\gamma^2), \tag{B.10}$$

where the dimensionless tunneling length $\gamma = \frac{\xi l}{\sqrt{2}}$, $x = \frac{x_0}{l}$, and the $-,+$ signs stands for the left and the right leads respectively.

Similarly, the lesser self energy may be calculated as

$$\Sigma^<_{n_0,n_1}(t_1,t_2) = \phi_{n_0,m}(t_1) g^<_{\alpha,\alpha}(t_1,t_2)\phi^*_{n_1,m}(t_2), \tag{B.11}$$

where $g^{<}_{\alpha,\alpha}(t_1,t_2)$ is the uncoupled Green's function in the leads and is given as

$$g^{<}_{\alpha,\alpha}(t_1,t_2) = \frac{1}{N}\sum_j g^{<}_{\alpha,j}(t_1,t_2) = \int_{-\infty}^{+\infty} n_\alpha d\varepsilon_\alpha g^{<}_{\alpha}(t_1,t_2) \tag{B.12}$$
$$= \int_{-\infty}^{+\infty} 2in_\alpha f(\varepsilon_\alpha) B_m d\varepsilon_\alpha \exp[-i(\varepsilon_\alpha + m\hbar\omega)(t_1-t_2)],$$

where B_m is the Boltzmann factor. We are going to consider that temperature is zero in the leads. So, we assume, when the oscillator appears in the leads it will always be in its ground state such that $m = 0$ ($B_m = \delta_{m,0}$) and the Fermi distribution function can be replaced with the theta function which in turn limits the integral. With the help of these approximations, and using the expressions for the tunneling matrix and the uncoupled retarded Green's function into equation (B11), the lesser self-energy may be written as

$$\Sigma^{<}_{n_0,n_1}(t_1,t_2) = \int_{-\infty}^{\epsilon_{F\alpha}} N2in_\alpha d\varepsilon_\alpha \frac{|V|^2}{N}\theta(t_1)\theta(t_2)\exp[-i\varepsilon_\alpha(t_1-t_2)] \tag{B.13}$$
$$\times \int dX A_{n_0} e^{-\frac{(X-x_0)^2}{2l^2}} H_{n_0}\left(\frac{X-x_0}{l}\right) V_0 e^{\mp\xi\hat{X}} A_0^* e^{-\frac{(X)^2}{2l^2}}$$
$$\times \int dX' A^*_{n_1} e^{-\frac{(X'-x_0)^2}{2l^2}} H_{n_1}\left(\frac{X'-x_0}{l}\right) V_0 e^{\mp\xi\hat{X}'} A_0 e^{-\frac{(X')^2}{2l^2}},$$

The above expression can be rewritten as

$$\Sigma^{<}_{n_0,n_1} = 2in_\alpha |V|^2 \theta(t_1)\theta(t_2) \int_{-\infty}^{\epsilon_{F\alpha}} d\varepsilon_\alpha \exp[-i\varepsilon_\alpha(t_1-t_2)] \tag{B.14}$$
$$\times \int dX A_{n_0} e^{-\frac{(X-x_0)^2}{2l^2}} H_{n_0}\left(\frac{X-x_0}{l}\right) V_0 e^{\mp\xi\hat{X}} A_0^* e^{-\frac{(X)^2}{2l^2}}$$
$$\times \int dX' A^*_{n_1} e^{-\frac{(X'-x_0)^2}{2l^2}} H_{n_1}\left(\frac{X'-x_0}{l}\right) V_0 e^{\mp\xi\hat{X}'} A_0 e^{-\frac{(X')^2}{2l^2}},$$

$$= i\Gamma_\alpha \theta(t_1)\theta(t_2) \int_{-\infty}^{\epsilon_{F\alpha}} \frac{d\varepsilon_\alpha}{2\pi} \exp[-i\varepsilon_\alpha(t_1 - t_2)] \tag{B.15}$$
$$\times \int dX A_{n_0} e^{-\frac{(X-x_0)^2}{2l^2}} H_{n_0}(\frac{X - x_0}{l}) V_0 e^{\mp\xi\hat{X}} A_0^* e^{-\frac{(X)^2}{2l^2}}$$
$$\times \int dX' A_{n_1}^* e^{-\frac{(X'-x_0)^2}{2l^2}} H_{n_1}(\frac{X' - x_0}{l}) V_0 e^{\mp\xi\hat{X}'} A_0 e^{-\frac{(X')^2}{2l^2}},$$

where Γ_α=$2\pi \left|V_{0,\alpha}\right|^2 n_\alpha$, with α representing the L or R leads, and the above equation can be rewritten as

$$\Sigma^<_{n_0,n_1}(t_1,t_2) = i\Gamma_\alpha \theta(t_1)\theta(t_2) \int_{-\infty}^{\epsilon_{F\alpha}} \frac{d\varepsilon_\alpha}{2\pi} \exp[-i\varepsilon_\alpha(t_1 - t_2)] \tag{B.16}$$
$$\times \int dX' A_{n_0} e^{-\frac{(X'-x_0)^2}{l^2}} H_{n_0}(\frac{X' - x_0}{l}) V_0 e^{\mp\xi\hat{X}'} A_0^* e^{-\frac{X'^2}{2l^2}}$$
$$\times \int dX A_{n_1} e^{-\frac{(X-x_0)^2}{2l^2}} H_{n_1}(\frac{X - x_0}{l}) V_0 e^{\mp\xi\hat{X}} A_0^* e^{-\frac{(X)^2}{2l^2}},$$

Which can be simplified by carrying out the integrals[63] and the final result is written as

$$\Sigma^<_{n_0,n_1}(t_1,t_2) = i\Gamma_\alpha \theta(t_1)\theta(t_2) \frac{\exp[\frac{-x^2}{2} + (\frac{\gamma \mp x}{2})^2]}{\sqrt{n_0!}} [\mp(\frac{\gamma \pm x}{2})]^{n_0} \tag{B.17}$$
$$\times \frac{\exp[\frac{-x^2}{2} + (\frac{\gamma \mp x}{2})^2]}{\sqrt{n_1!}} [\mp(\frac{\gamma \pm x}{2})]^{n_1} \int_{-\infty}^{\epsilon_{F\alpha}} \frac{d\varepsilon_\alpha}{2\pi} \exp[-i\varepsilon_\alpha(t_1 - t_2)],$$
$$\equiv \mathbf{\Sigma}^<(\mp)\Sigma^<_\alpha(t_1,t_2) = \mathbf{\Sigma}^<(t_1,t_2)$$

where $\gamma = \frac{l\xi}{\sqrt{2}}$, $x = \frac{x_0}{l}$, and the $-,+$ signs stands for the left and the right leads respectively.

Bibliography

[1] A. Schliesser, et. al., Nature Physics 5, 509 (2009).

[2] K. L. Ekinci and M. L. Roukes, Review of Scientific Instruments 76, 061101 (2005).

[3] K. L. Ekinci, Small 2005,1, No. 8-9, 786-797 (2005).

[4] M. L. Roukes, Technical Digest of the 2000 Solid State Sensor and Actuator Workshop; "Nanoelectromechanical Systems".

[5] H. G. Craighead, Science 290, 1532 (2000).

[6] P. Kim and C. M. Lieber, Science 126, 2148 (1999).

[7] M. P. Blencowe, Phys. Rep. 395, 159 (2004).

[8] A. N. Cleland, Foundations of Nanomechanics, 423, 2003 (Berlin: Springer).

[9] K. L. Ekinci, X. M. H. Huang, and M. L. Roukes, Appl. Phys. Lett. 84, 4469 (2004).

[10] R. G. Knobel and A. N. Cleland, Nature (London) 424, 291 (2003).

[11] H. J. Mamin and D. Rugar, Appl. Phys. Lett. 79, 3358 (2001).

[12] Michael Galperin, Mark A. Ratner, Abraham Nitzan, Alessandro Troisi, Science 319, 1056 (2008).

[13] Miles Blencowe, Science 304, 56 (2004).

[14] M. D. LaHaye, O. Buu, B. Camarota, and K. C. Schwab, Science 304, 74 (2004).

[15] K. C. Schwab and M. L. Roukes, Phys. Today 58 (7), 36 (2005).

[16] H. Park, J. Park, A. K. L. Lim, E. H. Anderson, A. P. Alivisatos, and P. L. McEuen, Nature (London) 407, 57 (2000).

[17] A. Naik et al., Nature (London) 443, 193 (2006).

[18] J. Koch and F. von Oppen, Phys. Rev. Lett. 94, 206804 (2005).

[19] J. Koch, F. von Oppen, and A. V. Andreev, Phys. Rev. B 74, 205438 (2006).

[20] M. Poot, E. Osorio, K. O'Neill, J. M. Thijssen, D. Vanmaekelbergh, C. A. van Walree, L. W. Jenneskens, and H. S. J. van der Zant, Nano Lett. 6, 1031 (2006).

[21] E. A. Osorio, K. O'Neill, N. Stuhr-Hansen, O. F. Nielsen, T. Bjørnholm, and H. S. J. van der Zant, Adv. Mater. (Weinheim, Ger.) 19, 281 (2007).

[22] E. Lörtscher, H. B. Weber, and H. Riel, Phys. Rev. Lett. 98, 176807 (2007).

[23] A. Erbe, C. Weiss, W. Zwerger, and R. H. Blick, Phy. Rev. Lett. 87, 096106 (2001).

[24] M. Poggio et al., Nature 4, 635 (2008).

[25] S. J. Bunch, et al., Science 315, 490 (2007).

[26] B. J. LeRoy et al., Nature 432, 371 (2004).

[27] G. A. Steele, et al., Science 325, 1103 (2009).

[28] A. D. Armour, M. P. Blencowe, and Y. Zhang, Phys. Rev. B 69, 125313 (2004).

[29] C. B. Doiron, W. Belzig, and C. Bruder, Phys. Rev. B 74, 205336 (2006).

[30] L. Y. Gorelik, et al. , Phys. Rev. Lett. 80, 4526 (1998).

[31] Andriy V. Moskalenko, Sergey N. Gordeev, Olivia F. Koentjoro, Paul R. Raithby, Robert W. French, Frank Marken, and Sergey E. Savel'ev, Phys. Rev. B 79, 241403(R) (2009), and references therein.

[32] A. D. Armour and A. MacKinnon, Phys. Rev. B 66, 035333 (2002).

[33] Miles Blencowe, Nature 424, 262 (2003).

[34] R.H. Blick, A. Erbe, H. Kömmer, A. Kraus, and J.P. Kotthaus, Physica E (Amsterdam) 6, 821 (2000).

[35] N. B. Zhitenev, H. Meng, and Z. Bao, Phys. Rev. Lett. 88, 226801 (2002).

[36] Hyun S Kim, Hua Qin, Michael S Westphall, Lloyd M Smith, and Robert H Blick, Nanotechnology 18, 065201(2007).

[37] Tomáš Novotný, Andrea Donarini, Christian Flindt, and Antti-Pekka Jauho, Phys. Rev. Lett. 92, 248302 (2004).

[38] T. Novotný, A. Donarini, and A.-P. Jauho, Phys. Rev. Lett. 90, 256801 (2003).

[39] Christian Flindt, Tomáš Novotný, and Antti-Pekka Jauho, Phys. Rev. B 70, 205334 (2004).

[40] D. Wahyu Utami, et al., Phys. Rev. B 74, 014303 (2006).

[41] A. Yu. Smirnov, L. G. Mourokh, and N. J. M. Horing, Phys. Rev. B 69, 155310 (2004).

[42] D. Wahyu Utami, et al., Phys. Rev. B 70, 075303 (2004).

[43] J. Villavicencio, et al., Appl. Phys. Lett. 92, 192102 (2008).

[44] D. Fedorets, L. Y. Gorelik, R. I. Shekhter, and M. Jonson, Phys. Rev. Lett. 92, 166801 (2004).

[45] L. V. Keldysh, Zh. Eksp. Teor. Fiz. 47, 1515 (1965).

[46] H. Huagand and A. P. Jauho, Quantum Kinetics in Transport and Optics of Semiconductors, Springer Solid-State Sciences Vol. 123 (Springer, New York, 1996).

[47] D. K. Ferry and S. M. Goodnick, Transport in nanostructure, Cambridge University press, 2001.; S. Datta, J. Phys.: Condens. Matter 2, 8023 (1990); R. Lake and S. Datta, Phys. Rev. B 45, 6670 (1992); 46, 4757 (1992).

[48] D. Fedorets, L. Y. Gorelik, R. I. Shekhter, and M. Jonson, Europhys. Lett., 58, 99 (2002).

[49] D. A. Ryndyk, R. Gutiérrez, B. Song and G. Cuniberti, Springer Series in Chemical Physics, Volume 3, pages 213-235 (2009).

[50] C. Caroli, R. Combescot, P. Nozieres, D. Saint-James, J. Phys. C: Solid St. Phys. 4, 916 (1971).

[51] C. Caroli, R. Combescot, D. Lederer, P. Nozieres, D. Saint-James, J. Phys. C: Solid St. Phys. 4, 2598 (1971).

[52] C. Caroli, R. Combescot, P. Nozieres, D. Saint-James, J. Phys. C: Solid St. Phys. 5, 21 (1972).

[53] Y. Meir, N.S. Wingreen, Phys. Rev. Lett. 68, 2512 (1992).

[54] N.S. Wingreen, A.P. Jauho, Y. Meir, Phys. Rev. B 48, 8487 (1993).

[55] A.P. Jauho, N.S. Wingreen, Y. Meir, Phys. Rev. B 50, 5528 (1994).

[56] D. Mozyrsky, and I. Martin, Phys. Rev. Lett. 89, 018301 (2002).

[57] Mozyrsky, I. Martin, and M. B. Hastings, Phys. Rev. Lett. 92, 018303 (2004).

[58] M. Tahir and A. MacKinnon, Phys. Rev. B (submitted), arXiv:1001.4250v1.

[59] Michael Galperin, Abraham Nitzan, and Mark A. Ratner, Phys. Rev. B 74, 075326 (2006).

[60] Michael Galperin, Abraham Nitzan, and Mark A. Ratner, Phys. Rev. B 73, 045314 (2006).

[61] M. Tahir and A. MacKinnon, Phys. Rev. B 77, 224305 (2008).

[62] V. Aji, J. E. Moore, and C. M. Varma, arXiv: cond-mat/0302222.

[63] I. S. Gradshteyn and I. M. Ryzhik, Tables of Integrals, Series and Products Academic, New York, (1980), P. 837-838.

[64] I. S. Gradshteyn and I. M. Ryzhik, Tables of Integrals, Series and Products Academic, New York, (1980), P. 66-67.

[65] A. D. Armour, Phys. Rev. B 70, 165315 (2004).

[66] D. A. Rodrigues and A. D. Armour, Phys. Rev. B 72, 085324 (2005).

[67] A. A. Clerk and S. M. Girvin, Phys. Rev. B 70, 121303R (2004).

[68] N. M. Chtchelkatchev, W. Belzig and C. Bruder, Rev. B 70, 193305 (2004).

[69] V. Nam Do, P. Dollfus and V. Lie Nguyen, Appl. Phys. Lett. 91, 022104 (2007).

[70] J. X. Zhu and A. V. Balatsky, Phys. Rev. B 67, 165326 (2003).

[71] J. Paaske and K. Flensberg, Phys. Rev. Lett. 94, 176801 (2005).

[72] K. Flensberg, Phys. Rev. B 68, 205323 (2003).

[73] Urban Lundin and Ross H. McKenzie, Phys. Rev. B 66, 075303 (2002).

[74] A. Yacoby, M. Heiblum, D. Mahalu, and H. Shtrikman, Phys. Rev. Lett. 74, 4047 (1995).

[75] L. D. Landau and E. M. Lifshiftz, Quantum Mechanics Nonrelativistic Theory (Pergamon, New York, 1977), p. 613.

[76] R. Schuster, E. Buks, M. Heiblum, D. Mahalu, V. Umansky, and H. Shtrikman, Nature (London) 385, 417 (1997).

[77] Akiko Ueda and Miko Eto, Phys. Rev. B 73, 235353 (2006).

[78] I. S. Gradshteyn and I. M. Ryzhik, Tables of Integrals, Series and Products Academic, New York, (1980), P. 310-311.

[79] T. Brandes and N. Lambert, Phys. Rev. B 67, 125323 (2003).

[80] D. A. Rodrigues, J. Imbers, and A. D. Armour, Phys. Rev. Lett. 98, 067204 (2007).